# AquaModel:

# Software for Sustainable Development of Open Ocean Fish Farms

**United States Department of Agriculture:**

**Small Business Innovation Research**

**Final Report**

Prepared by

**System Science Applications, Inc.**

**August 31, 2011**

**Authors:**

**Frank O'Brien**

**Dale Kiefer, Ph.D.**

**J.E. Jack Rensel, Ph.D.**

# Contents

# Table of Figures

# List of Tables

### Acknowledgements

This report should be cited as:

# Executive Summary

The development of open ocean marine aquaculture (mariculture) farms within suitable portions of the United States Exclusive Economic Zone (EEZ) offers the promise of profitable commercialization with low risk to the environment and wild fish stocks. The history of net pen fish farming has demonstrated that site selection involves many interacting and critical variables that are not easily assessed by traditional trial and error approaches. With support from the U.S. Department of Agriculture, we have helped to advance this industry by completing development of *AquaModel*, software that accurately predicts the environmental impacts and operations of fish farms both nearshore and in the open ocean. *AquaModel* is now available to assist industry and government to predict and meet proposed rules and performance standards and to provide quick access to information needed for permitting and planning. *AquaModel* provides a home for data used in these and related pursuits, the tools to visualize and communicate this information, and a comprehensive model to simulate operations and environmental impact of operations. Presently, there are no other comprehensive software systems to accomplish all these tasks.

The updated version of *AquaModel* provides mapping and modeling tools required by regulators and farm operators to manage sustainable mariculture development in coastal and offshore waters. Using this technology we have developed a mariculture information system for Hawai'i's Department of Agriculture that focuses on the main island. This is a region where the growth of open water mariculture is imminent. During this project we have completed all six of the tasks we identified in our Phase II proposal.

1. We developed an advanced visualization of a broad-scale (entire coastline), 3-dimensional coastal flow and built an interface to link this visualization in *AquaModel* to outputs from coastal circulation models.
2. We added contouring and statistics routines into *AquaModel* in order to better summarize the environmental impact of farm operations.
3. We wrote computer code to accelerate simulations in order to improve our ability to analyze the impact of sediment waste deposition in waters where waste accumulation and the response of the benthic community are slow.
4. We completed a greatly improved benthic dynamics subroutine and incorporated it into *AquaModel*.
5. We completed physiological studies of a culturally and commercially important species (moi, *Polydactylus sexfilis)* that has been the principal species cultivated in

Hawai'ian net pens. We also conducted similar studies with cobia (*Rachycentron canadum*) as this species is growing in importance worldwide in tropical seas.

6. We created an updated version of *AquaModel* and incorporated the Hawai'i Department of Agriculture GIS information system into our software.

In this report we applied basic components of *AquaModel* to a single, modestly-sized fish farm site near the NW coast of the big island of Hawai'i where we forecasted water column and benthic effects. Then, for six slightly larger farms in the same region, we studied potential interactions and effects on nutrients, phytoplankton and nearshore areas using the far field modeling system of *AquaModel*. The hypothetical farms were located relatively nearshore (1.5 to 2 km) but in deep water (~ 100m) and in areas of strong currents. The direction of water flow at each of the far field sites varied slightly, but was dominantly to the northeast and therefore onto the shore a few km away.

We found that the strong currents and modest production schedule resulted in essentially no measurable adverse effect upon the seabottom anywhere in the modeling domain. This was expected and the small amount of total organic carbon containing waste fish feces or waste feed that reached the bottom would be resuspended, moved, aerated and eventually assimilated by bottom dwelling organisms from bacteria to invertebrates and demersal fish.

The water column effects of the six farms were found mostly to be independent of each other, with the exception of two or three sites in the main bight of the Kohala coast. Waste nitrogen excreted by the fish is rapidly moved in several directions, but we were particularly interested in transport that would impinge upon the nearby shoreline areas that are replete with coral reefs. Nutrients in the water column around coral reefs can be detrimental to reef survival by enhancement of epiphytic growth of attached benthic algae, although the subject is controversial. Measurable amounts of nitrogen were seen to occur at the farm sites, but data "capture cells" located about one-half the distance to shore from the net pens show an order of magnitude decline of dissolved nitrogen concentration due in part to dilution and uptake of nitrogen by phytoplankton. Nearest shore, the concentration of net pen origin nitrogen would be near zero except for brief periods, particularly when the fish biomass was approaching maximum carrying capacity. At such times the concentrations nearshore would increase from the naturally low level of about 0.1 μM to 0.2 μM but would average much less. Larger or more numerous fish farm sites could increase the concentrations near shore and possibly initiate a problem for the coral reefs. We used a conservative estimate of dissolved nitrogen production that included both urea and ammonia produced by the fish, as well as other, usually neglected components through our own studies of the physiology of the targeted culture fish, moi.

Study of the distribution and amount of phytoplankton resulting from the single and six fish farm operations indicated that there were more optimal and less optimal sites in terms of phytoplankton accumulation and density. Although most phytoplankton are considered beneficial and part of the base of the food web of the sea, it would be prudent to minimize nearshore production of phytoplankton in the Hawai'ian Islands as there are already numerous anthropogenic and natural sources of nutrient flowing into the sensitive near shore areas. We found that effects nearshore were most pronounced from pens located inside the Kohala Coast bight, a sort of open bay that tended to reduce water flow. Effects were at times noted around the fish farm locations, but due to the lag period of nutrient production to uptake and cell division, the location of increased production due to the six fish farm operation could be some distance from the fish farm sites. Minimal nearfield effects were recorded for Site 5 near a major headland known as Keahole Point, due to the northeasterly currents that had no immediate nearby shore in the down current direction. The simulation shows evidence that dissolved nitrogen is taken up by photosnthetic phytoplankton, as downstream there are minor plumes of phytoplankton but the concentration of nitrogen in these plumes is similar to ambient conditions. In all cases, the production of phytoplankton at all locations was minimal, only a few tenths of a part per billion in units of chlorophyll *a* (a surrogate density measure of phytoplankton abundance).

This analysis indicates that some level of net pen based fish farming would be sustainable along the subject coastal area, but that there are limits or a carrying capacity where the effects would shift from non measurable or significant to measurable and potentially adverse. Presently, *AquaModel* is the only computer software in the world that is specifically designed for forecasting these effects.

# Description of AquaModel

## Background

To the best of our knowledge, *AquaModel* is the only software that provides a complete, dynamic model of farm operation and environmental impact. It is also the only software that fully integrates environmental information with model computations within a GIS. More information can be found at www.AquaModel.org and simplified demonstrations of model use can be found at http://netviewer.usc.edu/projects.htm (only use Internet Explorer and closely follow browser options). The GIS program EASy is described at http://www.runeasy.com/.

The GIS software EASy provides a 4-dimensional framework (latitude, longitude, depth, and time) to run simulation models and analyze field measurements as graphical, numerical and statistical outputs. EASy, whose components are summarized in Figure 1, runs in Windows. It is a geographical information system designed for the storage, dissemination integration, analysis and dynamic display, of spatially referenced series of diverse oceanographic data. It provides the tools to import, display, and analyzes environmental information obtained from satellite-ocean thermal and color sensors and field surveys of currents, nutrients, oxygen, chlorophyll and other related parameters.

EASy graphically renders dynamically in time, within their proper geo-spatial context, both field and remotely sensed data and model outputs as diverse types of plots, including vector, contour, false color images and includes a built-in data contouring feature. Vertical structure of data, critical in oceanographic applications, is depicted as vertical contours for transects or depth profiles at selected point locations. Time series for measurements and relationships such as vertical profiles within the database at individual stations can also be visualized interactively as XY-plots. Presently there are over 50 different XY-plots available for different parameters viewed as vertical profiles or horizontal cross sections that are dynamically updated in real time simulations. The software also provides access to data, integrated visualization products, and analytical tools over the Internet via Netviewer, a client-server, plug-in for EASy (Tsontos and Kiefer, 2002 and 2003).
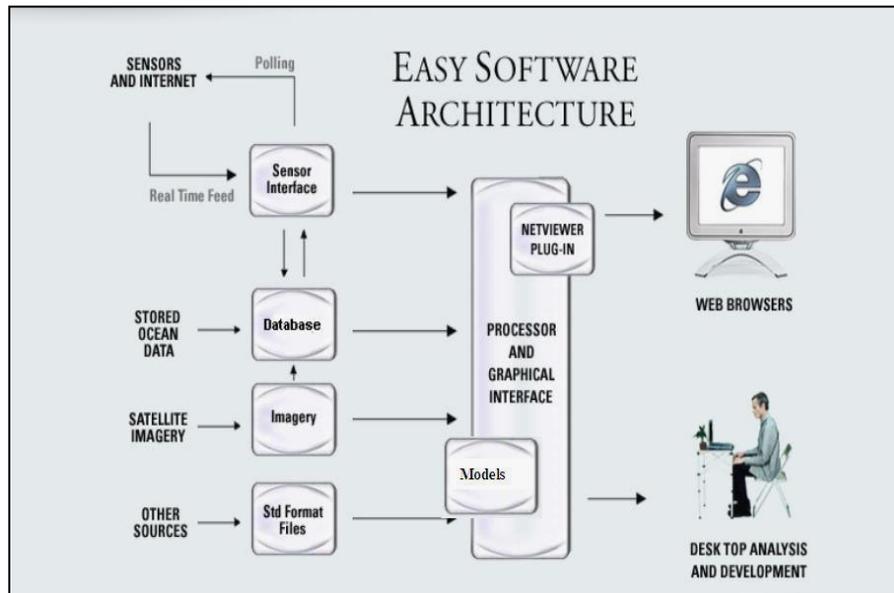
**Figure 1. EASy software architecture and data integration and communication capabilities.**

*AquaModel* is a plug-in model to EASy and simulates the dynamics of fish farms that can be "placed" within a selected water body and operated under the conditions found at that location. Most importantly, *AquaModel* fully integrates environmental conditions into the calculations of the growth and physiology of the penned fish.

The model is designed to simulate both the growth and metabolism of farmed fish species and the environmental impact of waste produced by the farm. It is to be used by developers and environmental agencies to assess both the optimal placement of farms and appropriate size of the farm for environmentally safe and sustainable operations. Several variables including the water temperature, the dissolved oxygen concentration, current speed, average wet weight of the fish, their density within each pen and the daily food ration define the initial state of conditions in the fish farm. Each pen is tracked separately and different species can be stocked in separate pens and each pen allows different initial size of fish. Outputs from the simulation include three dimensional maps of the two types of waste plumes (dissolved and particulate) created by egestion, excretion, and respiration by the farmed fish. Outputs also include the growth rate and standing stock of the fish, and the concentrations of nitrogenous nutrients, oxygen, and particulate waste (feces) within the farm. Many other parameters and plots of vertical profiles or transects can be viewed simultaneously, and all data can be written to spreadsheet or database for statistical and other types of post-model processing.
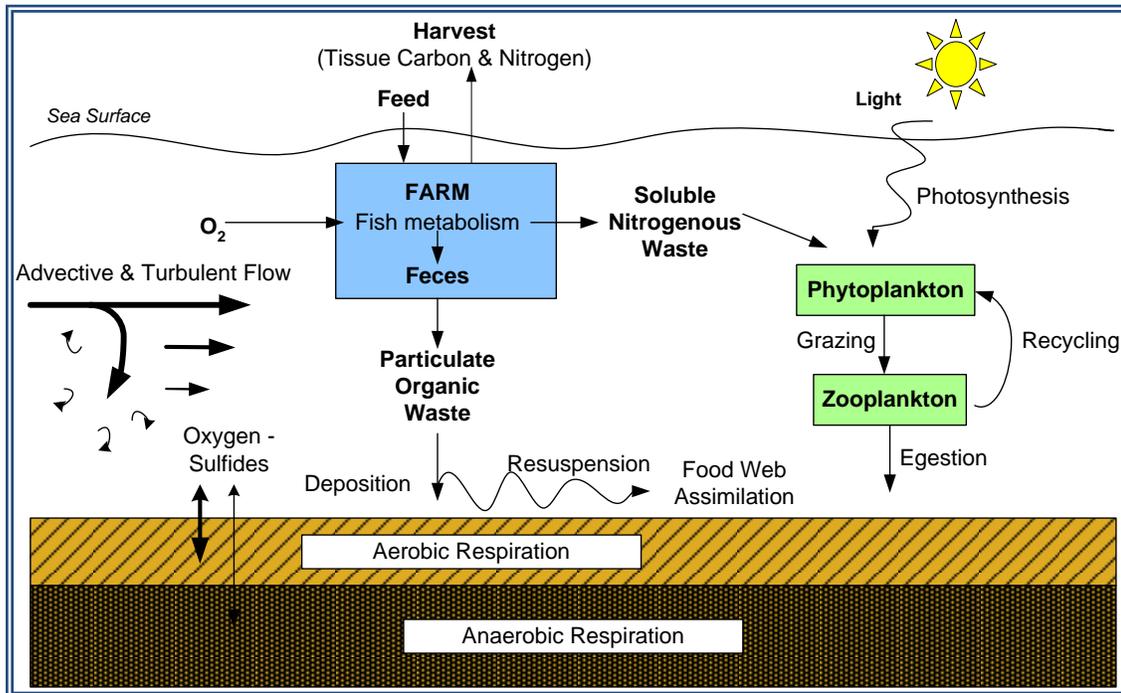
**Figure 2. Key processes simulated in *AquaModel* include the growth and metabolism of farmed fish, the flow of water through the pens and transport of dissolved and particulate wastes produced by the fish, and the ecological transformations of these wastes.**

The model is best described as consisting of 4 linked computational routines: a 2 or 3 dimensional description of water circulation, a description of the growth and metabolic activity of the cultured fish within the farm, a description of the planktonic community's response to nutrient loading, and a description of benthic effects (Figure 2). Carbon, nitrogen and oxygen fluxes are traced and rate functions vary with operational and environmental conditions. Operational conditions are the size and position of the pens, the quantity and composition or rations, and the density and size of the fish. Environmental factors that determine metabolic rates are current speed, the temperature of the water and the concentration of oxygen in the water. As water passes through the farm, a "waste water plume" and a "waste particle plume" are created downstream. The characteristics of this plume will depend upon the metabolic activities within the farm as well as the advective and turbulent flows that shape the plume.

*AquaModel* is also designed to be user friendly so that it can be quickly put in the hands aquaculture stakeholders with basic understanding of commercial software. Thus, virtual farms are first designed by the stakeholder and simulations are then run using several graphical interfaces. For example, Figure 3 is such an interface in which the user enters information on the location, size, and operation of a virtual (or real) fish farm as well as key environmental information. In this figure the "Pens" tab has been selected in which the user selects the number of pens in the farm, the species of fish in each pen, the

geographical position of the pens, the size and shape of the pens, the average weight of fish at the start of grow out, and the stocking density of these fish. In addition, from this interface the user can also chose to run a simulation, run and capture the results in a file, or replay a "results file". Moreover, one can select whether to run the simulation with a 2-dimensional or 3-dimensional flow field.
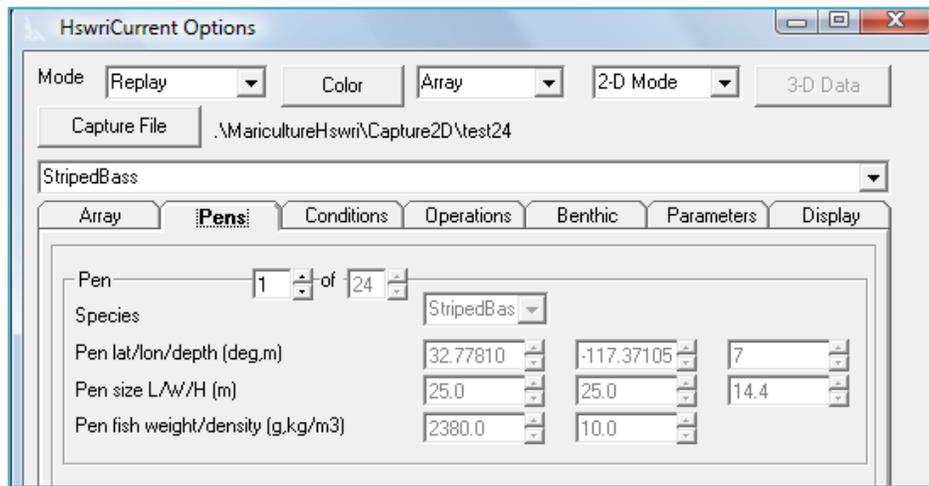


**Figure 3.  The user interface for entering information on the location, size, and operation of a virtual (or real) fish farm as well as key environmental conditions.**

## Circulation Routine

*AquaModel*'s circulation routine flushes cages with ambient waters and transports wastes from them. The computations during each step of the simulation occur within each element of a 3-dimensional grid of rectangular cells that populate an array of such cells. The size, orientation, and geospatial location of the array as well as the number and dimension of the cells that populate the array are entered by the users. The array of cells begins at the sea surface and extends to the sea floor. The geometry and flow at the sediment/water interface is described in more detail in the Benthic Routine Section and the farm layout is described in the site description section. The time steps for the simulation vary between 1 and 5 minutes depending upon the speed of the currents.

The system of equations describing circulation is a simple finite element description of advection and dispersion. Each element of the array is treated as a box model in which materials flow across the 6 interfaces of each element, top, bottom and the four sides. Each element is treated as instantly mixed throughout. These movements are tracked using a simple, finite difference calculation. Conservative tracers such as water and elements are conserved within the computational array.

Water and dissolved and suspended materials also move across the boundary of the array; however, here the values for the concentrations of dissolved and particulate materials at the boundaries are determined by the boundary conditions of the computational array. During the course of our NMAI project we added the capability to vary the values of current velocities and the concentration of tracers at the boundary to vary at a time step specified by the user. If the calculations of such a model are to be trusted, the array must be sufficiently large such that the exchange across the boundary does not significantly perturb the results of calculations. At the sediment-water interface uneaten feed and feces from the farm are transported, deposited into the sediments, resuspended from the sediments, or consumed by benthic organisms. These processes will be described in the next section.

The flow field in *AquaModel* can be either 2- or 3-dimensional. In 3-dimensional simulations the movement of water between adjacent cells has no constraints other than the requirement of conservation of mass. Convergent and divergent motion can be represented within the array as well as local eddies. In addition, the water depth can vary within the array. Since 3-dimensional flow on small spatial and temporal scales is rarely measured in the field, our 3-dimensional simulations draw upon 3-D coastal circulation models. The spatial scale of these models is generally no smaller than 1 km and thus small scale turbulence is not included in the output. However, *AquaModel* provides the user the option to add specified levels of horizontal and vertical eddy diffusivity. While rates of horizontal dispersion are constant throughout the computational array, the rates of vertical dispersion can be specified for two layers, the upper mixed layer and the underlying stratified waters. The depth intervals of the mixed layer and the stratified layers vary with season as a sinusoidal oscillation.

In 2-dimensional simulations advection only occurs horizontally; neither divergence nor convergence flow occurs within the array. Small scale horizontal and vertical turbulent motions are treats as described in the previous paragraph. Much of the data on circulation collected at mariculture sites come from field measurements with acoustic Doppler current profilers, drogues, or current meters. In other cases information may come from simple tidal models. Such information is well suited to 2-dimensional simulations.

*AquaModel* provides a user interface for importing both 2- and 3-dimensional output from current meters and circulation models, and automatically interpolates in time and space such output in order to "fit" the computational grid selected by the user.

# Farm Operations and Fish Metabolism Routines

The fish farm is characterized by physical layout and size of its cages and by its stocking, feeding, and harvesting regime. The physical layout of the farms requires one to enter:

- The number of cages.

- The location of the cages as described by their geographic co-ordinates (latitude, longitude, depth).

- The size of the cages including the length, width, and height. These setting may have to be adjusted to best fit the size of the cells within the computational array.

- The fractional difference between the current speed within the cages and ambient current speed.

Farms operations require one to enter for each cage:

- The species of farmed fish. Although the system of equations describing the growth and metabolism is invariant with species, the coefficients found within these equations will likely vary with species.

- Mean weight of fish in grams wet weight at initial stocking or at selected time intervals.

- Density of fish in mass of fish per cubic meter at initial stocking or at selected time intervals.

- Feed rate in grams dry weight of feed per day. This rate can be entered manually or calculated automatically by *AquaModel* as an optimal feed rate.

- Estimated percentile of uneaten feed loss from the cages.

Prior to this project we developed the fish metabolism routine that is based upon extensive review of the literature describing the growth and metabolism of commercial species (e.g. see Brett's work on sockeye salmon in references). This information has been supplemented by our own unpublished laboratory experiments and has been incorporated into a series of equations that track the transformations of oxygen, carbon, and nitrogen. (See Rensel, Kiefer, and O'Brien 2006 and Rensel et al. 2007 for more background.) The routine includes a description of oxygen-limited metabolism- an important feature since fish are raised at high densities, and in some cases farms are found in ambient waters of moderate or low dissolved oxygen concentration.

As indicated in Figure 4, the routine includes the processes of ingestion, egestion, assimilation, respiration, excretion, and growth. Carbon, nitrogen, and oxygen fluxes are all computed, and of course the rates of these fluxes vary with operational and environmental conditions. The operational independent variables are listed above while the environmental variables that determine metabolism are:

- Water temperature.

- Ambient oxygen concentration which is one of the determinants of the concentration of oxygen with a cage.

- Ambient current velocity, which is another determinant of oxygen concentration within the cage as well as a determinant of the respiration rate required of the fish to swim at a speed in order maintain their position within the cage.
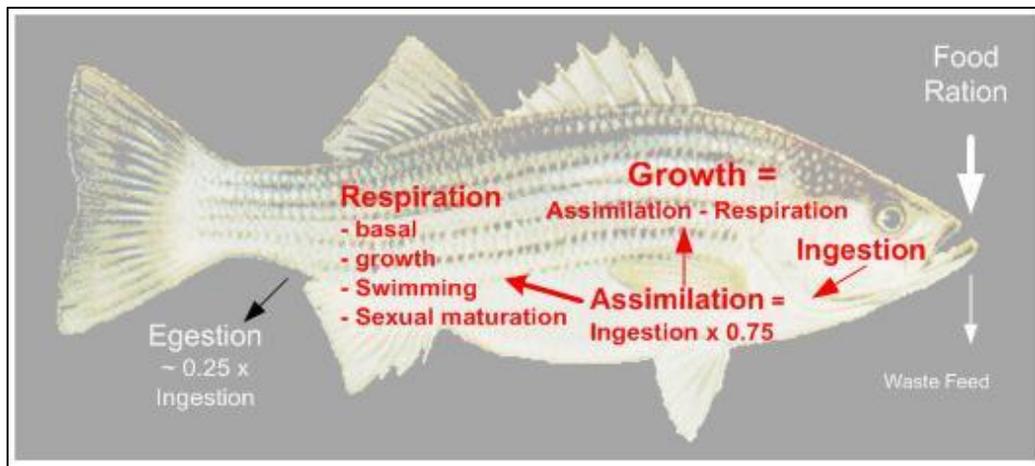


**Figure 4. Metabolic processes described by our metabolic routine for fish metabolism. (*Background drawing by Duane Raver, USFWS*).**

The striped bass routine consists of a series of functions describing the fluxes of carbon, nitrogen, and oxygen as determined by the basic features of metabolism, ingestion, egestion, assimilation, respiration, and growth. Specifically, each element is tracked according to these 5 basic features, which are related to each other by conservation of mass:

1. ingestion rate = egestion rate + assimilation rate

2. rate of growth = assimilation rate - rate of respiration

3. respiration rate = resting rate of respiration (i.e. basal) + respiration rate of activity (i.e. swimming) + respiration rate of anabolic activity (i.e. growth)

4. rate of feces production = egestion rate

5. rate of loss of uneaten feed = feed rate – ingestion rate

The functions for the 5 basic metabolic processes can be summarized as follows. Ingestion rate is determined by both the rate of supply of food and rate at which the fish can assimilate ingested food (Process 1). If the rate of supply of food exceeds the sum of the rate of egestion and the rate of assimilation, then a fraction of the food will be uneaten and contribute to the particulate waste produced by the cage (Process 5). Egestion is assumed to be a fixed fraction of ingestion; the value of this fraction is determined largely by the nutrient composition of the feed. The rate of egestion is in fact the rate of feces production (Process 4). The assimilation rate of the fish will be a function of the size (age) of the fish, the temperature of the water, and the concentration of oxygen within the cage. The assimilated nutrients are then either consumed by respiration or contribute to the growth of the fish (Process 2). Note that we assume that there are no reproductive demands within the cage. The rates of respiration, which include both the consumption of oxygen and excretion of nitrogen, are determined by three processes, basal metabolism, swimming metabolism, and anabolic metabolism demanded by growth (Process 3). Basal metabolism is a function of water temperature and the size of the fish, swimming metabolism is a function of the fish size and its swimming speed, and anabolic metabolism is proportional to growth rate. The growth rate of the fish is simply calculated by subtracting the rate of respiration from the rate of assimilation.

Information on *Salmo salar* and *Morone saxatilis* metabolism that we used to determine the values for coefficients found in the system of equations for the two species came from a number of sources including publications of growth and metabolism in the laboratory and field (see our references), reports provided by our collaborators, and FishBase, which distributes data over the Internet on morphometrics, respiration rates, growth rate, and in some cases gill surface area. Data from these sources were used to tune the equations of the metabolism by searching for coefficient values that provided the best fit to the data. Because of its commercial value, *Salmo salar* has been thoroughly studied, and data for tuning is comprehensive. *Morone saxatilis* is less studied and our review of the literature included information for wild stocks (e.g., Hung et al. 1993, Chesney et al. 1993, Duston et al. 2004) as well as stocks by our collaborators at the Hubbs Sea World Research Institute. Examples of the goodness of fit between routine predictions and measurements for both species follow *(*Rensel, et. al. 2006).

Figure 5 compares our routine predictions (dashed lines) of the growth of sockeye salmon, *Oncorhynchus Nerka*, with laboratory measurements (continuous lines) at different temperatures and feeding rates (Brett 1964). The accuracy of predictions is also good. The growth rates are in units of the fractional change in body weight per day, and the feed rates of 0.06, 0.03 and 0.015 are in units of fractional body weights of food per day. Note that the routine accurately predicts the decreases in the temperature of optimal growth with decreases in feed temperature. The predicted growth rates are calculated

from the functions describing all the physiological aspects shown in Figure 4. We wish to acknowledge here the importance of the measurements and concepts of Brett and co-workers in designing our routine (Brett, Shelbourne, and Shoope 1969; Brett and Zala 1975; Brett 1976).
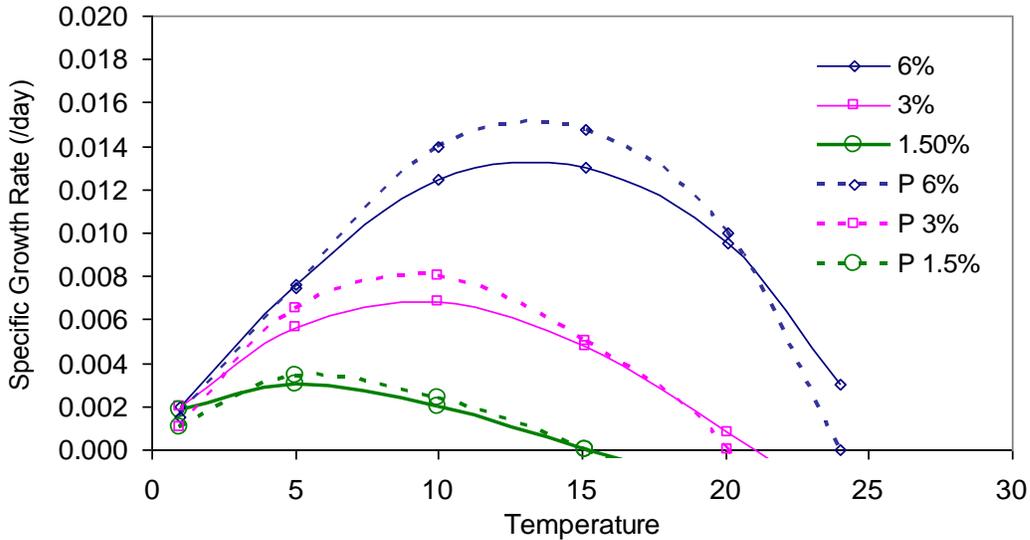


**Figure 5. Predicted (dashed line) and measured (continuous line) specific growth rates for sockeye salmon grown at different temperatures and feed rates. The specific growth rates are the daily fractional change in fish weight and the feed rates in the upper right corner are the daily fraction of the fish weight provided by dry feed. The fish weights are about 200 g (Brett 1964).**

Figure 6 shows predicted (dashed lines) and measured (solid lines) respiration rates for young sockeye salmon swimming at different speeds (legend) and at different temperatures (abscissa). The swimming speeds found in the legend are in units of body lengths per second. Although our model describes steady state conditions as opposed to the short time interval during which the measurements was made, the fit is still good except at maximal swimming speeds.

Figure 7 is a third example of the performance of the fish metabolism routine, in which the calculated specific growth rate of *M. saxatilis* plotted against the weight of the fish over time. Two curves are plotted; one is results of calculations with our *AquaModel* routine and the other is derived from the von Bertalanffy growth curve (von Bertalanffy 1960). The two curves fall nearly perfectly on top of each other. The fish metabolism routine was calculated for fish that are well fed, at rest, and cultured in water that is aerated and at a temperature of 15 °C.
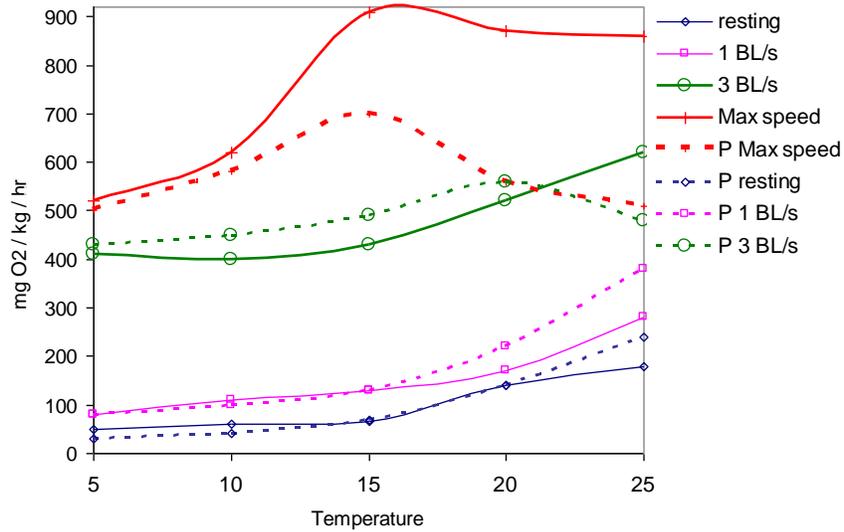
**Figure 6. Predicted (dashed lines) and measured (continuous lines) respiration rates for sockeye salmon grown at different temperatures and swimming speeds. The respiration rates are in units of mg $O_2$/(kg fish wet weight/ hour) and swimming speed is in units of body lengths per second. Fish weights are about 200 g (Brett 1964).**
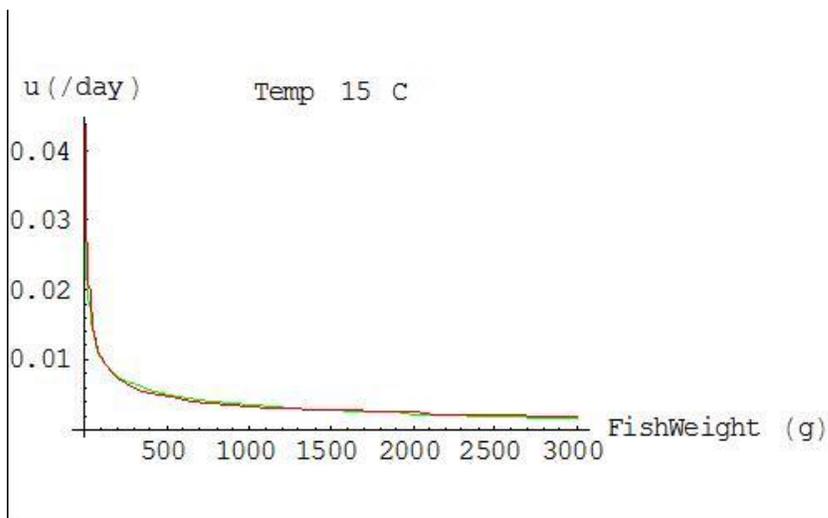


**Figure 7. The specific growth rate of striped bass of differing size (age). The red line is calculated from the von Bertalanffy growth curve found in FishBase and the (almost exactly superimposed) green curve is the predicted growth rate under optimal culture conditions from the *AquaModel* fish metabolism routine.**

# Plankton Routine

The plankton routine describes the cycling by plankton of nitrogen and oxygen within each element of the array, both within the farm and the surrounding waters. This model is similar to the PZN models that have been published by Kiefer and Atkinson (1984) and Wroblewski, Sarmiento, and Flierl (1988). The "master" cycle describes the transforms of nitrogen between three compartments, inorganic nitrogen, organic nitrogen in phytoplankton, and organic nitrogen in zooplankton. The three biological transforms are:

- Photosynthetic assimilation of inorganic nitrogen by phytoplankton which is a function of temperature, light level, DIN (dissolved inorganic nitrogen consisting of ammonia, nitrite and nitrate) concentration.

- Grazing by zooplankton on phytoplankton which is a function of temperature and concentrations of zooplankton, and phytoplankton.

- Excretion of DIN by zooplankton, which is a function of temperature and the concentration of zooplankton.

All three components are transported by advective and turbulent flow as described above. The model displays predator-prey oscillations, which dampen over time and reach a steady state. The default simulations for DIN, phytoplankton, and zooplankton stabilize at roughly 1 mg-at N m$^{-3}$, for all 3 components respectively. In order to calculate the concentrations and rates of loss by respiration and production by photosynthesis, we have assumed a constant flux ratio of oxygen to nitrogen of 6 moles $O_2$ gm-at N, consistent with the Redfield ratio. The inputs to this model consist of the time series of exchange coefficients produced by the hydrodynamic model, surface irradiance, and water temperature as well as concentrations of dissolved oxygen, dissolved inorganic nitrogen, cellular nitrogen in phytoplankton and zooplankton. Outputs of this model consist of a time series of the concentrations of dissolved inorganic nitrogen and oxygen, phytoplankton (traced as chlorophyll), and zooplankton. This routine provides estimates of the response of the planktonic community to the discharge of nitrogenous nutrients from fish farms. Specifically, it focuses on the question of whether such discharges can initiate phytoplankton blooms.

Figure 8 is a schematic of the plankton routine. During the simulation, this subroutine runs within each cell of our 3-dimensional computational grid. As shown, the subroutine calculates within each cell transformations of two tracers, nitrogen and oxygen, by the planktonic community. In fact the concentrations of oxygen and nitrogen within each cell vary with time because of both the local transformations with each cell and the vertical and horizontal transport of these elements among cells.

Although oxygen is shown as two components, atmospheric oxygen and dissolved oxygen in seawater, we assume that the concentration of atmospheric oxygen remains at a constant value of 0.209 atmospheres (i.e., the normal sea level concentration of oxygen as about 21% of air), and thus only the concentration of dissolved oxygen varies with time. For computational cells at the sea surface, local variations are caused by the rate of exchange across the air-water interface (indicated by the blue horizontal line) and rates of photosynthesis by phytoplankton and respiration by zooplankton. Below the sea surface, local changes are caused only by the rates of photosynthesis and respiration. The routine consists of five components: atmospheric oxygen, dissolved oxygen, phytoplanktonic nitrogen, zooplanktonic nitrogen, and dissolved inorganic nitrogen. The concentrations of inorganic nitrogen and oxygen will vary with environmental conditions as well as rates of fish metabolism within the fish pens and transport from the pens. The routine includes descriptions of the influence of temporal and spatial variations in temperature and light on rates of photosynthesis and grazing. The description of light intensity includes calculations of the concentration of chlorophyll within the water column and its influence on the diffuse attenuation of downwelling irradiance. The routine also includes a tuning algorithm to obtain values for the coefficients for zooplankton grazing and excretion that provide a best fit to field measurements of concentrations of phytoplankton, zooplankton, and nutrients.
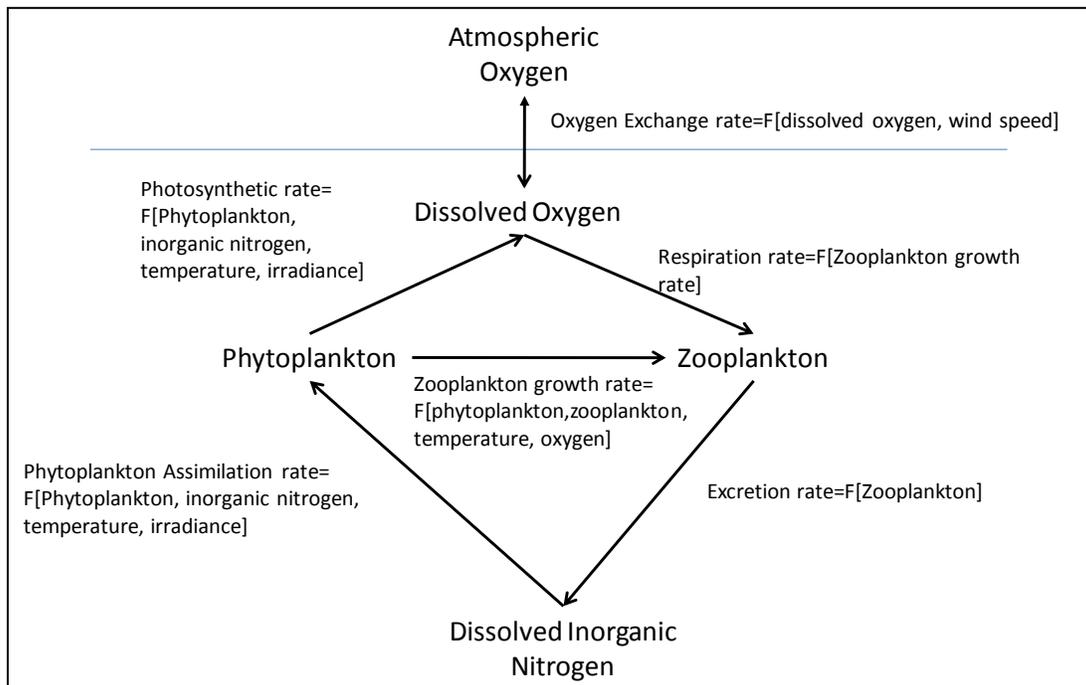


**Figure 8. Processes and components of the *AquaModel* plankton routine. Processes include oxygen exchange across the air-sea surface (but of course not in the computation cells below the surface), the cycling of nitrogen by phytoplankton, zooplankton, and dissolved inorganic nitrogen, and the biological production and consumption of oxygen associated with the cycling of nitrogen.**

Figure 9 shows an example of the dynamics of the plankton routine when it is tuned to the conditions in the Southern California Bight. This simulation shows the response of the phytoplankton and zooplankton community to a sudden increase in dissolved inorganic nitrogen in a closed system in which there is neither transport of material in nor out of the system. The conditions within the system are those of the summer upper mixed layer several kilometers off the San Diego coast: because of warm water and high irradiance in a shallow mixed layer the growth rate of phytoplankton is only limited by nutrient concentration.
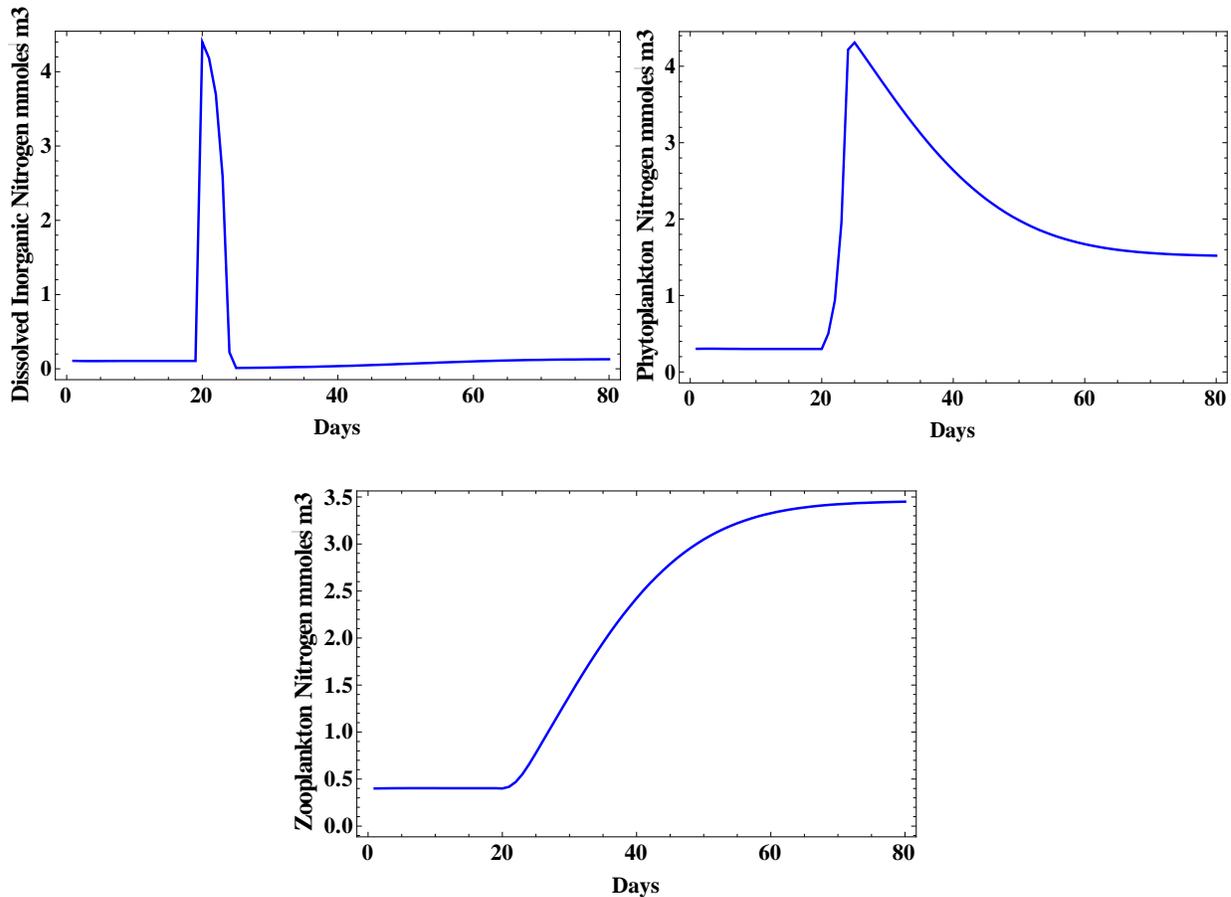






**Figure 9. A simple simulation of the plankton routine for a closed system in which there is no transport of material into or out of the system. The environmental conditions are constant during the 80 day simulation except that on day 20 the concentration of dissolved inorganic nitrogen is suddenly increased from 0.2 to 4.4 mg-at. N m$^{-3}$. This increase in the limiting nutrient stimulates a phytoplankton bloom and subsequently a zooplankton bloom.**

During the first 20 days of the simulation the planktonic community is in a nutrient-limited, steady state in which the concentrations of dissolved inorganic nitrogen, phytoplankton nitrogen, and zooplankton nitrogen are 0.2, 0.3, and 0.4 mg-at. N m$^{-3}$, respectively. On day 20 the concentration of dissolved inorganic nitrogen is suddenly increased from 0.2 to 4.4 mg-at. N m$^{-3}$. This increase in the limiting nutrient stimulates a

phytoplankton bloom that assimilates the excess nutrient within a week.  This bloom then quickly grazed by the zooplankton, and a new steady state is established by the end of the simulation in which the concentrations of nutrient, phytoplankton, and zooplankton are 0.2, 2, and 3.5 mg-at nitrogen m$^{-3}$, respectively.

This simulation is provides a sense of the type of plankton response one might expect within the nutrient enriched plume downstream of a very large commercial fish farm, provided that there is no dispersion of the plume as it is transported from the site.  In fact, given the time scales of the plankton response, the mixing of the plume with ambient waters will greatly reduce concentrations within the plume well below the values shown in this figure.

Figure 10 is an example of the dynamics of the plankton routine when it is subjected to a simple tuning to the conditions at the Gulf of Maine site, from a recent study by our *AquaMode*l group.  It shows a one year simulation for a closed system in daily changes in the concentration of dissolved inorganic nitrogen is an input to the calculation.  Here the phytoplankton and zooplankton communities respond to the large seasonal changes in the water temperature, nutrient concentration, mixed layer depth, and sea surface irradiance. A comparison of these calculated time series with field measurements at the Gulf of Maine farm found in this report indicates that the routine provides a reasonably good description of the spring and fall bloom of phytoplankton and zooplankton. The timing of the bloom and the variations in phytoplankton crop are good; however variations in zooplankton biomass are much too large. This is the consequence of assuming a closed, cycling system with only 3 components.

The tuning algorithm that is referenced above is executed by solving the system of differential equations found in the plankton routine for values of coefficients found in these equations.  The solutions are obtain by assuming that there exists quasi-steady state conditions for the key dependent variables of the plankton routine, i.e., the concentrations of nutrients, phytoplankton, and zooplankton.  Under such conditions one can solve for the value of unknown coefficients that provide a "best-fit" between calculated values the independent variable and values for these variables measured in the field. Tuning for the Gulf of Maine simulation matched predicted and measured values during the summer period when the concentrations of the three dependent variables were low and both the spring and fall periods of the phytoplankton bloom.  Tuning a separate Southern California Bight simulation matched predicted and measured values during the summer period when the concentration of nutrients are low and zooplankton high and the winter period when the concentration of nutrients are high and zooplankton low.
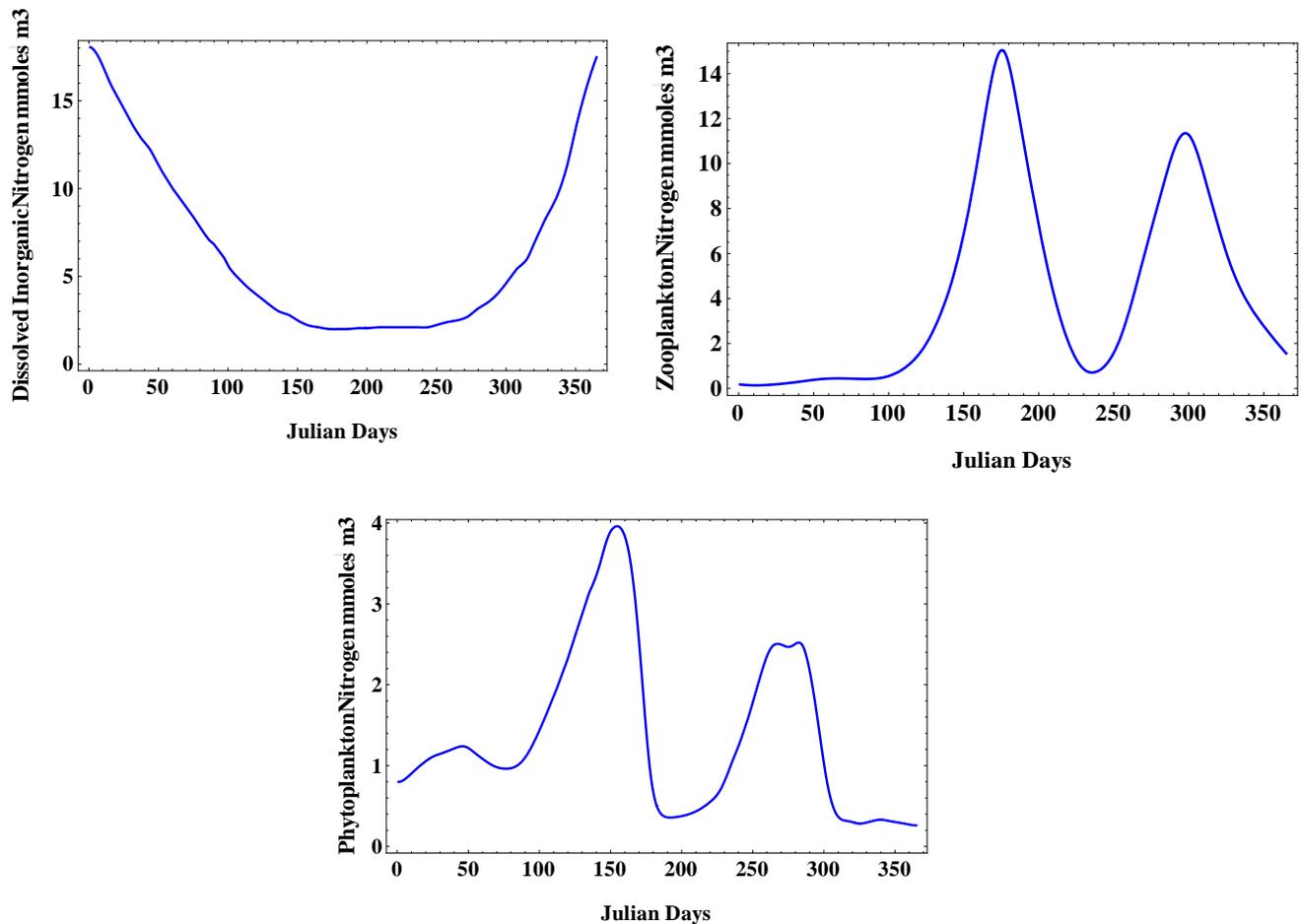
**Figure 10. A one year simulation by the plankton routine for a closed system in which there is no transport of material into or out of the computational cell. A comparison of these calculated time series with field measurements at a Gulf of Maine farm found in sections 4.7- 4.8 indicates that the routine provides a reasonably good description of the spring and fall bloom of phytoplankton and zooplankton.**

The development and application of the tuning algorithm provided us with information on the sensitivity of calculated values for the dependent variables to uncertainties in the values for independent environmental variables such as water temperature, current flow, and nutrient concentration as well as uncertainties in the value of coefficients. In the case of the plankton routine it appears that predictions are most sensitive to the values of such environmental variables as vertical and horizontal eddy diffusivity, mixed layer depth, water turbidity, and primary and secondary macronutrient concentrations. Coefficients most critical to accurate predictions are those that describe zooplankton dynamics. These are the two scalar coefficients that determine specific rates of grazing and excretion and the two exponential coefficients that describe the variation in the specific rates of grazing and excretion with the size of the zooplankton biomass. Finally, the sinking rate of the

phytoplankton, which we have set to zero in our simulations, is most important. Unfortunately, the values for most of these parameters are difficult to measure and predict.

## Benthic Routine

The benthic loading component of our model is based upon several literature citations and functions found in the existing, previously-verified DEPOMOD model (Cromey et al. 2002 a &b; Cromey, Provost, and Black 2003; Cromey and Black 2005) that in turn was based on the G-model of carbon degradation (Westrich and Bernier 1984; see also Panchang, Cheng, and Newell 1997; Brooks and Mahnken 2003). DEPOMOD is presently the international standard for assessing the impact of loading of organic carbon in sediments underlying fish farms and in some countries calculations with the code are a requirement for obtaining fish farm permits. Since DEPOMOD only addresses the transport of particulate waste from the pens to the sediments, we have written a more comprehensive environmental description of fish farms that includes waste production within the pens, transport from the pens to the sediments, and the biochemical response of the benthic community to waste deposition.

As uneaten feed and feces produced by fish in each cage sink through the water column, they are transported downstream of the cage. Since uneaten feed pellets are larger and denser than feces, the routine tracks both uneaten feed and feces. Not only will these different classes of particles sink at different rates and be transported at different distances from the farm, but also when they reach the bottom boundary layer their shear thresholds for deposition and resuspension will also differ, leading to further separation. Eventually, both uneaten feed and feces will either be consumed by the benthos or consolidated into the sediments and no longer subject to resuspension. Thus, *AquaModel* has three categories of particulate waste within the sediments, uneaten feed, feces, and consolidated waste.

## Physical Description of Deposition

As illustrated in Figure 11, we have simplified the formulation of physical processes. This was required because simulations running on a PC became too time-consuming or mathematically unstable with a more detailed formulation. For each time step the waste particles produced in the farm are "collected" as "capsules" that sink through the water column at a rate determined from measurements in the laboratory. These capsules are shown as brown dots in the figure. As these capsules sink, the ambient currents transport them through the 3-dimensional array of cells. This is somewhat analogous to water moving through an unsecured garden hose that is in continual motion but in this case is driven by variations in current velocity and direction. The waste particles are however not

subject to turbulent dispersion as is the case for the dissolved wastes. As the capsules near the bottom the waste particles are "released" and evenly distributed into the cells of the suspension layer as indicted in Figure 11. This array of cells consists of a single layer that lies immediately above the sediment surface. The length and width of these computational cells are the same dimensions as the cells within the overlying water column, but their depth is user selectable. In the case of the demonstration farm, we have chosen a depth of 1 meter. Once released into the suspension layer the particles are now treated as suspended particles and subject to both advection and turbulent dispersion.
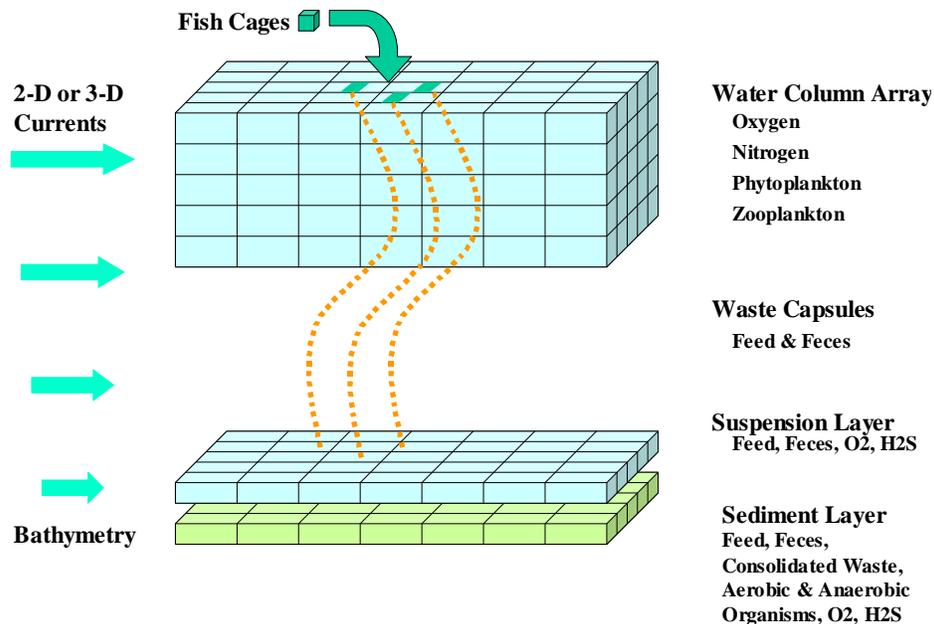


**Figure 11. The physical layout of the transport and deposition of particles in the benthic routine. Fish wastes consisting of uneaten feed and feces are transported by advection to the suspended layer that is immediately above the sediment layer. Depending upon the shear at the sediment surface waste particles within the suspended layer will either remain suspended and transported within the suspended layer or deposited in the sediments. The value of shear at the interface will also determine whether waste particles in the sediment layer will remain there or be resuspended into the suspended layer.**

Once particles reach the "suspension layer", the routine executes the formulations of DEPOMOD (Cromey et al. 2002a, 2002b) to calculate whether these particles stay in suspension and transported further from the pen or deposited in the sediments. According to these formulations, waste particles in the suspension layer are deposited into the sediment layer when shear between the sediment and the bottom water falls below a threshold value (See also Fox 1988). The rate of deposition increases with the concentration of particles in the layer and with decreases in shear. On the other hand when shear at the interface exceeds a threshold value, waste particles in the sediment layer will be resuspended into the suspension layer and thus subject to further transport and dispersion from the site. The thresholds for deposition and resuspension differ with

the size, density, and stickiness of the particles and thus will differ between feed and feces. When shear at the bottom falls between the threshold for deposition and the threshold for resuspension, the particles in the suspension layer will be remain in suspension and thus transported further from the pen. Finally, wastes deposited in the sediment will compact into organic particles that are no longer subject to resuspension. Cromey and his co-workers have derived a function for this process in which compaction begins at a given rate after a 4 day delay. We have on the other hand chosen a simple first order rate function in which a fixed fraction of the mass of feed and feces in the sediments consolidates each day.

## Biochemical Processes in the Benthic Community

The 3 types of waste found in the sediments, uneaten feed, feces, and consolidated feed and feces are to varying degrees energy and nutrient sources for the benthic community, which consist of both macroscopic and microscopic organisms. Although the compounds found in feed and feces will consist of refractive and labile fractions, we have assumed in our simulations that all compounds are labile. We feel that this is a worst case assumption. Thus, at a given time, the concentration of waste in the vicinity of a farm will depend upon the previous physical processes of deposition and resuspension as well as the previous biochemical processes of growth and remineralization by the benthos. As shown in Figure 11, we treat the sediment layer as a single layer; this is despite the fact that vertical profiles within sediments indicate sharp, predictable biological and chemical gradients. In our simulations we have chosen a depth interval of 2 cm for each cell of our sediment array. This depth was chosen because it is the standard depth for sediment monitoring (core collection) in and around fish cages in many North American jurisdictions. The length and width of these cells are the same as those within the water column and the suspension layer. Our functions provide predictions of average biological and chemical conditions within the layer.

Describing the complexity of biochemical processes within the sediments has challenged marine scientists, and the models that have been developed (including ours) are relatively crude and lack comprehensive testing. Despite these limitations, field data describing benthic responses to variations in organic loading of the sediments show clear understandable patterns, and that when tuned to local conditions models such as the pioneering G-Model of Westrich and Bernier (1984), can provide good quantitative estimates of the response. Figure 12 shows the components and processes that are described by our benthic routine. These components consist of dissolved compounds, oxygen, sulfate, hydrogen sulfide, carbon dioxide, which flow between the suspension and sediment layers by diffusion. These components also include particulate organic

carbon (POC) produced in overlying waters from farm waste or the planktonic community.  Finally, they include two communities within the benthos, the community of aerobic species that respire only oxygen and the community of anaerobic species that respire sulfate.   Although these communities consist of both macroscopic and microscopic species, it is our view that the biochemical transformations shown in Figure 12 are largely mediated by microbes.
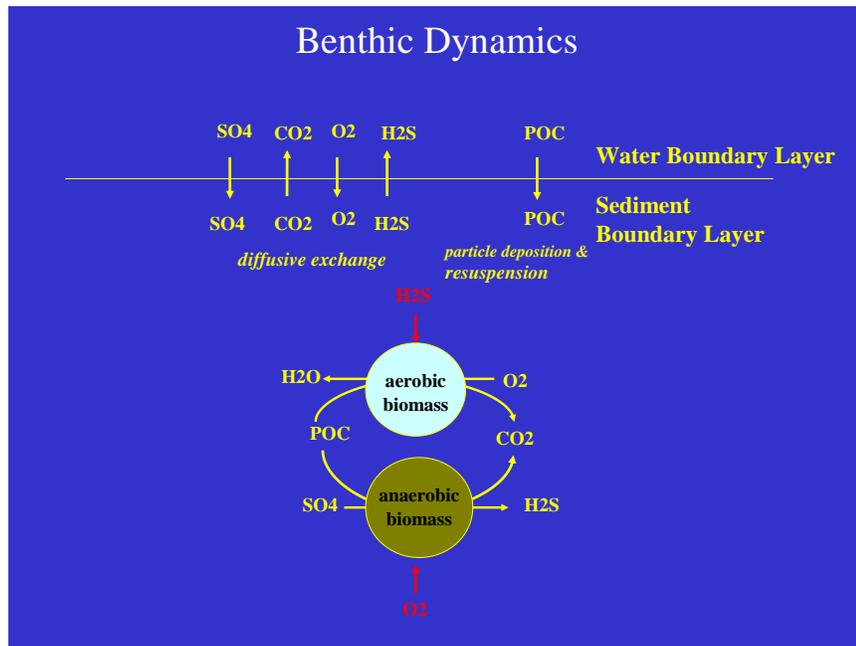


**Figure 12. The biochemical components and transformations of the benthic routine.  The transformations are mediated by two communities consisting of aerobic and anaerobic species.   These two communities compete for organic carbon supplied by particulate organic carbon (POC) produced in the farms and plankton communities in the overlying water column.  The rates of assimilation by these two communities will depend upon the supply of POC, the biomass of the two communities, and the concentration of respiratory substrates (here limited to $O_2$ & $SO_4$) and metabolic inhibitors ($O_2$ and $H_2S$) of the two communities.**

These dissolved compounds will be transported across the sediment-water interface depending upon both their diffusivity and the size of the concentration gradient at the interface. The same can be said for their transport within the sediment.   The local concentration gradient will depend upon local rates of metabolism by the benthos as well as diffusivity.   Furthermore, diffusivity itself will depend upon the porosity of the sediment, temperature, and the chemical properties of the compound.

The aerobes respire dissolves organic compounds released from the particulate organic material and oxygen in order to grow and meet other metabolic demands.  The main by-products of their metabolism are carbon dioxide and water. If either the concentration of

oxygen or POC decreases below saturating concentrations, rates of growth and respiration will decrease. Furthermore, at the lower extremes of oxygen or POC availability, aerobe growth will stop and respiration will be reduced to a basal level. The anaerobes, which here consist only of the sulfate reducing micro-organisms, respire POC and sulfate in order to grow and meet other metabolic needs. The main by-products of their metabolism are carbon dioxide and hydrogen sulfide (or other reduced sulfur compounds). If either the concentration of sulfate or POC decreases below saturating concentrations, rates of growth and respiration will decrease. Additionally, at the lower extremes of oxygen or POC growth will stop and respiration will be reduced to a basal level. If produced at a sufficient rate the hydrogen sulfide produced by anaerobes will inhibit the growth of the aerobes. On the other hand, oxygen inhibits the growth of the anaerobes.

It is clear from Figure 12 that the size and growth rate of the aerobes can be limited by the supply of oxygen from the overlying water column. In our routine the rate of supply of oxygen to the sediments is determined by the diffusion of oxygen from the suspension layer into the sediment layer, and the rate of diffusion will be determined by the difference in the concentration of oxygen in the suspension layer and the sediment layer, the thickness of the diffusion boundary layer at the interface:

$$JO2 = \frac{O2DiffCoef[temperature] * (O2\ suspended - O2sediment)}{Z[velocity]}$$

Here $JO_2$ is the flux of oxygen into the sediment layer, $O_2DiffCoef$ is the diffusion coefficient of oxygen, which varies with temperature, $O_2$suspended is the concentration of oxygen in the suspended layer, $O_2$ sediment is the concentration of oxygen in the sediment layer a, and Z is the thickness of the diffusion boundary layer, which is less than a millimeter in most open waters, and as indicated varies with the velocity of flow in the suspended layer. If the current speed in the suspension layer increases the thickness of the boundary layer will decrease and the rate of diffusion will increase. The concentration of oxygen in the sediments is in steady state such that the rate of oxygen consumption by the aerobes, which varies with the concentration of oxygen and the concentration of particulate organic carbon within the layer, is equal to the rate of oxygen supplied by diffusion.

One should note that at each of the two steady states the growth rate of the aerobic community is zero and the community's respiration rate is basal. At the higher loading rate the aerobic community is much larger, but the steady state growth rate of the community is zero because of oxygen limitation. This limitation to aerobic growth

allows the anaerobic community to grow by assimilating the flux of POC that is unassimilated by the aerobes. At the lower loading rate the aerobic community is much smaller, but the steady state growth rate of the community is zero because of the limited supply of POC. The growth of anaerobes remains check because of the high concentrations of oxygen.
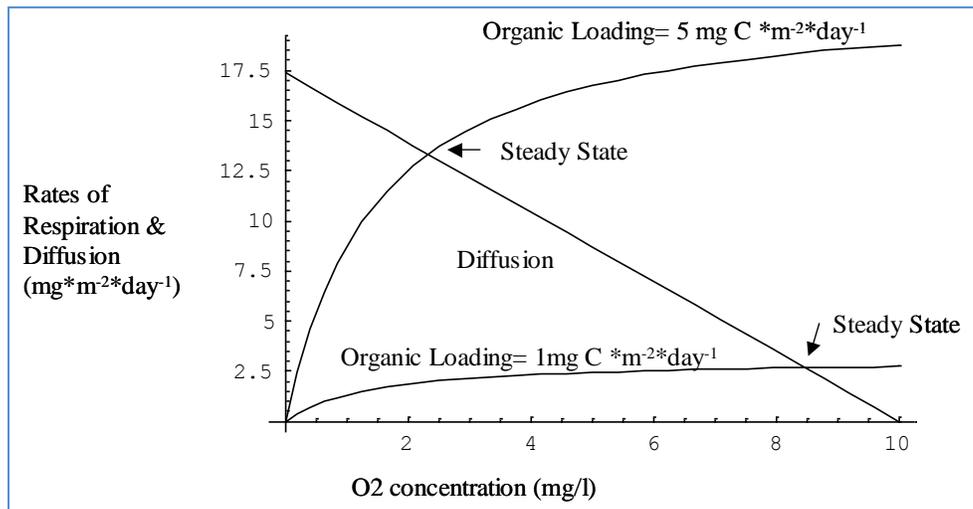


**Figure 13. An example of the calculation of the relationship between the organic loading of sediments and the concentration of interstitial oxygen in the sediment layer. The abscissa is the $O_2$ concentration in the sediment layer and the ordinate show the rate of diffuse of oxygen into the layer as well as the rate of aerobic respiration in the layer. The straight line is the steady rate of diffusion into the layer when the concentration of $O_2$ in the overlying water is 10 mg $L^{-1}$. The 2 hyperbolic curves are the rates of aerobic respiration in the sediment for rates of loading of 1 and 5 mg carbon/(m$^2$*day). The steady state conditions for the two rates are indicted by the arrow.**

A similar diagram and similar arguments can be presented for regulation by POC deposition and sulfate diffusion for the anaerobes. However, because of the high concentrations of sulfate in seawater, the rates of diffusion of sulfate into the sediments layer are sufficiently high to rarely constrain the growth rate and biomass of the anaerobic community in the upper sediments. It is clear from this diagram that increases in organic loading decreases the concentration of oxygen in the sediments, thereby releasing anaerobic organisms from their oxygen limitation of growth. As a consequence, the biomass of anaerobes will increase and possibly competing for POC with the aerobes and producing hydrogen sulfide. The latter may inhibit the metabolism and growth of the aerobes. Consequentially, if the aerobic community declines, oxygen concentrations will increase inhibiting growth of the anaerobes. Such interactions will tend to drive the system toward a well-defined steady state determined by the rate of organic loading, as well as the temperature, concentration of oxygen, and current velocity in the suspended layer above the bottom.

The differential equations that are found in the routine can be solved for steady state conditions in which the state variables of the routine are constant with time or solved during each time step of a simulation. The results of simulations for our New England and southern California studies will be shown in the sections that follow. Here we present an example of the behavior of the routine for steady state conditions. We then compare these results with field observations.

In Figure 14 we plot calculated concentrations of oxygen, hydrogen sulfide, and the biomass of aerobic and anaerobic species as a function of the rates of deposition of particulate organic carbon under conditions typical of those found under the Atlantic salmon farms of New England and British Columbia. Panels A to G show in the upper sediment layer for the concentration of aerobic biomass, anaerobic biomass, O2, particulate organic carbon (POC), and H2S, respectively. Figures F and G show calculations.

In Figure 14A we see that the concentration of aerobic biomass in the upper sediment layer increases with deposition up to a rate of about 0.3 g carbon/(m$^2$*d); above this threshold it remains constant. In Figure 14B we see that the concentration of anaerobic biomass is 0 until deposition reaches a rate of about 0.3 g carbon/(m$^2$*d); above this threshold it increases linearly (not obvious on this log-linear plot) with deposition. In Figure 14C we see that the concentration of oxygen in the upper sediment layer is decreases with increases in deposition until it reaches a value of 2.38 mg O$_2$ m$^{-3}$ at which deposition has increased to of about 0.3 g carbon/(m$^2$*d); above this threshold it remains constant. In Figure 14D we see that the concentration of POC in the sediments remains relatively constant at a value of about 270 g carbon m$^{-3}$ over the range of deposition rates. This organic carbon is almost exclusively the refractive component with little nutritive value. The labile fraction particulate carbon is assimilated by the benthos. In Figure 14E we see that the concentration of hydrogen sulfide in the upper sediment layer is 0 until deposition increases to 0.3 g carbon/(m$^2$*d); above this threshold it increases linearly with deposition (not obvious on this log-linear plot). In Figure 14F we see that the flux of O$_2$ g /(m$^2$*d) diffusing into the sediments increases with deposition until deposition reaches 0.45 g/(m$^2$*d); above this threshold it remains constant at a value of 50 g O$_2$/(m$^2$*d).

Unfortunately, although there are abundant measurements of the concentration of organic carbon under fish farms, there have been very few direct measurements of the daily deposition of waste carbon. There are even fewer such measurements that have been supplemented by measurements of current velocity, the biomass of the communities of aerobic and anaerobic organisms, and concentrations and fluxes of oxygen, hydrogen sulfide, and carbon dioxide. The studies of Findlay and Watling (1997) and Chamberlin and Stucchi (2007) are not only comprehensive but also praiseworthy, and in fact the

work of Findlay, Watling and co-workers has helped guide development of the benthic routine. In 1991 Findlay and Watling undertook a comprehensive study during summer grow-out of the benthic community beneath an Atlantic salmon farm off Swans Island, Maine (Findlay, Watling, and Meyer 1995; Findlay and Watling 1997). This study is important because it clear demonstrated that there is a critical threshold rate of waste deposition that determines the biochemical response of the benthic community. If rates of deposition are below this threshold the rate of growth and respiration of the community is sufficient to remineralize most if not all of the particulate organic material reaching the sediments.

In short, below this threshold a steady state appears to be established in which the rates of organic carbon deposition are matched by the rates of release of respired carbon dioxide; neither organic waste nor biomass of the benthos will increase significantly. Above this threshold, this balance is lost and the rates of carbon dioxide release are much lower than the rates of organic carbon deposition. This imbalance appeared to reflect an increase in the biomass of the benthos and possibly an accumulation of waste carbon.

Figure 15 summarizes their field measurements of organic deposition, CO2 flux from sediments, and O2 flux into sediments. The left graph shows the flux of particulate organic carbon to the sediments beneath the farm and the rate of CO2 release from sediment cores incubated in the laboratory. At loading rates of less than 400 mmoles m-2*day carbon deposition is roughly equal to respiration. The single point above this threshold indicates a net accumulation of organic carbon beneath the farm.
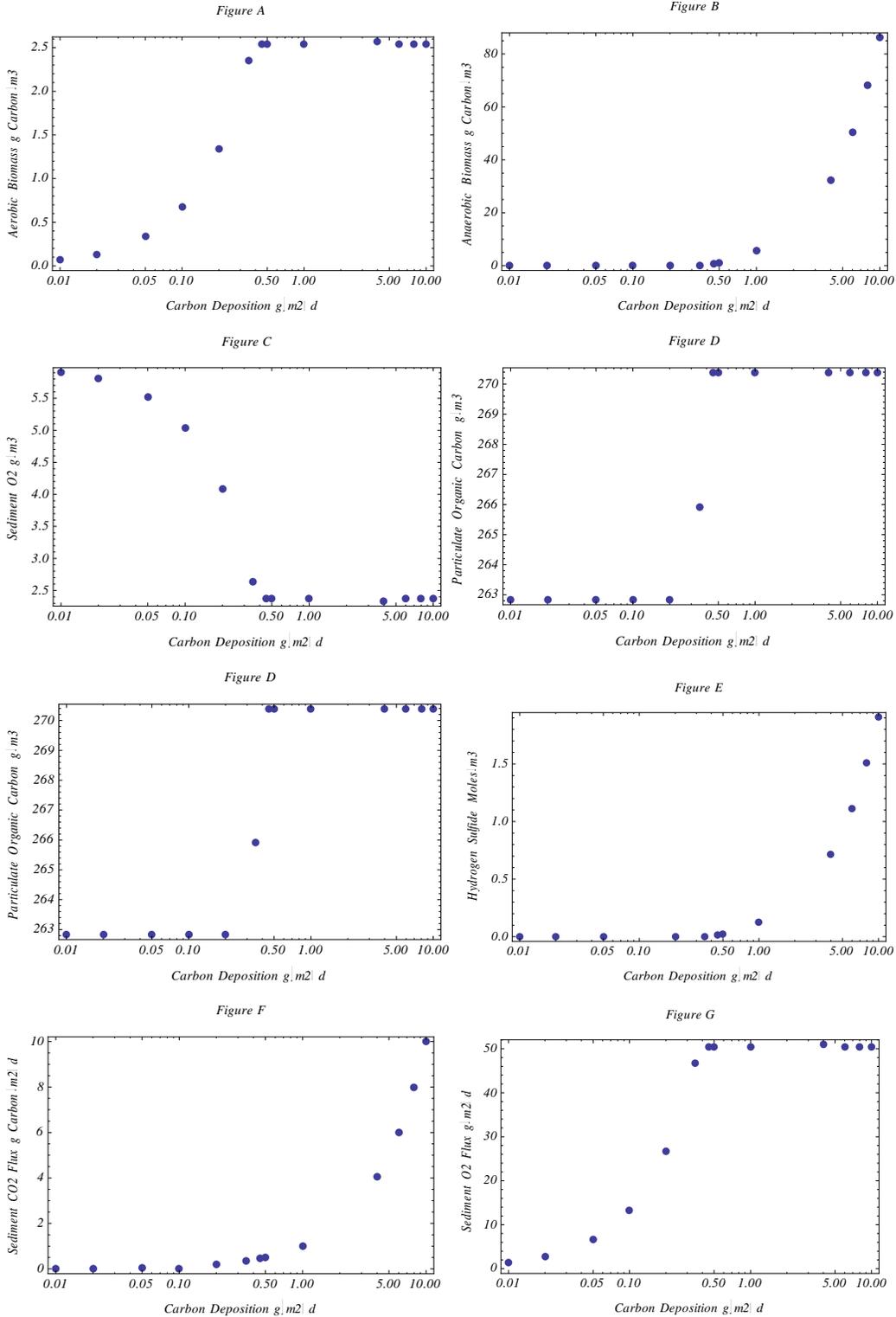
**Figure 14. Steady state solutions of the benthic routine. Benthic community response to changes in particulate carbon deposition plotted under conditions common to the sediments in Atlantic salmon farms. of the flux of CO2 out and O2 into the sediments over the range of deposition.**
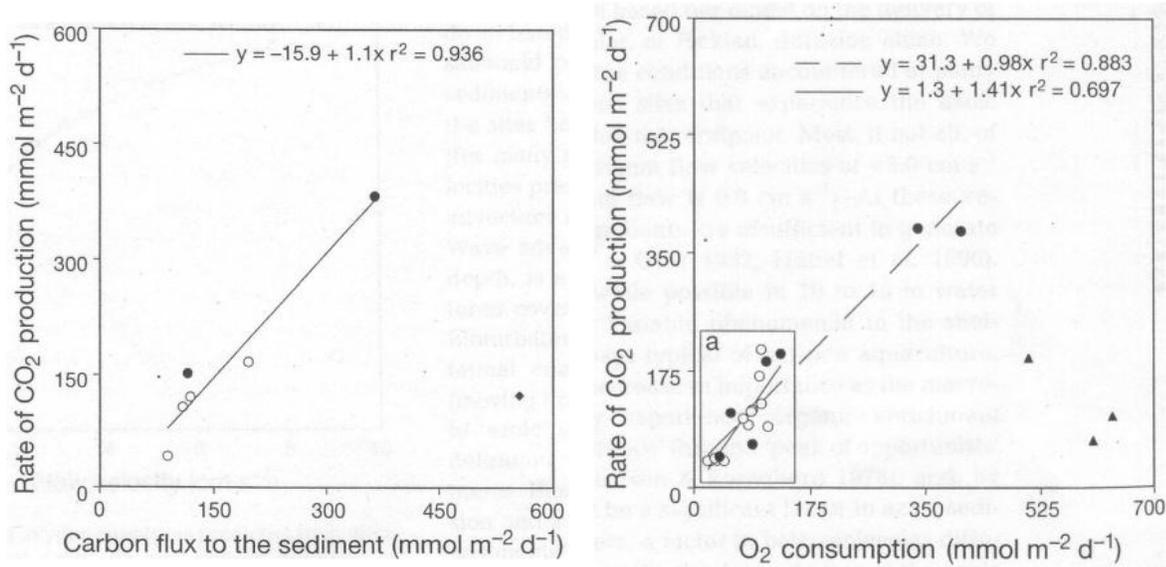
**Figure 15. Field measurements of organic deposition, $CO_2$ flux from sediments, and $O_2$ flux into sediments collected during the growing season at an Atlantic salmon farm off Swans Island, Maine. The left graph shows the flux of particulate organic carbon to the sediments beneath the farm and the rate of $CO_2$ release from sediment cores incubated in the laboratory. The right graph shows the respiratory stoichiometry of $CO_2$ to $O_2$ of sediment cores sampled during the growing season (Findlay and Watling 1997).**

The right graph of Figure 15 shows the respiratory stoichiometry of CO2 to O2 of sediment cores sampled during the growing season. The expected ratio of 1.4 fell rapidly as rates of deposition exceeded the deposition threshold of than 400 mmoles carbon m-2*day. This imbalance coincided with the sudden appearance and rapid growth of *Beggiatoa*, a Proteobacteria, that not only respires sulfide and oxygen but also fixes $CO_2$. Although itself a chemolithoautotroph, this species is key indicator of the development of a dominant anaerobic benthos. Its presence as a dense mat at the sediment surface explains both the drop in $CO_2$ release. The disappearance of respiratory stoichiometry for $CO_2/O_2$ may be explained by the onset of both anaerobic and chemioautrophic metabolisms.

Although the scales abscissa of Figure 14 is logarithmic and that of Figure 15 is linear, a careful comparison of the two figures indicates that general features of our benthic routine fits well with these field data. An examination of Figures 14F and 14G show calculated rates of $CO_2$ release and $O_2$ assimilation as functions of organic deposition. In Figure 14F one sees that the benthic routine predicts that the respiratory release of $CO_2$ by aerobes at low rates of deposition combined with respiratory release of $CO_2$ by anaerobes at high rates of deposition will balance rates of carbon deposition over a broad

range of deposition rates. We propose as do the authors that the presence of a threshold deposition at 400 mmoles carbon m$^{-2}$*day is set by the appearance and growth of *Beggiatoa* when the rates of production of hydrogen sulfide by anaerobes is sufficient to support colonization by this species. With the addition of a 3$^{rd}$ benthic component consisting of sulfide oxidizing autotrophs to our routine, such a threshold will emerge.

In Figure 14G one sees that O$_2$ assimilation matches rates of carbon deposition up to a deposition threshold of 0.5 g carbon m$^{-2}$*day or 42 mmoles carbon m$^{-2}$*day; above this threshold the rate of O$_2$ assimilation is fixed and no longer matches the increased rates of deposition. This is about 10-fold lower than the threshold measured in the study. Although large, this difference may be easily by a the differences between calculated and field variables such as the oxygen concentration of water at the sediment interface, the bottom current speed, the porosity of the sediments, and the biomass of epibenthic aerobic species. We also note that the benthic routine was not tuned to the Swan Island study and adjustments in the values for several coefficients would certainly much improve quantitative predictions.

More recently Chamberlin and Stucchi (2007) have assembled time series field data on sediment conditions including concentrations of organic carbon and sulfide concentration, currents, and waste production at an Atlantic salmon farm in British Columbia. Simulations with DEPOMOD provided them with a corresponding time series of deposition rates beneath the farm which they then compared to their field measurements. Figure 16, which is one of their most interesting results, shows the relationship between sulfide concentration and organic carbon deposition. Their log-linear plot can be directly compared to the benthic routine's predictions shown in Figure 14E. The fit is good despite the fact that there was no tuning of the routine.

Because we have not yet obtained a comprehensive and diverse dataset on the benthic impact of fish farms, we have not been able to test the accuracy of our benthic routine much beyond the comparisons shown in Figures 14-16. However, during the development of the benthic routine and its initial runs, we have been able to identify those environmental and mathematical parameters whose variation most influences the benthos.
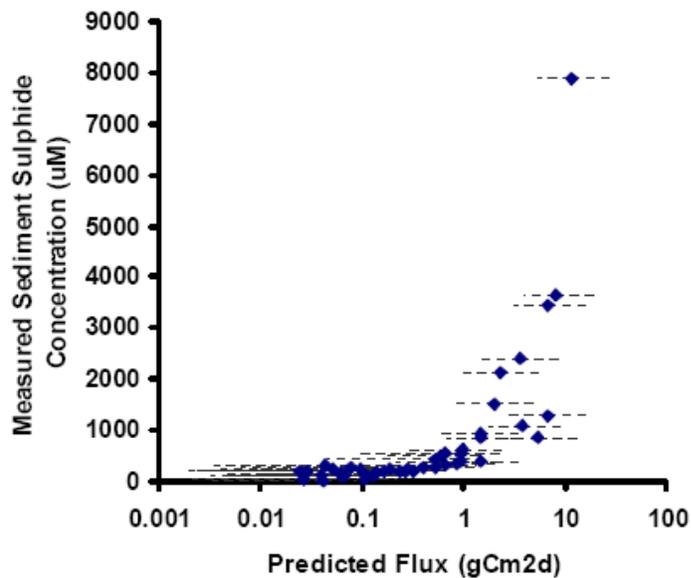
**Figure 16. Field measurements of sulfide concentration in sediments and organic loading of sediments calculated with DEPOMOD under salmon farms in British Columbia (Chamberlin and Stucchi, 2007). The increase in sulfide concentration with deposition is an indication of increases of total metabolism of anaerobes in the surficial sediment layer. Comparisons of such field data with predictions by our benthic routine shown in Figure 14 indicate good agreement.**

The most important physical parameters are the areal rate of waste production by the farm (in units of g waste $m^{-2}$ $day^{-1}$), current speeds throughout the water column and particularly the bottom layer, the depth of the water column, the oxygen concentration and temperature in the bottom layer, and the porosity of the sediments. The most important biochemical parameters are the values for threshold for deposition, erosion, and resuspension, the maximum specific assimilation rates of particulate organic carbon for aerobes and anaerobes, the half saturation constant for oxygenic respiration, and the half saturation constant for oxygen inhibition of anaerobic respiration.

This relatively long list of key parameters indicates that there is no fixed "short list" of critical variables that can be applied to fish farms of differing sizes and locations. According to our routine, the dynamics of the benthic community is highly nonlinear because of thresholds and fundamental nonlinearities in the response of benthic species to the concentration of diverse electron donors and acceptors as well as their response to metabolic inhibitors. Because of this complexity we propose that accurate predictions of impact will require computations with models such as our benthic routine that have been tuned and validated.

# SBIR Project Accomplishments

As stated in the executive summary, we have completed the six tasks found in our Phase II SBIR proposal that is discussed below.

## Task 1. Development of broad-scale, 3-dimensional coastal flow system to couple *AquaModel* to existing coastal circulation models

During this project we added new interfaces that allow the *AquaModel* simulation to incorporate output from detailed bathymetry as well as complex coastal circulation models. The detailed bathymetry combined with 3-dimensional ocean current data allows the *AquaModel* to accurately track the movement of uneaten feed and fish feces as it sinks through the water column so that *AquaModel* can determine whether such waste is deposited near the mariculture site or transported away from the site by water column or bottom currents. Accurate tracking of waste is the most important factor in determining the environmental impact of open ocean fish farms, and is even more important that nearshore aquaculture locations that may be predictably driven by repeating tidal cycle-forced currents.

*AquaModel* can display coastline data from several different sources including World Data Bank (WDB-II), World Vector Shoreline (WVS), or from ArcShape files. For this project we used World Vector Shoreline because it is relatively detailed (1:250000). WVS is provided by NOAA National Geophysical Data Center. The raw data however, consists of a series of disconnected line segments that are suitable only for an outline display of land masses. A filled shoreline such as that shown in Figure 17 requires that line segments are first connected into ordered polygons. EASy includes an interactive tool that provides this capability.
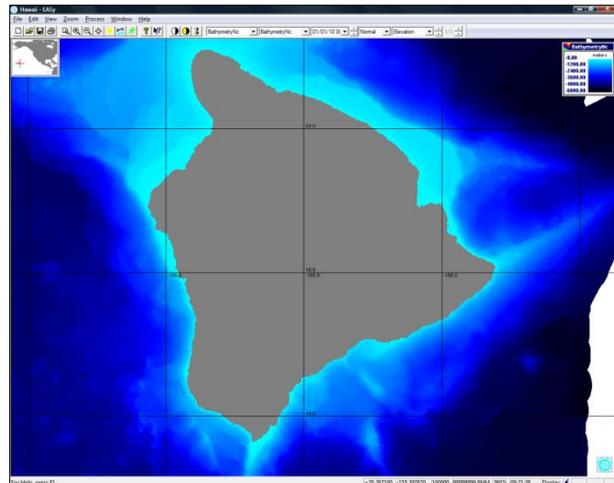


**Figure 17. *AquaModel* uses detailed bathymetry to determine the spatial distribution of where farm waste products are deposited.**

The new version of *AquaModel* utilizes detailed bathymetry shown in Figure 17 to define the depth of the water column at each grid cell location. Prior versions were restricted to a uniform grid where the

ocean bottom was modeled as flat and level. Waste products transported by ocean currents may travel further from a farm site if the bottom depth is deeper. Modeling of an uneven bottom depth therefore provides for a more assessment of the distribution of farm waste products.

In addition to measured current meter data, *AquaModel* now interfaces with three types of modeled 3-dimensional ocean curent data. This detailed data provides a basis for analyzing the effects of convergent and divergent current flows as well as eddy circulation. The new program feature addresses the problem of matching differences in temporal and spatial resolution between the circulation model output and that used by *AquaModel* to simulation the processes of waste production, waste transport, and the biological transformations of the waste.

The first circulation model that we interfaced with *AquaModel* was the NASA Jet Propulsion Laboratory ROMS (Regional Ocean Modeling System). This model computes 3-dimensional current vectors for specific regions. We accessed current data for the Southern California Bight region with ocean current data with a temporal resolution of 3 hours and a spatial resolution of 2 kilometers. This data was used to run simulations of a proposed open ocean experimental farm near San Diego as shown in Figure 18.
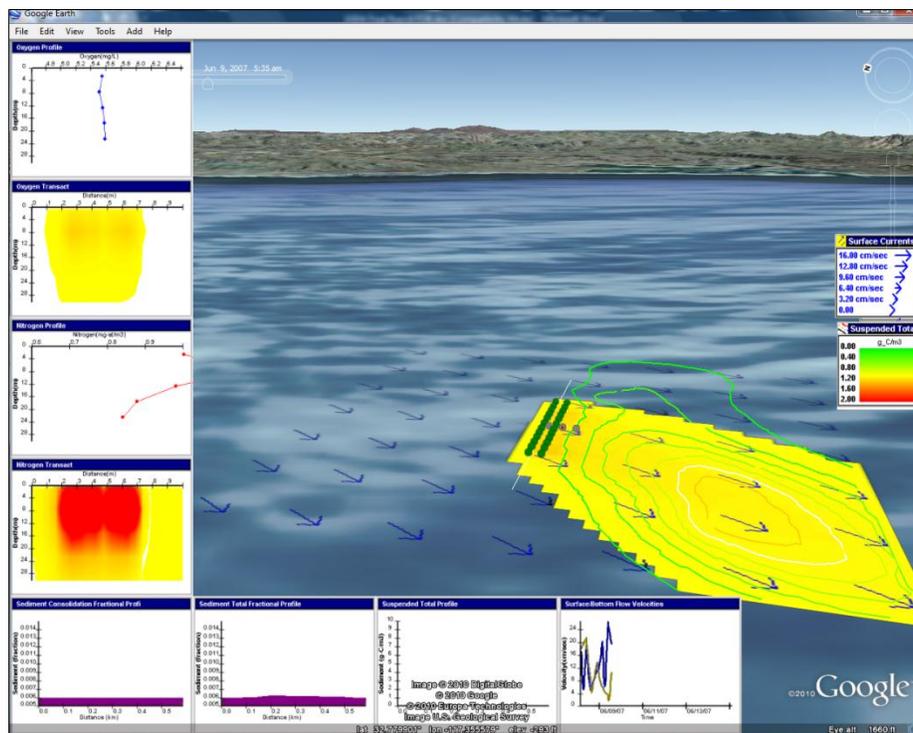


**Figure 18. Using NASA JPL's ROMS 3-D current data the *AquaModel* was used to simulate a proposed mariculture farm near San Diego, California.**

Although the ROMS data are relatively high resolution, it is only available for relatively few geographic regions. To evaluate mariculture farms in other geographic regions, we added an interface to the NASA JPL ECCO2 model. This model produces current data worldwide with a temporal resolution of 6 hours and a spatial resolution of 25 kilometers. In addition to 3-dimensional flow field, the ECCO2 model also outputs predicted temperature, and salinity. This is useful since temperature is another parameter that is critical in determining the environmental impact of mariculture operations. Figure 19 shows an example of ECCO2 surface velocity vectors.
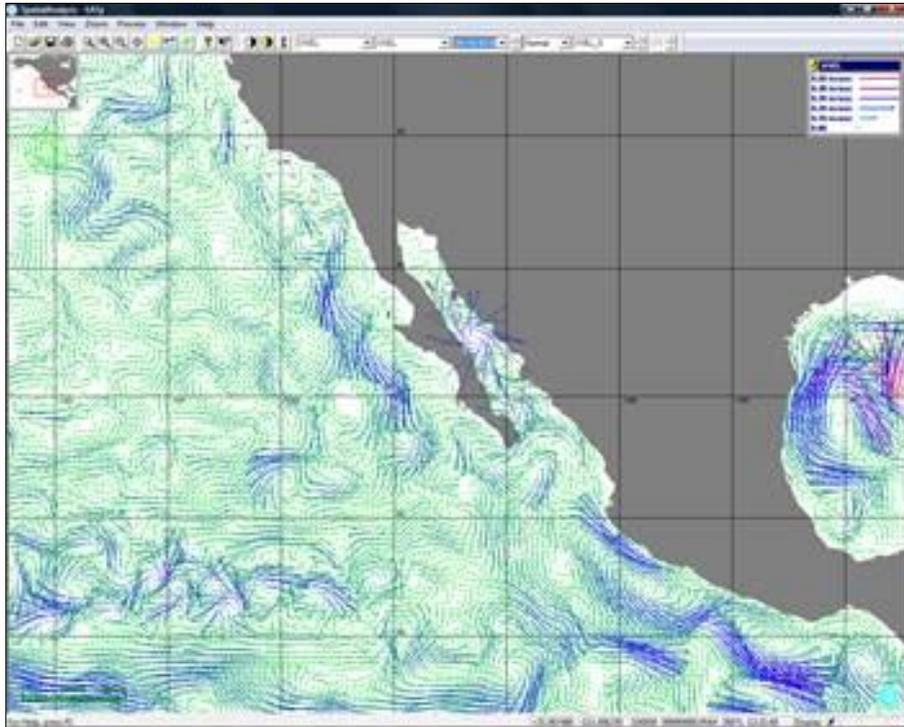


**Figure 19. The NASA JPL ECCO2 model current data allows *AquaModel* to evaluate the environmental impact of mariculture operations anywhere in the world.**

For the Hawai'i Department of Agriculture information system we interfaced the *AquaModel* with the University of Hawai'i ocean circulation model. This model creates a detailed ocean current data shown in Figure 20 around individual Hawai'ian Islands with a temporal resolution of one hour and a spatial resolution of one kilometer.
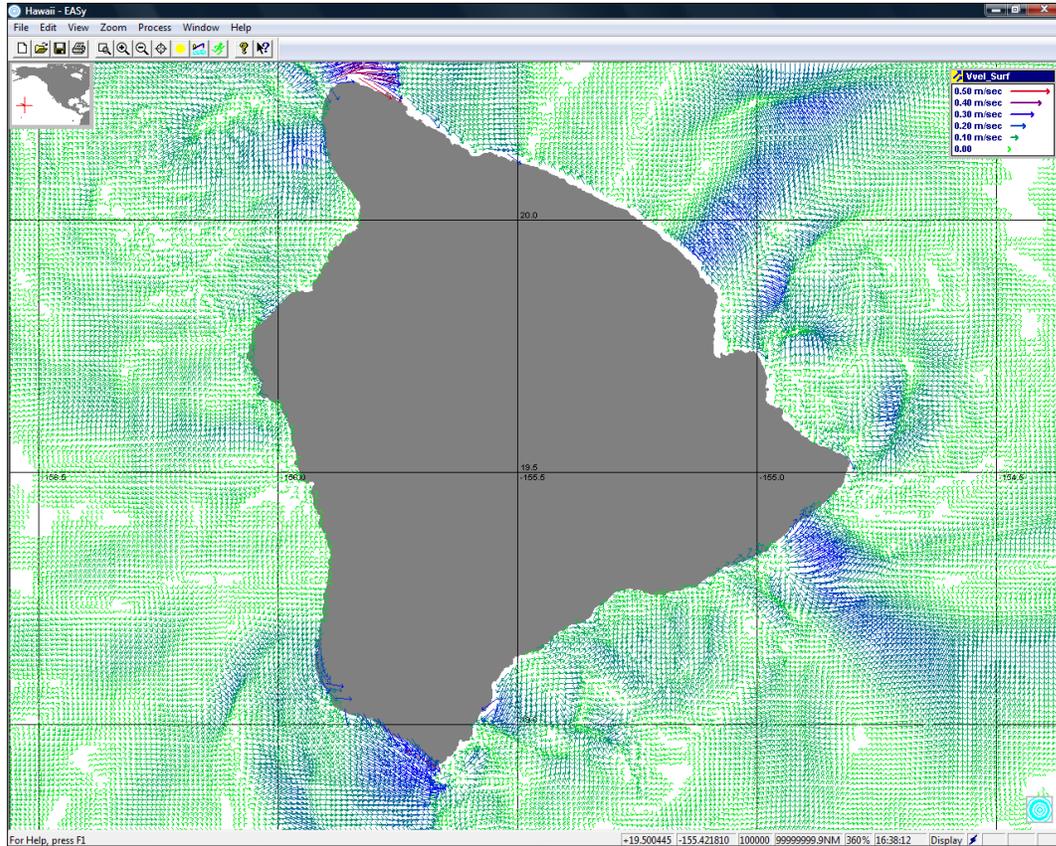
**Figure 20. The University of Hawai'i ocean current data provides detailed information that *AquaModel* can use to evaluate proposed mariculture sites.**

Finally for this task, we improved the *AquaModel* simulation replay capability so that the user can now skip forward or backward to display results at any specified simulation time. Prior versions provided for capturing and replaying of simulation results, but the replay was restricted to a sequential display of simulation results starting at the beginning of the simulated period. While this replay mode progressed about six times faster than the original simulation, it still took a significant period of time to progress to the end of long simulation run. Using the new simulation replay capability the user can immediately skip to the end or to any other point of the simulation period by either moving the red line in the time bar with the mouse or by entering a 'current' date/time as shown in Figure 21. The new capability also allows the user to play the simulation forward or backward from any selected point as well as to adjust the simulation replay time step. These features allow the user to more easily investigate the dynamic nature of the environmental impact of mariculture farms such as seasonal changes.
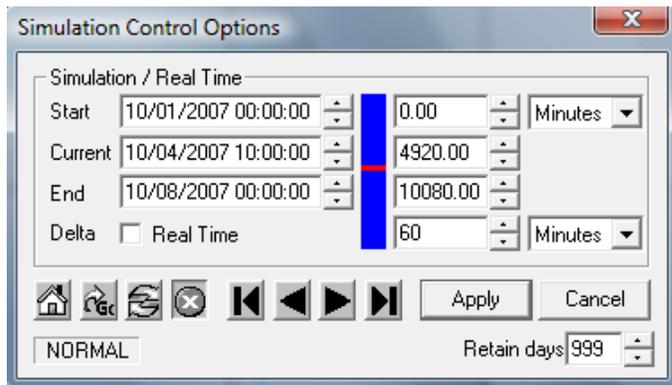
**Figure 21. The new simulation control panel allows the user to skip to any point in a previously captured simulation and to play the simulation either forward or backward.**

## Task 2. Develop contouring and statistics routines into *AquaModel* in order to better summarize the environmental effects of fish farms

We added a capability to contour any user-selected simulation variable. The program now provides the ability to view patterns in the distribution of farm wastes as either false color raster images or as contours. This capability also allows the user to compare the spatial distribution of two variables by viewing one as a false color image overlaid by a second displayed as a contour. Figure 22 shows an example of surface oxygen overlaid by the distribution of surface nitrogen.
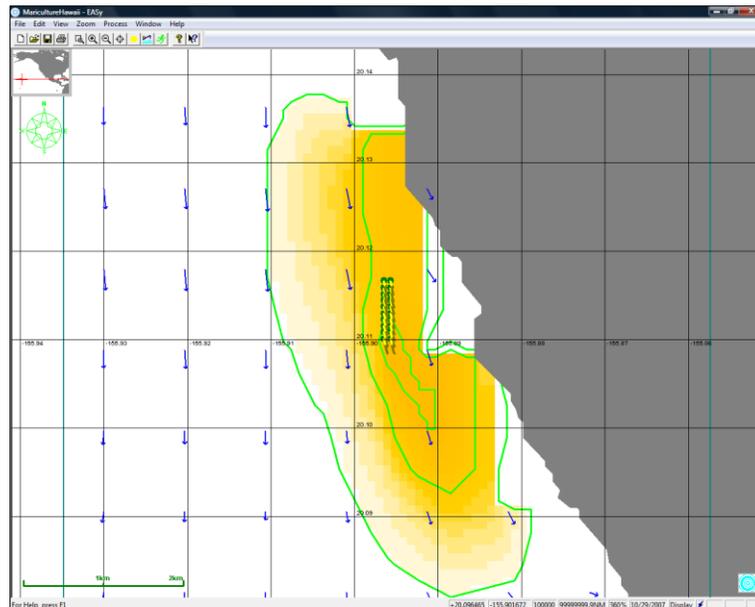


**Figure 22. The new contouring tool allows the user to view the relationship between two spatial distributions such as surface oxygen (false color image) overlaid by surface nitrogen (contours).**

*AquaModel: Software for Sustainable Development of Open Ocean Fish Farms* 35

We also added a capability to calculate statistics for a user selected window of any selected spatial image. This tool displays the selected window height, width, and area as well as the number of valid pixels within the selected window, the pixel minimum and maximum values, the mean, and standard deviation. It also displays a 3-dimensional perspective view of the selected region. Figure 23 shows an example of the computed statistics for a selected region (red box) of the oxygen false color image. The statistics tool exports pixel values in the selected region as well as the calculated statistics for off-line analysis.
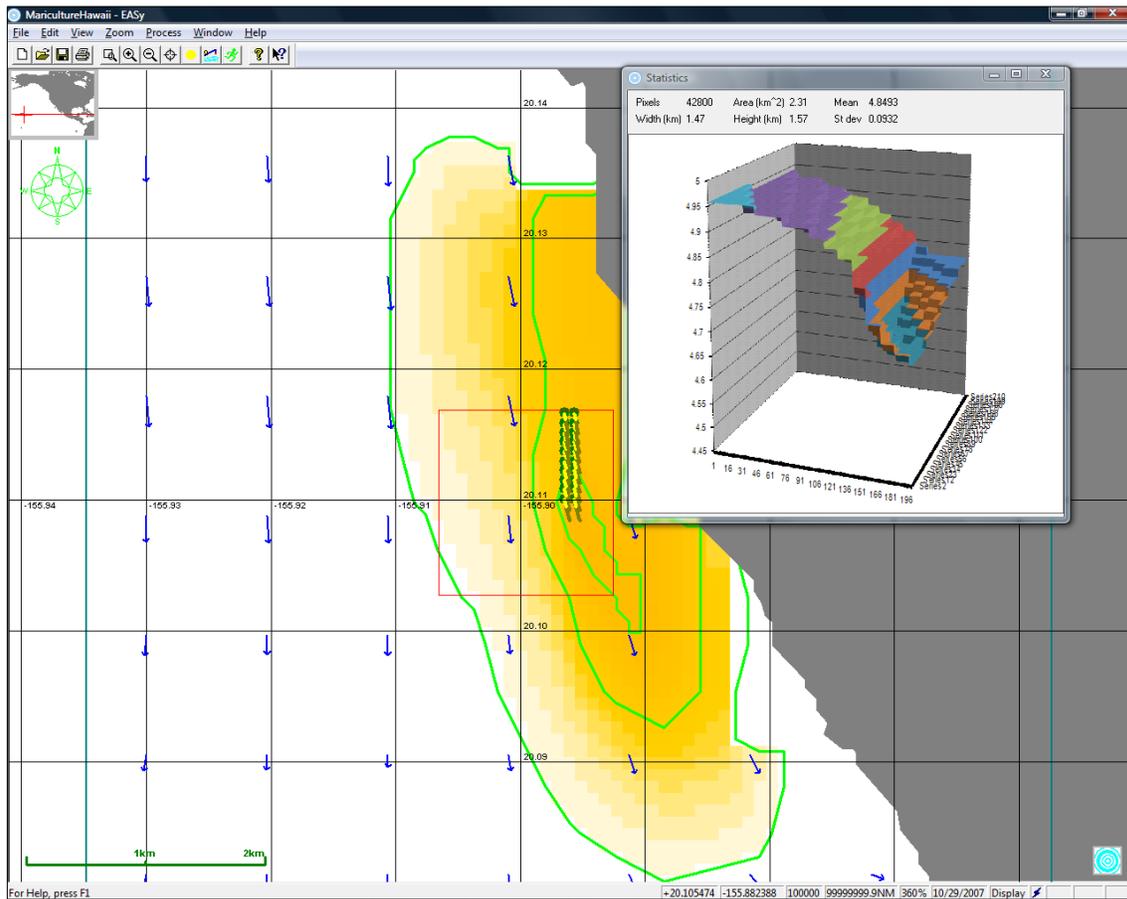


**Figure 23. Image statistics for a user selected regions provide for rapid analysis of critical oceanographic properties.**

# Task 3.  Provide computer code to accelerate simulations of sediment waste deposition and resuspension.

We have increased the speed of computations by a factor of four by re-designing *AquaModel* to operate in three separate modes:

- The transport and ecological transformations of both dissolved (oxygen depletion and nitrogenous enrichment within the water column) and particulate wastes (organic carbon of uneaten feed and feces)

- The transport and ecological fate of the dissolved wastes alone

- The transport and ecological fate within the sediments of the particulate wastes.

The speed at which each of the 3 simulations runs depends on the time step of the calculations and the size of the 3-dimensional, computational grid. Generally a 1 month simulation for both dissolved and particulate wastes requires about 3 hours on a modern PC. Thus, a simulation of 1 year will require about 36 hours. Usually 12 to 18 month simulations are required to evaluate the response of the benthic community to organic loading and to determine if seasonal changes in farm operations and environmental conditions are significant.  We acknowledge that the new computations for dissolve and particulate wastes alone are still time consuming, and we hope to make additional improvements as we continue to improve *AquaModel*. Such improvements are easily achieved by embedding code in modern graphic boards, for example, that can speed up the routines by an order of magnitude or two.

# Task 4.  Complete testing of an improved benthic dynamics subroutine.

Design and implementation of the benthic routine is now complete. *AquaModel* now provides a detailed and comprehensive description of the fate of uneaten feed and fish feces deposited in the sediments beneath the farms.   Other methods for computing sediment loading from farm wastes provide general calculations that are limited to the aerobic remineralization of carbon and the associated consumption of oxygen.   As discussed below, our implementation expands this description to include changes in the relative abundance of aerobic and anaerobic organisms, the remineralization of waste carbon by anaerobic organisms that respire sulfate (rather than oxygen), and the production of hydrogen sulfide by the anaerobes.  A fraction of hydrogen sulfide is toxic in marine water and it is a key indicator of excess loading by farms.  It is commonly used

to monitor fish farm environmental compliance through the measurement of free sulfide. *AquaModel* calculates total sulfide, a measure which can be related to free sulfide.

The development of the benthic routine is an important accomplishment of this project. The benthic routine addresses the question of whether the deposition of organic waste in the vicinity of the farm will adversely affect the taxonomic composition of the benthic community and the fluxes of oxygen and hydrogen sulfide between the sediments and overlying waters. The physical processes of the routine consist of the transport of fish feces and uneaten feed to the bottom and their deposition and consolidation. The bio-chemical processes consist of the growth of aerobic and anaerobic taxa of the benthic community as determined by increased rates of organic deposition beneath the pens. Such growth will increase the demand for oxygen and potentially to the depletion of oxygen and production of hydrogen sulfide.

To run *AquaModel* the user first identifies the sources of environmental data including bathymetry, ocean currents, and environmental conditions such as water temperature, wind speed, ambient oxygen, ambient nitrogen, ambient phytoplankton, ambient zooplankton, mixed layer depth, and average daily irradiance. *AquaModel* provides a flexibility set of options for entering each type of data. Bathymetry can be specified by an ASCII file of depth measurements, by a set of vector contours, or by a raster image. Ocean currents can be specified by a time series of current meter measurements or by a time series of 3-dimensional vectors. Environmental conditions can be specified by entering static constants into *AquaModel* or by specifying one or more Excel files that include time series data for measured values. An example of this time series data is shown in Figure 24.

The user interface for specifying sources of ambient time series data, bathymetry, and ocean currents is shown in Figure 25. This interface also allows the user to scale the available ocean current vectors to evaluate a range of extreme current conditions. It also provides a capability to merge measured ocean current data with 3-D modeled tidal current data to account for global ocean currents and/or weather conditions.

**Figure 24. Ocean currents and other measured properties can be used to describe ocean conditions around the specified farm pens.**
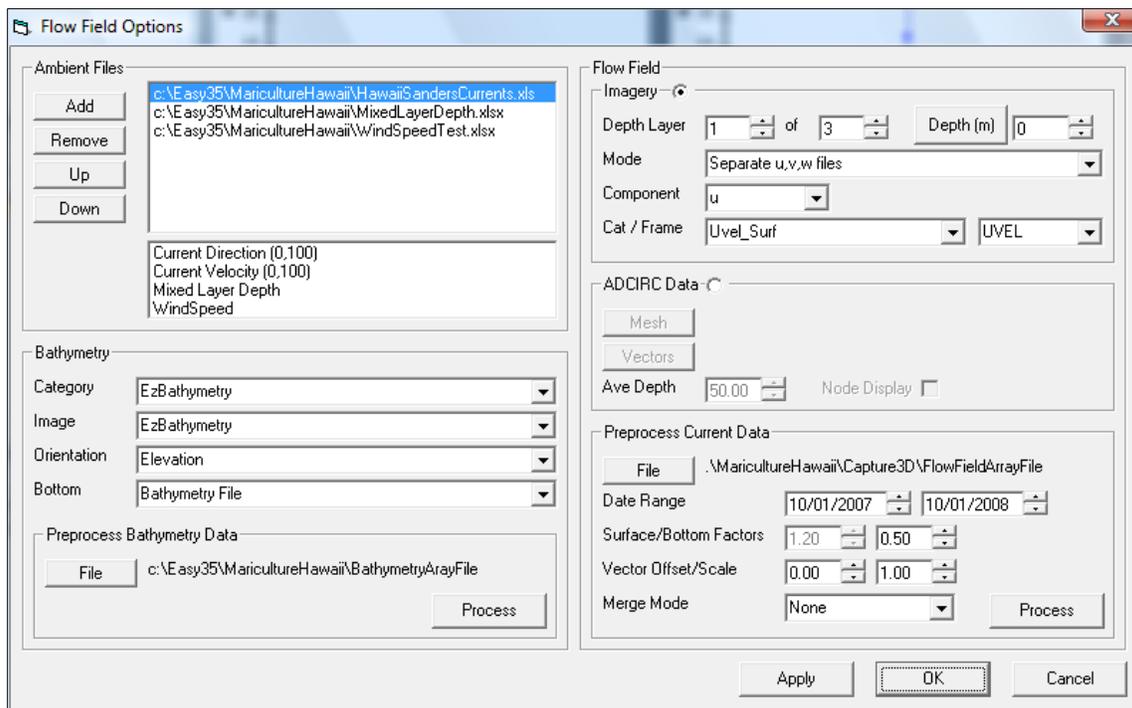


**Figure 25.** *AquaModel* **provides flexible options for entering both static and time series environmental data.**

Static environmental conditions are entered within the 'Conditions' tab of the graphic user interface shown in Figure 26. These conditions include water temperature, average daily irradiance, mixed layer depth, and nominal wind speed for winter and summer, diffusion coefficients, tidal period and maximum tidal velocity, and ambient oxygen, nitrogen, phytoplankton, and zooplankton. It also includes parameters that are used to

*AquaModel: Software for Sustainable Development of Open Ocean Fish Farms*     39

tune the program's plankton model to local normal ambient and plume conditions. These static parameters are superseded by measured time-series data if it is provided by the user.

**Figure 26. Static environmental conditions can be used to simulate farm operations if more detailed time series or ocean current data are unavailable.**
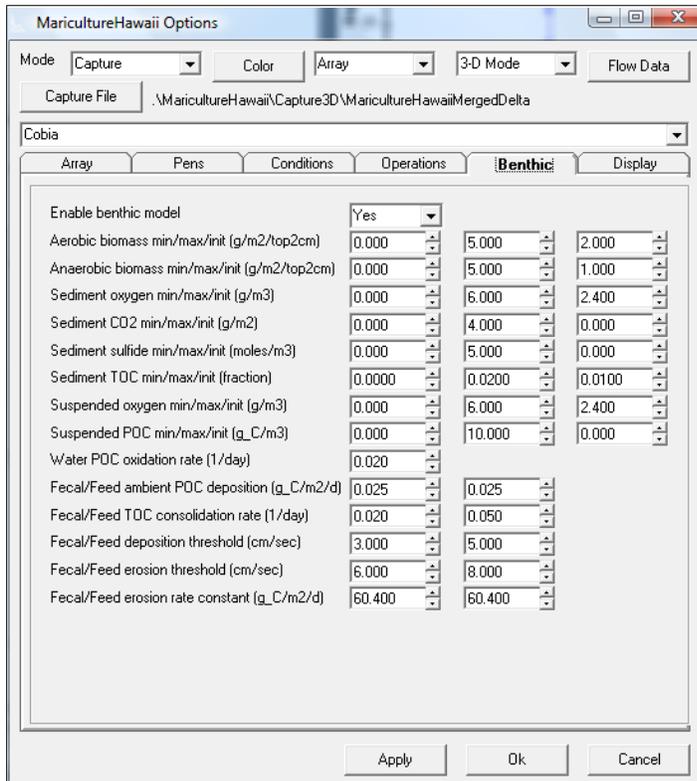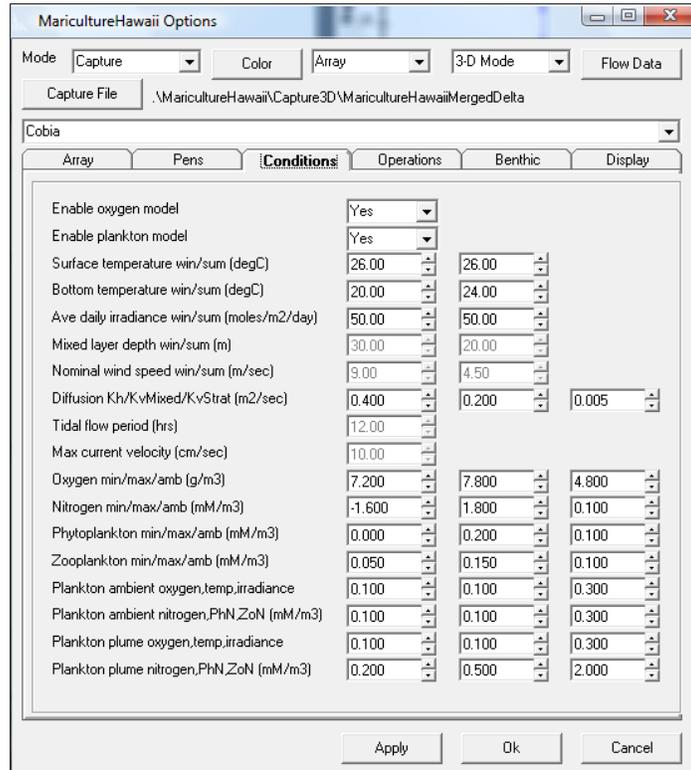




**Figure 27. Sediment and suspended layer parameters define how waste materials effect the environment after they reach the ocean bottom.**

*AquaModel: Software for Sustainable Development of Open Ocean Fish Farms*     40

Sediment and suspended layer conditions are specified by the 'Benthic' tab of the graphic user interface shown in Figure 27. Sediment conditions include minimum, maximum, and initial values for aerobic and anaerobic biomass, sediment oxygen, $CO_2$, sulfide, and TOC. The suspended layer is the layer of water just above the sediment. This layer is the source of ambient oxygen that is diffused into the sediment. It also transports and diffuses suspended materials along with the bottom currents. Suspended layer parameters include minimum maximum and initial values for oxygen and POC. Finally, this tab defines feed and fecal deposition, consolidation, and erosion rates and thresholds.

The *AquaModel* analysis array is specified by the 'Array' tab of the graphical user interface shown in Figure 28. This tab defines the center and orientation of the analysis array, the array size and resolution, and the default bottom depth. The results of a simulation run are displayed as false color images, contours, and profile plots. In addition, *AquaModel* creates an Excel export file that contains a time series of calculated simulation values that can be used for post simulation offline analysis. The 'Array' tab includes three user specifiable analysis array locations. Calculated values for these capture array cells will be appended to the standard values in the Excel export file.
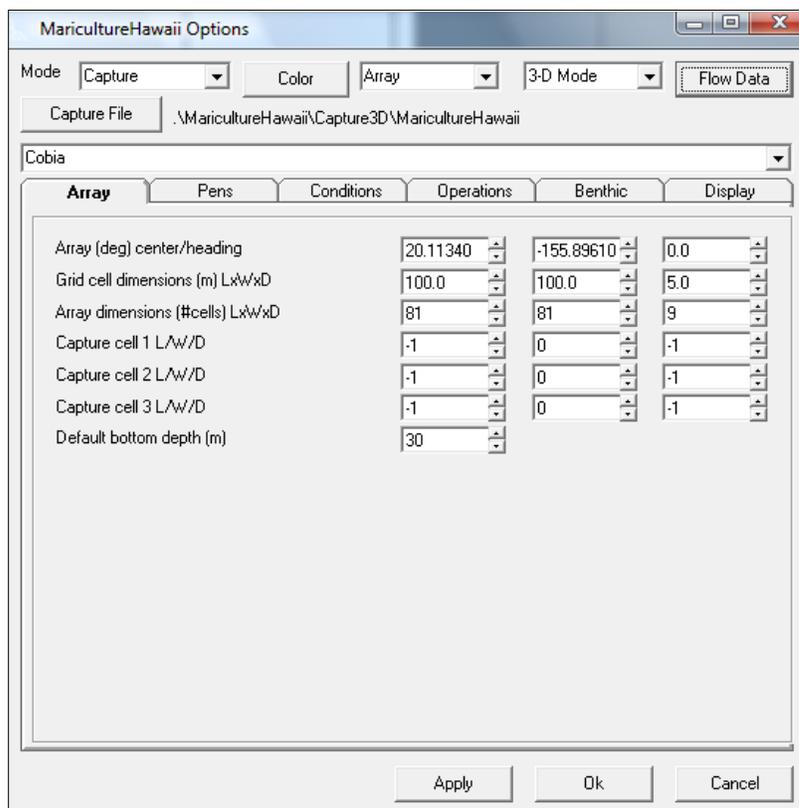


**Figure 28. The analysis area of interest is specified by a geographic location, array orientation, size, and resolution.**

The simulated mariculture farm pens are specified with the 'Pens' tab of the graphical user interface shown in Figure 29. The location size of each individual pen is specified

along with the fish species, initial fish weight, and fish density. Pens must be located within the analysis array. While each pen must contain only one species, separate specified pens may contain different species. The user may specify as many as 99 pens although this limit could be easily increased to any practical limit. Each specified pens are simulated as a separate entity so it may represent either an individual pen for a single mariculture farm or the effect of multiple pens for a number of farms.
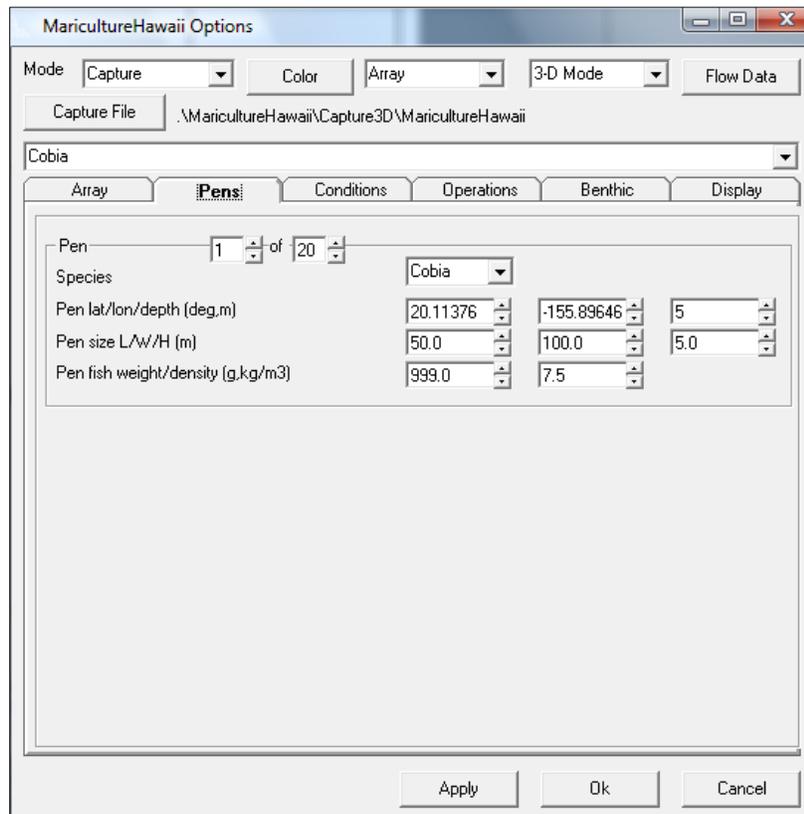


**Figure 29. Net pens or multiple farms are modeled as independent interties with separate geographic locations. The pens may also be of different sizes and may contain different fish densities or species.**

Farm operational parameters are specified with the 'Operations' tab of the graphical user interface shown in Figure 30. The pen feed rate parameters and initial pen oxygen and nitrogen concentrations are specified along with feed and fecal settling rates. The specified minimum and maximum growth rates are used only to control the profile plot range of values.
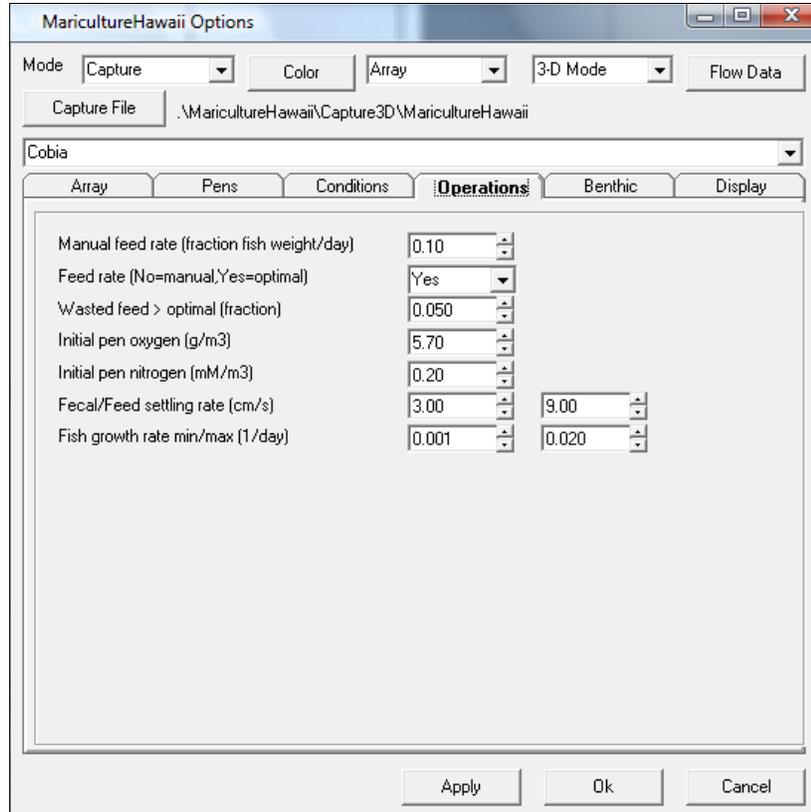
**Figure 30. The operational parameters provide a capability to evaluate various farm operating scenarios including the effect of altering feed rates.**

*AquaModel* display options are specified with the 'Display' tab of the graphical user interface shown in Figure 31. These options are used in conjunction with EASy display options to control the display of array grid cells, contours, ocean current vectors, and POC waste tracks. They also specify a mouse selection mode that determines if a left mouse double click event will display detailed pen or POC track values or will be used to identify the drill point user for profile plots.

Program operation and display parameters are located at top of the graphical user interface dialog box. These include the program mode (Display, Normal, Capture, or Replay), the ocean current vector type (2-D or 3-D), and the capture file folder. Finally, the 'Color' button allows the user to change the color of selected display items including the computational array boundary, current vectors, feed and fecal streams.
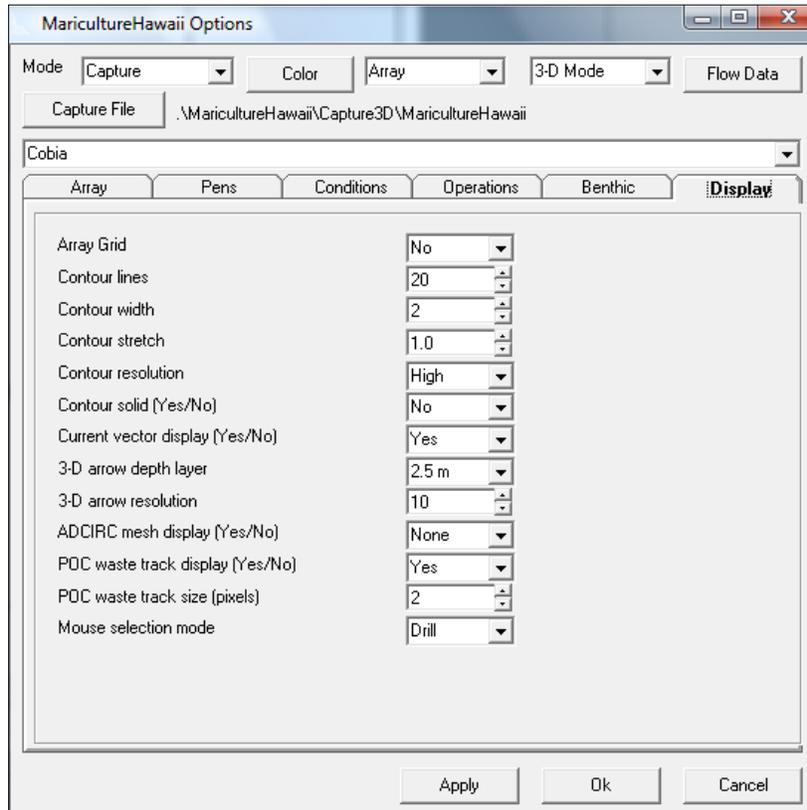
**Figure 31.** *AquaModel* **and EASy display parameters allow the user to tailor false color images, contours, and profile plots to evaluate the results of a simulation run.**

The EASy graphical user interface provides additional display parameters including the selection of false color images, current vectors, contours, and profile plots and associated color and size display settings. The 'Browse Images' toolbar shown in Figure 32 is used to select the false color or satellite image that is displayed in the main graphic window prior to the beginning of the simulation. During the simulation the graphic image is controlled by the 'Images' tab of the 'Data Graphics' dialog box as described below.
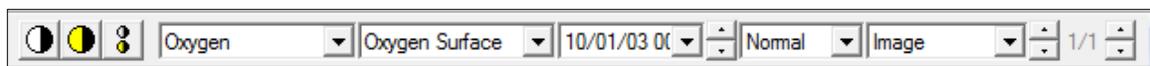


**Figure 32. The 'Browse Images' toolbar allows the user to display selected false color or satellite images in the main graphic window.**

The 'Images' tab of the 'Data Graphics' dialog box shown in Figure 33 allows the user to select a false color (or satellite) image type and/or the *AquaModel* ocean current vectors that are displayed on the EASy main graphic window during the simulation. The program animates the selected sequence of images and/or ocean current vectors to show how spatial changes occur over time.
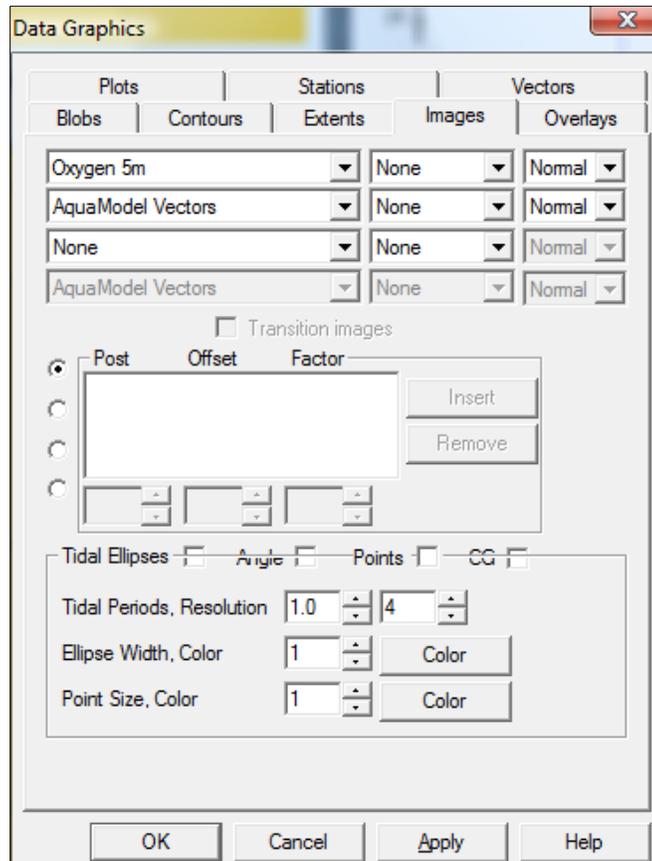


**Figure 33. False color images shown in the main graphic window allow the user to visualize both spatial and temporal changes in critical ocean properties.**

Available ocean properties that may be displayed as false color images include array oxygen, nitrogen, phytoplankton or zooplankton at each simulated array cell depth; suspended oxygen, feed, fecal, and total waste concentration; and sediment oxygen $CO_2$ or hydrogen sulfide concentrations; feed, fecal, average waste, cumulative waste, and total waste concentration, total consolidation waste, and aerobic or anaerobic abundance. This tab is also enables the display of calculated tidal ellipses for 3-D ocean currents.

 The 'Contours' tab of the 'Data Graphics' dialog box shown in Figure 34 allows the user to select an ocean property that will be displayed as a contour during the simulation. Ocean properties that can be displayed as false color images may also be displayed as contours. The selected contour is displayed over the selected false color (or satellite) image so that the user may determine how two parameters interact spatially. During the simulation the selected contour is animated along with the selected image to show how the two properties interact over time.

Profile plots are selected for display with the 'Plots' tab of the 'Data Graphics' dialog box shown in Figure 34. Four types of plots are available: depth plots (property vs. depth), time plots (property vs. time), transact plots (property vs. distance along a user defined transact line), and false color image plots (color image representing property values at array depths along a user selected transact line). Examples of the four plot types are shown below in Figure 35. The upper left figure shows a depth plot of oxygen at a user specified 'drill point', the upper right figure shows a false color image plot of oxygen along a user specified transact line, the lower left figure shows a transact plot of suspended total waste along the same transact line, and the lower right figure shows a time plot of average surface and bottom ocean current magnitude.
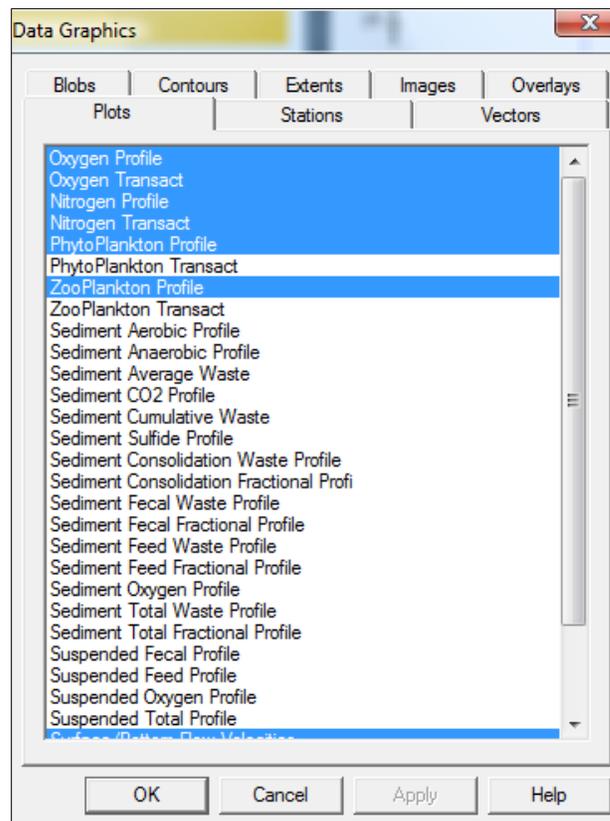


**Figure 34. User selected contour options are displayed over selected images show how two ocean parameters interact.**
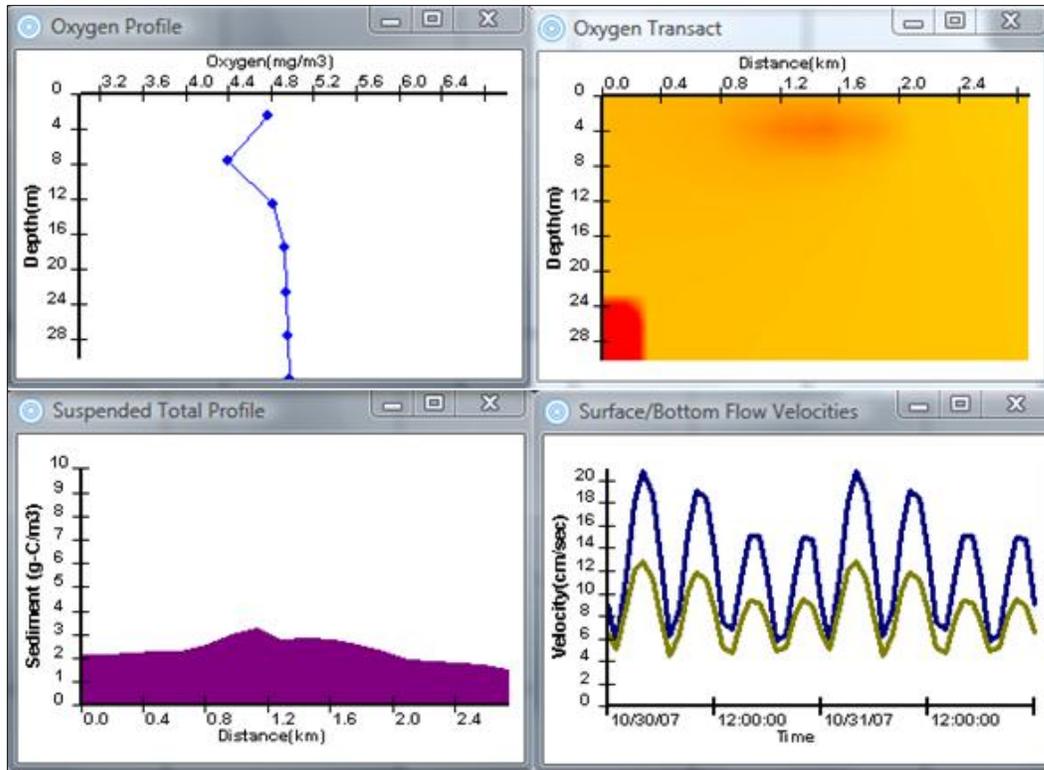
**Figure 35. Four types of X-Y profile plots provide flexibility in evaluating critical ocean properties.**

The 'Settings' tab of the 'Display Settings' dialog box enables general display objects and associated color, size, and resolution as shown in Figure 36. The *AquaModel* ocean current vector display is controlled by the 'Vector Arrows' panel of this tab. It defines vector length, width, and color, arrow head type and size, and vector array display resolution. Other display items that are controlled by this tab include distance units (metric or English), latitude/longitude units, legend types, display projection (Mercator, Lambert, or Arc), and geographic and profile plot background colors.

**Figure 36. EASy setting controls allow the user to tailor the geographic and profile plot displays.**



*AquaModel: Software for Sustainable Development of Open Ocean Fish Farms* 47
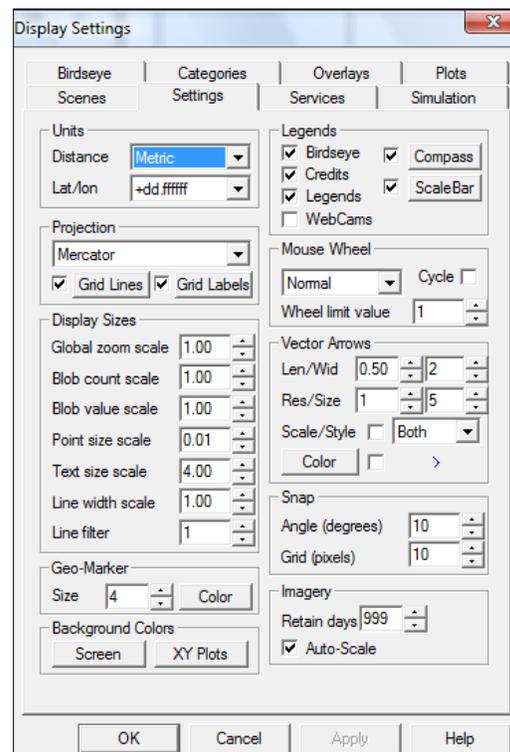
The 'Simulation' tab of the 'Display Settings' dialog box is used to initialize the simulation start and end dates and the display frequency as shown in Figure 37. The 'Restricted Simulation Capabilities' settings are ignored in this dialog box as they are automatically set by the *AquaModel* service depending on the selected operating mode (e.g. 'Normal', 'Capture', or 'Replay').
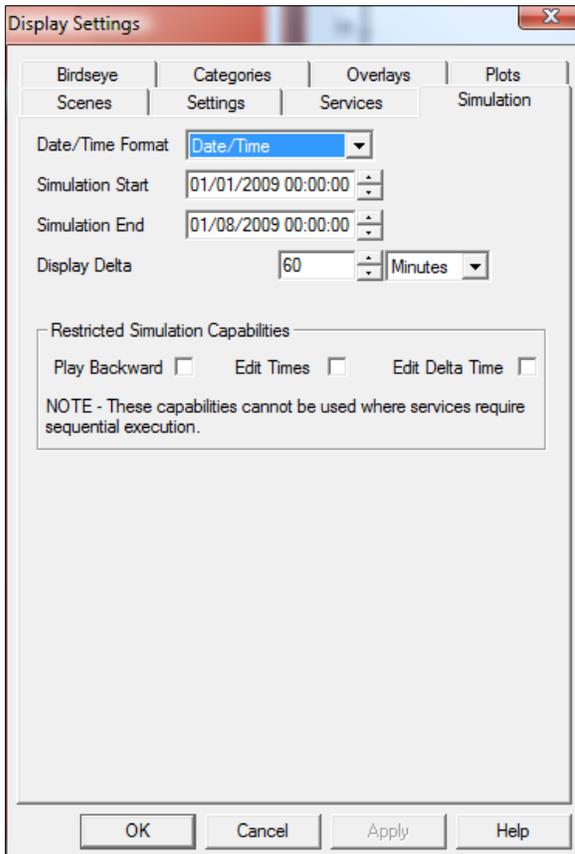


**Figure 37. The simulation settings control allows the user to set the simulation start and end times as well as the display interval.**

Execution of the simulation is then controlled by the 'Simulation Control Panel' shown in Figure 38. This dialog box allows the user to step, run, stop, or reset the current simulation. During the *AquaModel* replay mode the user may also skip to any point in the simulation or play the simulation either forward or backward.

**Figure 38. The new simulation control panel allows the user to skip to any point in a previously captured simulation and play the simulation either forward or backward simply by clicking and dragging on the red slide area in the blue bar.**
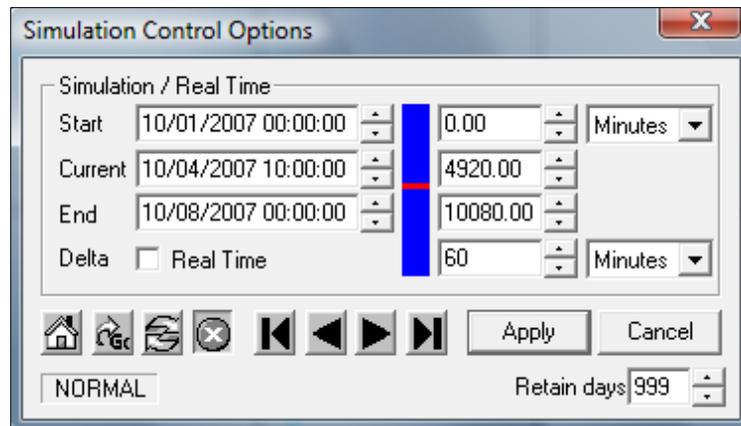
Figures 39 through 42 illustrate various combinations of geographic false color image, contour, and profile plots for a 24 cage farm near the big island of Hawai'i. The array of dark green dots in the center of the displays is the farm pens. A dot near the center of the array is the selected 'drill' location and the red line traversing through the array is the selected transact. Finally, the blue arrows show ocean current vectors at the displayed simulation time.

Figure 39 shows a false color image of oxygen concentration at five meters depth. The red rectangles partially obscured by land are an artifact that resulted from the bathymetry source that identified those areas to have zero depth (e.g. land). As a result *AquaModel* assumed an oxygen concentration of zero (red). The false color image is overlaid by contours that show the concentration of total waste in the near-bottom suspended layer. Profile plots include depth and false color image transact plots for oxygen, nitrogen, phytoplankton, and zooplankton; transact plots of suspended layer and sediment total wastes; and a time plot of average surface and bottom ocean currents.

Figure 40 shows a false color image of nitrogen concentration at five meters depth overlaid by contours of sediment total waste.

Figure 41 shows a false color image of phytoplankton concentration at five meters depth overlaid by contours of nitrogen concentration at five meters depth.

Figure 42 shows a false color image of zooplankton concentration at five meters depth overlaid by contours of phytoplankton concentration at five meters depth.
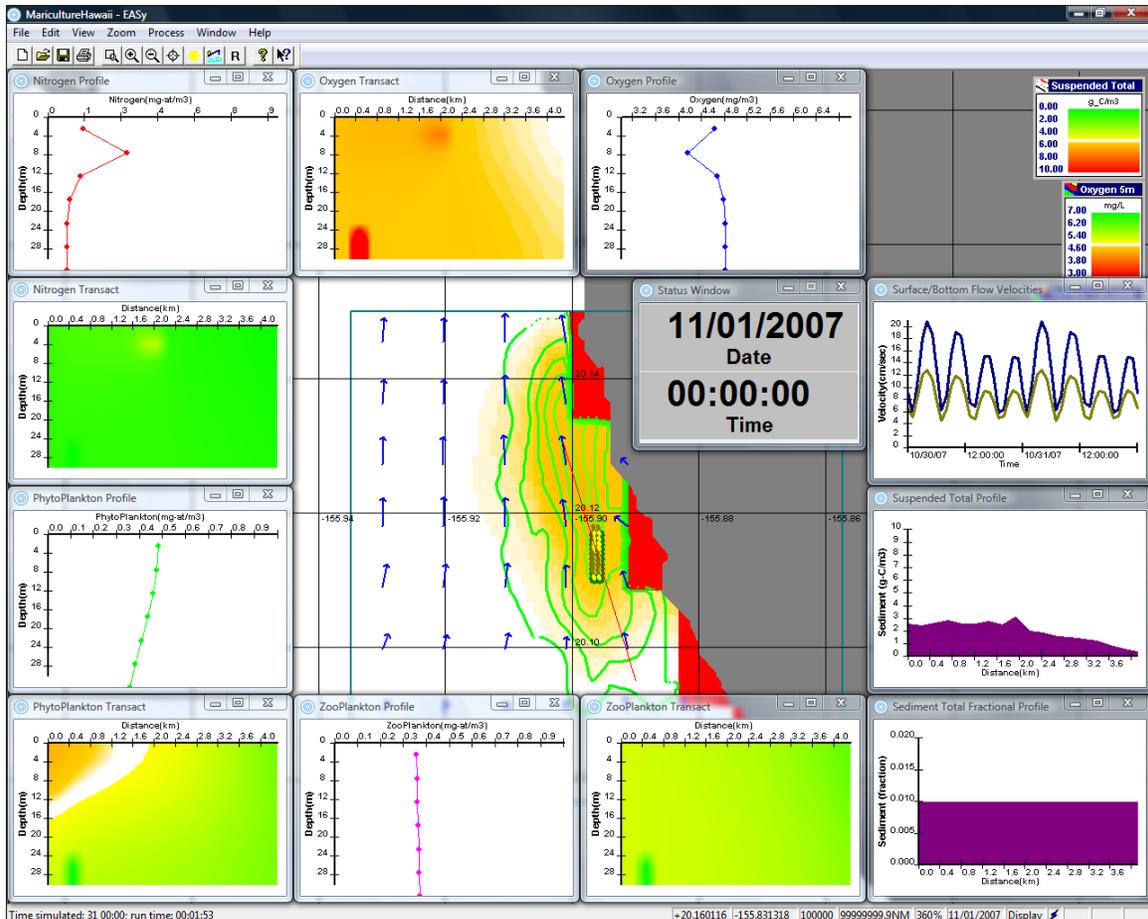
**Figure 39. The combined display of a false color image (oxygen), contours (suspended total waste), current vectors, and profile plots provides users with a comprehensive tool for the analysis of critical ocean conditions.**
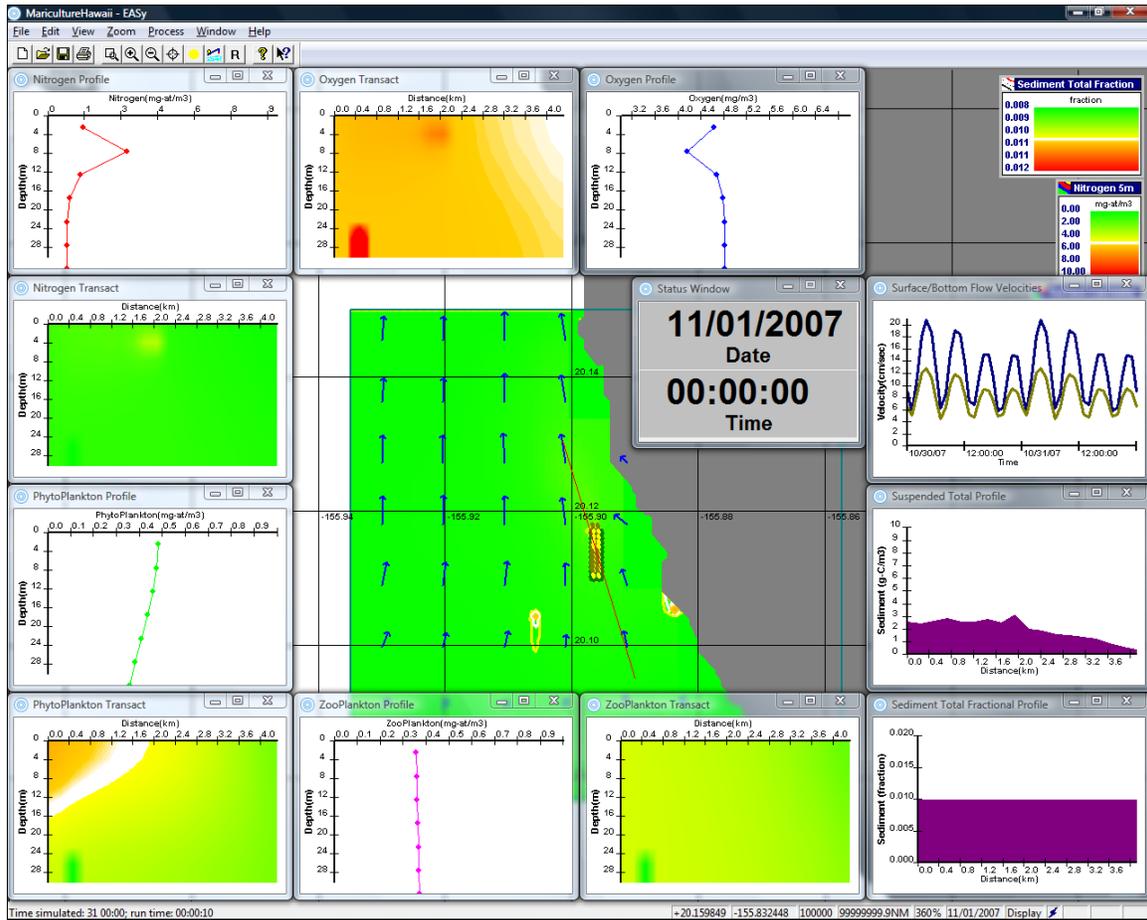
**Figure 40. The lack of a nitrogen plume (false color image) shows that excess nitrogen is being consumed by the available phytoplankton. The contours show only tiny areas where waste is being accumulated.**
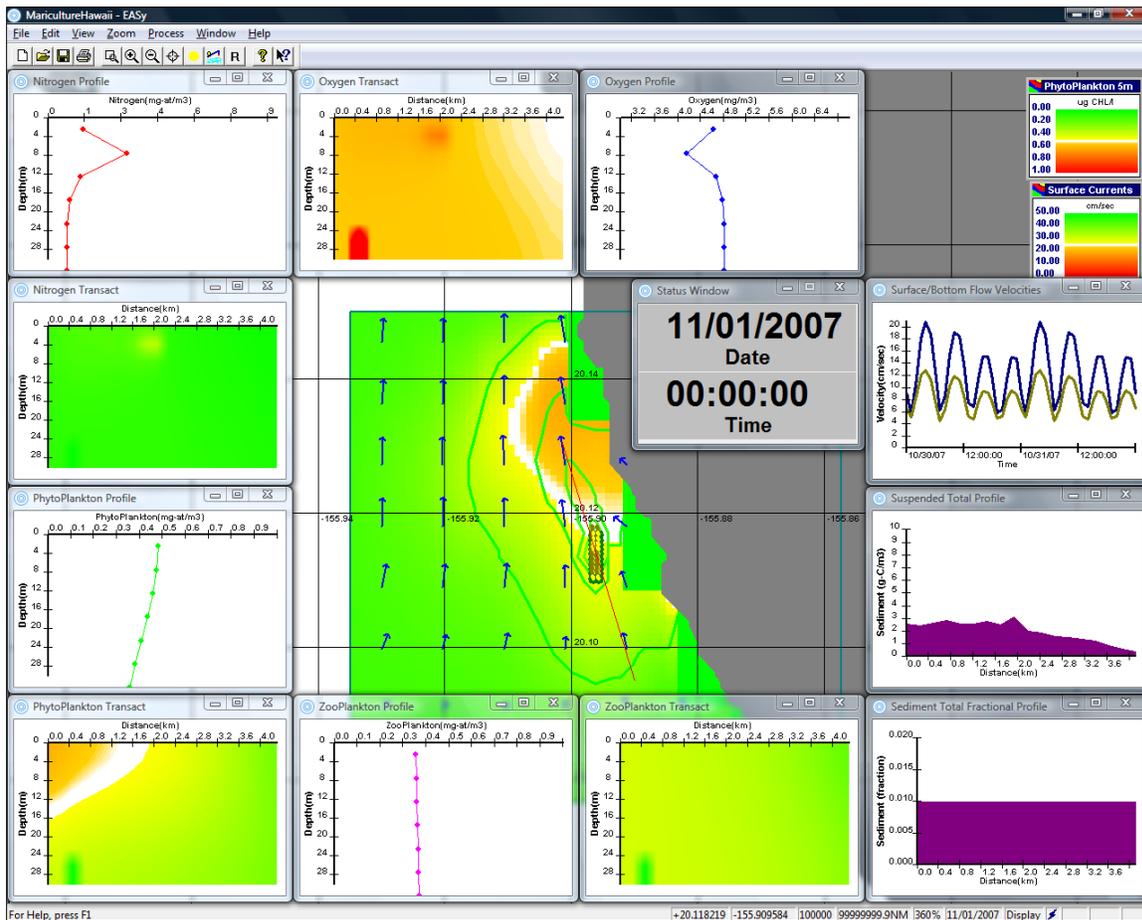
**Figure 41. Phytoplankton is abundance (false color image) near the farm eliminates excess dissolved nitrogen (contours).**
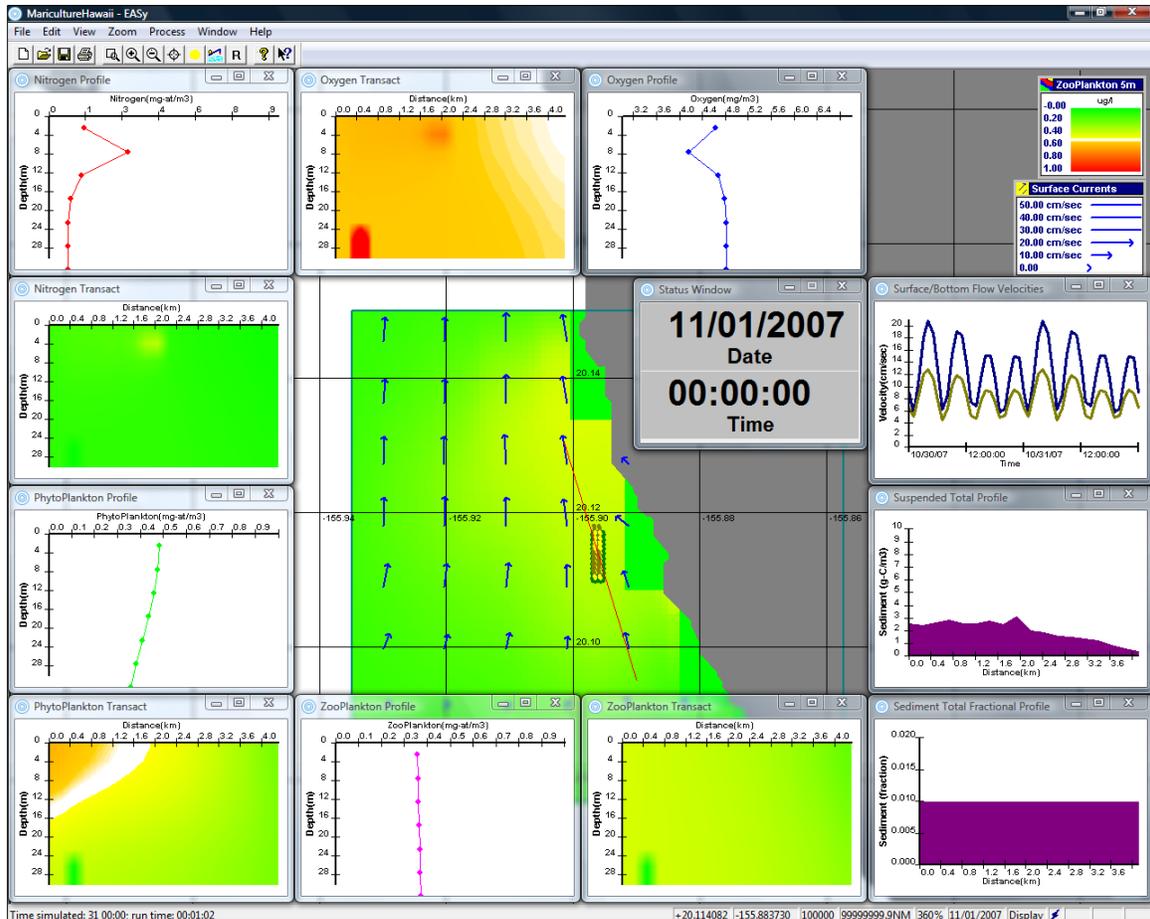
**Figure 42. Zooplankton abundance (false color image) near the farm controls excess phytoplankton growth (contours).**

# Task 5. Fish Physiology Studies of Moi and Cobia

We have completed laboratory studies on the growth and metabolic activity of two species of fish that are candidates for large open water commercial farming. These species are relatively new to American mariculture and although larval and very small juveniles have been studied, little is known about their physiology, particularly for the grow-out phase. Our studies of larger sized fish have provided information necessary to run simulations of operations and environmental impact for the growing mariculture industry in Hawai'i. The focus of this work is determination of basal (resting) and active respiration, excretion rates of ammonia, urea and total N, fecal settling rates and N and C digestibility and composition of fecal matter. The species included moi (*Polydactylus sexfilis),* which was the first species to be reared in net pens in Hawai'i. This task was managed by Dr. Jack Rensel with the cooperation of Dr. Michael Rust and Mr. Thomas Scott of NOAA NW Fisheries Science Center (NWFSC) in Seattle.

## Respirometry Methods

All respirometry work was performed at the Northwest Fisheries Science Center, Seattle, WA, USA in collaboration with researchers from the University of Idaho, Aquaculture Research Institute. The fish were raised in a large, recirculating seawater system. Water quality parameters remained within normal limits during grow-out for both species. Photoperiod was set to 12 hours on 12 hours off. System water was sand-filtered natural seawater from Puget Sound, Washington maintained at 30 g $L^{-1}$ salinity and 26.5°C. Fresh, de-chlorinated municipal water was used to maintain salinity and overcome evaporation and overall water quality results are shown below in Table 1.

**Table 1. Summary of water quality measurements during fish rearing.**

| Parameters | |
|---|---|
| NH3-N | 0.05 ± 0.05 |
| NO2-2 (mg L-1) | 0.12 ± 0.1 |
| Alkalinity (mg CaCO2L-1) | 912.4 ± 254.2 |
| Salinity (ppt) | 30.1 ± 0.4 |
| Temperature (C°) | 26.6 ± 1.31 |
| Dissolved Oxygen (mg L-1) | 10 |
| pH | 8.34 ± 0.2 |

Approximately 1200 Moi (*Polydactylus sexfilis*) juveniles were obtained from Hukilau Foods, Hawai'i, USA and air shipped to the lab in Seattle, Washington, USA. Juvenile weights at arrival ranged from 700 to 1000 mg. Initially, fish were stocked at a density of two fish per liter and hand fed four times daily (BioDiet Grower, Bio-Oregon, Longview, WA, USA). Later, as fish grew and consumed more feed, belt feeders were used. Fish

reached the target weight (~100g) for the first respirometry trials approximately 130 -140 days after arrival.

Approximately 1000 Cobia (*Rachycentron canadum*) juveniles were obtained from Virginia State University (from Dr. Michael Schwartz). Cobia weights at arrival were approximately 2 g. Initially, cobia were stocked at a density of 2 fish per liter and fed Otohimi diet. (Reed Mariculture). Later they were transitioned to BioDiet Grower and fed five days a week by belt feeders.

While studying the bioenergetics of sablefish from a previous study, we noted that the variability results when using both a galvanic dissolved oxygen meter and Winkler digital titration assays was unsatisfactory and were flagged as a quality control issue. We believed the dissolved oxygen meter was major part of this problem, although a widely used design that tested to be in good condition. We therefore purchased a new LDO dissolved oxygen meter and probe (Hach, Loveland, CO, USA model #HQ40d multi portable meter with LDO 10101 probe), that represents breakthrough technology in that it does not rely on the polargraphic or Clark style membrane method but rather uses a luminescent, light based system that is EPA approved for field sampling and reportedly is much more accurate and stable than older systems. Briefly, the LDO uses a sensor that measures the light emission characteristics from a luminescence-based reaction that takes place at the sensor-water interface. A light emitting diode (LED) provides incident light required to excite the luminophore substrate. In the presence of dissolved oxygen the reaction is suppressed. The resulting decay of the excited luminophore is evaluated and equated to DO concentration.

The three swim respirometers and the numerous static respirometers were fitted with new mounts to accept these probes. The new probes and two modified Winkler methods were then evaluated on the same water samples to determine if the new probes were indeed a better option. This testing showed the LDO probes to be the most repeatable method with the lowest repeat measurement variation of the three methods evaluated (data not shown).

Following that trial, oxygen consumption rates for both static and swim chamber respirometry were determined using an LDO meter. There are no known interferences with DO detection and quantification using this non-consumptive method. The probes used in the study were calibrated to ambient air saturation, and adjusted for salinity prior to each run.

The following equation was used to determine the mass corrected oxygen consumption rates for static and swim respirometry.

$$C = ((a/M)/(V))(K)$$

C = Consumption in mg oxygen per Kg fish weight per hour

a = Slope of the regression line relating time with oxygen consumption (mg $L^{-1}$ $minute^{-1}$).

M = Mass of fish (grams)

V = Chamber volume less volume displaced by the fish (liters)

K = 60 seconds/minute x 1000 grams/kg to report data in mg $O_2$ consumed per Kg fish weight per hour.

The volume displaced by the fish was ignored in the calculation (V term) for swim respirometers because it was small relative to the volume of the swim chambers (0.1-0.5% of volume). However, for the smaller static respirometers, the correction factors were estimated by developing a weight to volume regression for each species and then using the weight of each fish to calculate its volume. The weight to volume relationship was determined by measuring the displacement of seawater obtained when an anesthetized (MS-222, Argent, Redmond WA, USA) pre-weighed fish was added to a partially filled graduated cylinder. This procedure was repeated with ten fish from each species. The slope of the regression line between volume displaced and weight was used as the correction factor for each run (0.9008 ml $g^{-1}$ for moi and 0.8849 ml $g^{-1}$ for cobia). The correction factor multiplied by the weight of the fish was subtracted from the volume of the chamber for calculations. The correction factor was determined on fish of approximately 100 g, and applied to fish of all sizes from 100 g up.

A series of blank runs were conducted with each chamber but with no fish to determine the background oxygen consumption for both types of chambers (data not shown) and it was determined to be negligible and was not included in calculations.

## Swim Chamber Respirometry Methods

The basic design of the swim chambers employed in our studies is a modification of the Blazka style (Blazka et al. 1960) respirometer for larger fish (Smith and Newcomb 1970). The specific units we used were built to study swimming in young salmon (Flagg 1981) and later swim fatigue during the development of the pit tag system (Prentice et al. 1986). The chamber body is constructed of two clear, 0.25 inch think, acrylic tubes; an outer twelve inch diameter tube and an inner 10 inch diameter tube. The inner tube is loosely centered inside the larger tube by small supports at either end. Flanges were glued to the chamber ends for attaching the removable end-caps. The chamber and motor are secured to a wood base and set onto a metal framework supported by a central axel. The axel allowed the chamber to be tilted forward for dumping water or backward for filling and adding fish. A watertight, motor-driven, driveshaft attached to a small propeller passes through the end block into the chamber. Water is pulled toward the propeller through the

inner tube then forced back around in the space between the inner and outer tube. Fish were protected from the propeller by a screen. The proximately of the fish to the screen during trials was used to gage swimming behavior. To further approximate laminar flow, a straw pack was added to the end of the inside chamber on the upstream side of the fish. The straw pack was composed of several hundred 10 inch long clear plastic drinking straws banded together. The chamber design creates a low turbulence, nearly laminar flow and velocities up to 60 cm sec$^{-1}$. A vent at the top of the chamber was fitted with an airtight plug. A hole that runs through the center of the plug was topped with an airtight mount for the LDO probe. Temperature was taken at the beginning and end of the runs.



**Figure 43. Moi swimming in swim respirometer.**



**Figure 44. Three swim respirometers used in this study being used at the NOAA NWFSC AquaLab.**

Swim chamber velocity calibrations were calculated as follows: The driveshaft RPMs, determined with a hand held digital infrared tachometer (TIF 780, Digital Infrared Phototachometer), were turned into velocity (cm sec$^{-1}$) measurements by determining a standard curve for each swim respirometer using a Swoffer mini-prop current meter

placed at the center of an active swim chamber.  Manufacturers calibration techniques were used to calibrate the mini-prop (Swoffer Instruments, Tukwilla, WA, USA).  RPM was varied and velocity recorded to develop a calibration curve for each chamber.

Starting oxygen concentration was the value taken just prior to turning on the swim chamber propeller or as soon as the chambers were sealed for static chambers. Oxygen concentration was determined every two to five minutes from the time the trial started until the DO level in the chamber fell below 70% saturation.  A linear regression of DO concentration with time was performed for each run and those with an $r^2$ value lower than 0.85 were discarded.

Trials were run to determine oxygen consumption of moi and cobia during swimming at three different water velocities (15 cm sec$^{-1}$, 30 cm sec$^{-1}$ and 45 cm sec$^{-1}$).  Cobia ranged in size from 61 to 623 g (N = 81 trials) and moi were from 56.4 to 494.7 g (N = 78 trials). Data was taken so that individual fish weight was paired with its respiration rate so that data could be analyzed by regression.  The swim chamber was half filled with water prior to adding a single fish directly from the holding tank.  The chamber end was sealed and the chamber was filled. Three chambers were run simultaneously.  The end point for each assay was 70% of saturation or approximately 4.5 mg L$^{-1}$. Readings were stopped prior to fish becoming stressed. Oxygen concentration (mg L-1) values were manually logged every 2-5 minutes.  A typical run would have 10-20 points to make up the regression relating oxygen consumption with time. Each fish was observed and ranked for its swimming performance, activity level and general healthful appearance to ensure we did not include subpar appearing fish.  At the end point fish were observed for robustness and weighed before being placed into a recovery tank.  Fish were fed normally the morning of the day prior to trials but feed was withheld the morning and day of trials.

## Static Chamber Respirometry Methods

The six-liter static chambers were rectangular in shape and made from black, polycarbonate plastic with clear polycarbonate plastic tops.  The actual volume of each chamber was measured and recorded.  A black foam rubber gasket created an airtight seal between the chamber and the lid.  The four corners were secured with 0.48 cm stainless steel bolts that fit through a flange surrounding the lip of the chamber and the overlapping lid.  A 0.635 cm drip irrigation valve was attached to the side of each chamber to allow for continuous flow (~200 ml min$^{-1}$) during acclimation and to maintain oxygen saturation prior to the addition of fish.  The tops had a small fitting designed to accept and seal around the oxygen probe. The chambers were set into a 26.5°C water bath to maintain temperature.

**Figure 45. Static respirometers constructed for this work. The first three units in the foreground with LDO dissolved oxygen probes inserted.**

Trials were run to determine oxygen consumption of moi and cobia at rest at two different weights (moi 88.6 ± 4.9g, n=18, 343.7 ± 23.4g, n=9; cobia, 71.7 ± 2.0g, n=15, 270.7 ± 29.6g, n=12). Data were taken so that individual fish weight was paired with its respiration rate so that data can be analyzed by regression on paired samples. Treatment fish were moved from the general population tank directly to the static chambers. Tops were put on quickly, residual air was displaced by water, and the unit was sealed. Fish were allowed to adjust for 5 minutes in with water flowing through the chambers. At time zero, the inflow and effluent tubes were turned off and the beginning oxygen reading was taken. The end point for each assay was 70% of saturation (~4.5 mg $L^{-1}$). This point was chosen to minimize low oxygen stress on the fish. Measurements were read from the meter every 2 minutes and manually logged. Fish were observed throughout the run to ensure behavior was normal. At the end point, fish were observed and weighed before being placed into a recovery tank. Fish were fed normally the morning of the day prior to trials. Feed was withheld the morning and day of trial.

Note that the respiration rate of small fish held in "stirred" static respiration containers was significantly higher than not stirred containers (Table 2). This adds to our prior conclusion that the stirred containers without fish (blanks) added more oxygen than anticipated and therefore we have selected to rely on the unstirred data as most representative. Variability within replicates was smaller for the not stirred containers; hence the results are useful and probably reasonable given the large number of replicated trials.

**Table 2. Summary of preliminary tests of stirred vs. non stirred static respirometers for small-sized moi.**

| Treatment and No. of replicates | Mean (SD) Fish Weight (g) | Mean (SD)Respiration Rate (mg kg$^{-1}$ d$^{-1}$) | Salinity (psu) & Water Temperature (C°) | Range of ending Dissolved Oxygen (mg L$^{-1}$) |
|---|---|---|---|---|
| Not stirred* N = 9 | 81.6 (14.3) | 357.4 (44.6) | 30.5 psu 28.8 °C | 4.4 - 4.5 (~ 70% saturation) |
| Stirred N= 9 | 86.7 (21.5) | 418.4 (74.5) | 30.5 psu 28.8 °C | 4.4 – 4.6 (~70% saturation) |

# Fish Fecal Settling Rate Methods

Dr. Rensel devised a new, practical and inexpensive method to assess speed and volume of fish fecal settling rates. Fish fecal settling columns consisted of clear acrylic 7.6 cm diameter pipes 142.2 cm long, with Imhoff cones sealed to the bottom using silicone aquarium sealant. The length of the water column in these cylinders for each trial varied between 120 cm and 131 cm, due to changes in the mounting systems used between trials. Fish were fed to satiation in the early morning and in the afternoon. After being anesthetized with MS-222 (Argent, Redmond WA, USA), anesthetized fish were manually stripped of their fish feces by carefully squeezing the ventral edge of the fish anterior of the anus into the top of the column. Care was taken only to express fish feces that were ready to be naturally discharged, and several trials were judged not useful on this account. Settling was measured by recording the amount of feces in depth at the bottom of the Imhoff cone at periodic intervals after stripping and the rate/volume results calculated accordingly. For this assessment, moi weighed 405.6 ±114.05 g. Cobia were sampled twice weighing 351.4 ±86.02 g (n=22) for the first trial and 1854 ±344.4 g (n=10) for the second. This method was previously used by Rensel and colleagues for sablefish.

# Excretion Rate Determination Methods

Suitably-sized and clean containers such as 5 gallon buckets fitted with lids were washed with 10% HCL acid and rinsed with recirculating seawater from the culture system and fitted with airstones and lines to provide aeration during short term (6 to 12 hour) bioassays to estimate excretion rate. Container tops were fitted to allow gas exchange and aeration lines but also to prevent fish from jumping out.

Each of five replicate treatment of control containers were filled with seawater to a specified level representative of a known volume and aeration initiated. Before moving the fish into these tanks, background nitrogen samples were collected for total ammonia, nitrate+nitrite, dissolved total nitrogen, and in many cases urea. Samples were quickly processed and frozen immediately for later analysis using standard autoanalyzer methods for DIN and a CHN analyzer for total N except for the urea samples that were analyzed using the method of Revilla et al. (2005). After fish were placed in the containers, samples were collected after turning off the aeration for several minutes and inspecting each container for the presence of solids that would have indicated that the fish either defecated or regurgitated stomach contents. Both were relatively rare but if it did occur, that replicate was no longer sampled on that sampling day. At the same time, fish were inspected for condition and any fish observed to be stressed or respiring unusually was discarded as a replicate. All assays were conducted from 6 to 24 hours depending on the size of the fish and species. Moi were less suited to this type of assay, and data collected for large moi past 6 hours was discarded due to obvious signs of stress. Cobia were much more adaptable and were assayed for 12 hours.

## Apparent Digestibility Coefficients Determination Methods

Apparent digestibility is a common method used in fish nutrition studies to estimate the percentage of a nutrient or compound ingested by the fish that is retained by the fish. Subtracting the apparent digestibility coefficient (ADC) from 100% would represent an estimate of the percentage of the nutrient of interest excreted in the feces. ADC does not consider background or endogenous losses; however these are small relative to the amount of those nutrients from the diet. ADC's are calculated based on the ratio of an indigestible marker in the feed and feces of the animal being used for the estimate.

Cobia and moi were fed to satiation a fishmeal-based diet containing an Yttrium marker daily for three days. The apparent digestibility of dry matter, lipid, carbon, and nitrogen (protein) were determined via the incorporation of an inert rare earth mineral, yttrium oxide, into the feed as described by Austreng et al. (2000). Wet feed and fecal samples were weighed, dried and reweighed to determine dry mater. Dried and weighed feed and fecal samples were ashed overnight at 550 ºC, cooled, and then digested with an aqueous 20% (v/v) mixture of concentrated HCl and $HNO_3$. Samples were diluted as appropriate and analyzed for yttrium using a Perkin Elmer Optima 3000 Radial ICP-OES (Perkin Elmer Instruments, Norwalk, CT, USA) employing a detection wavelength of 371.029 and appropriate standards. Freeze-dried feed and feces samples were analyzed for nitrogen and carbon and compared to that of the feed, using a CHN analyzer at the University of Idaho, Analytical Services Laboratory (Moscow, Idaho). After lipid, carbon, nitrogen and marker contents were determined in feed and feces samples, ADCs

were calculated from the following formula.

$$ADC = 100\% \times \left( 1 - \frac{[\text{marker}]_{\text{feces}}}{[\text{marker}]_{\text{feed}}} \times \frac{[\text{nutrient}]_{\text{feed}}}{[\text{nutrient}]_{\text{feces}}} \right)$$

Preparation: We have completed work on the bioenergetics of sablefish, we noted that the variability results when using both YSI dissolved oxygen meter and Hach digital titration assays was unsatisfactory and was flagged as a quality control issue. We believed the dissolved oxygen meter was major part of this problem, although a widely used design that tested to be in good condition. We therefore purchased a new LDO dissolved oxygen meter and probe manufactured by HACH, that represents breakthrough technology in that it does not rely on the polargraphic or Clark style membrane method but rather uses a luminescent, light based system that is EPA approved for field sampling and reportedly is much more accurate than older systems. The three swim respirometers and the numerous static respirometers were fitted with new systems to accept these probes. The new probes and two modified Winkler methods were then evaluated on the same samples. This testing showed the LDO probes to be the most repeatable method with the lowest repeat measurement variation of the three evaluated.

Testing of the respirometers was then conducted to insure the units were leak proof and "blank" runs were conducted to test for flux of dissolved oxygen in the absence of fish. These tests proved satisfactory, in that only small change in dissolved oxygen concentrations were recorded over long periods. Dr. Rensel then recalibrated the swim respirometers for flow rate, using a Swoffer mini-prop streamflow sensor and meter.

We found that the static respirometers they had been cannibalized for parts, and NOAA staff had to construct new fish-size specific units from sealed units that fitted with water and probe ports. The units were then tested, and we found those units equipped with stirrers had blank oxygen change rates consistently higher D.O. (+0.13 mg L$^{-1}$) than those without (-0.09 mg L$^{-1}$). Accordingly, we elected to remove the stirrers for all future tests. Larger static respirometers will be constructed for larger fish in the near future.

We obtained juvenile moi (*Polydactylus sexfilis)* that were shipped from O'ahu Hawai'i and donated by Cates International Co. (Mr. Randy Cates). These fish were very small when shipped and were reared to about 90 grams for the first of two or three size class trials, depending on the parameter involved. The fish grew rapidly and were very active but at about the 70 gram size they experienced some mortality from an unidentified *Pseudomonas* bacterial outbreak. In part, this may have been due to handling that was necessary for growth sampling. Cobia juveniles were provided by Michael Schwartz, Virginia Seafood Agricultural Research and Extension Center. Laboratory methods manual was constructed and updated as methods evolved and were adapted.

# Moi Swim and Static Respiration Results

Moi swim respiration results for different swimming speeds are shown in Figure 46 and indicate an expected gradual increase from about 400 to 1200 mg kg$^{-1}$ hr$^{-1}$ dissolved oxygen use at 0, 15, 30 and 45 cm sec$^{-1}$ velocity.
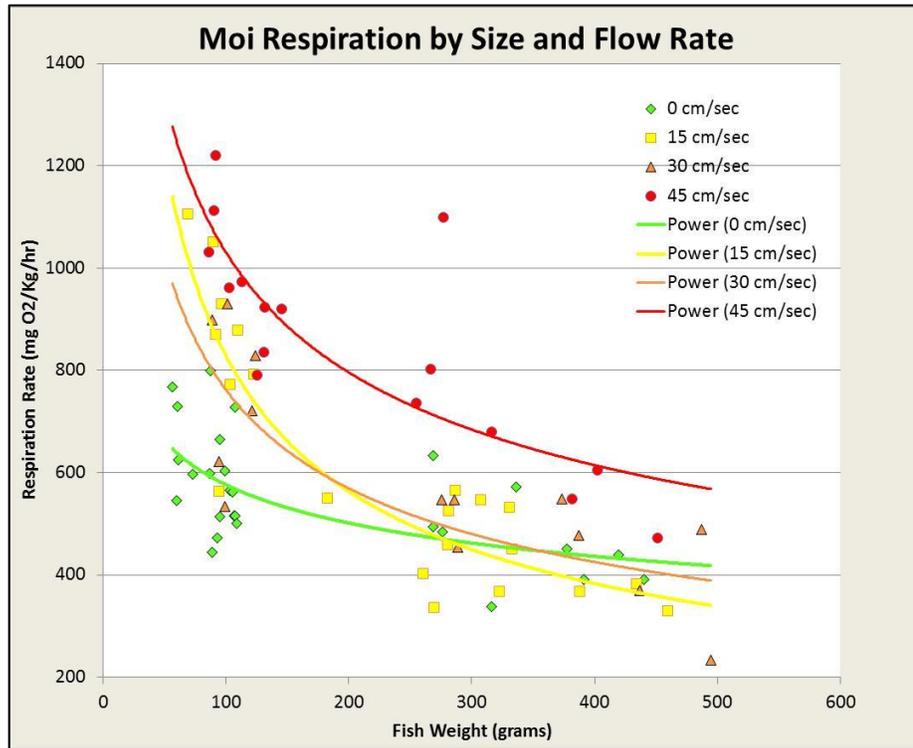


**Figure 46. Moi respiration rates by fish weight and swimming speeds cm sec$^{-1}$.**

A power curve was fitted to these data for a close approximation of a regression line. The results for moi formed relatively cohesive curves, with correlation coefficient of determination ($R^2$) ranging from 0.42 to 0.80. These are good considering normal biological variation among individual fish and all curves showed decreasing respiration rates with increasing body size.

Cobia respiration results are shown in Figure 47 and are somewhat different. Zero and 45 cm sec$^{-1}$ results are similar to appearance to moi, although much lower respiration rates. Curiously, both the 15 and 30 cm sec$^{-1}$ results formed relatively flat (no slope) lines indicating no effect of size on respiration rate for these swimming rates. This was an artifact, especially for the 15 cm sec$^{-1}$ rate, because we observed the fish resting on their pectoral fins and wedged in against the currents. The data were corrected for this artifact before using the functions that were derived.
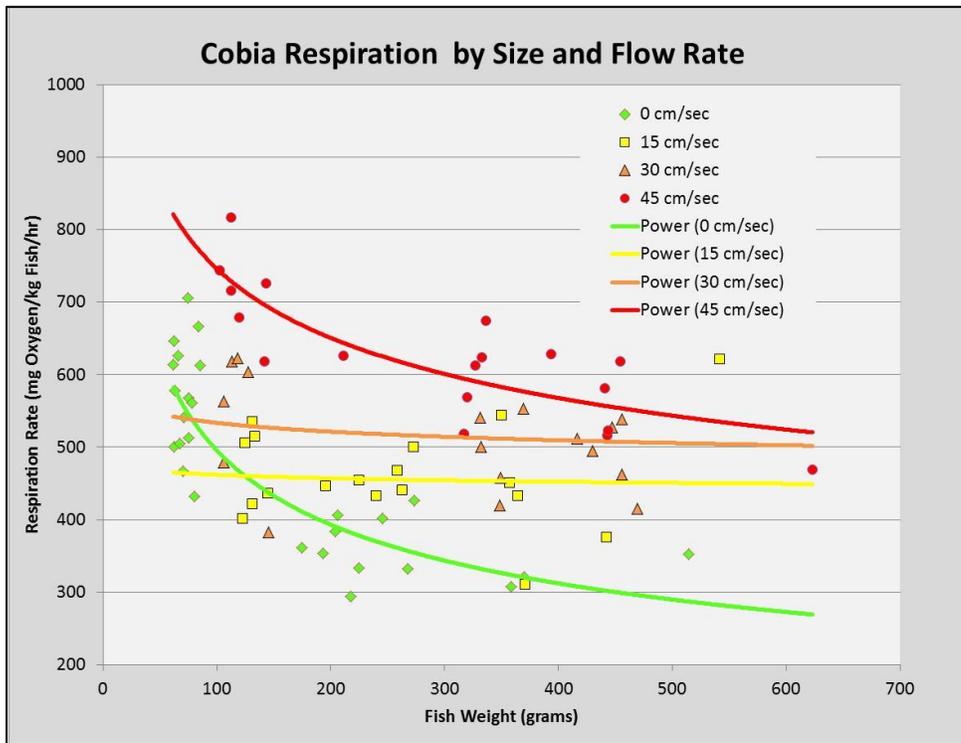
**Figure 47.  Cobia respiration rates by fish weight and swimming speeds cm sec$^{-1}$.**

Figure 48 presents moi and cobia data together to emphasize the differences in respiration rates between the species.
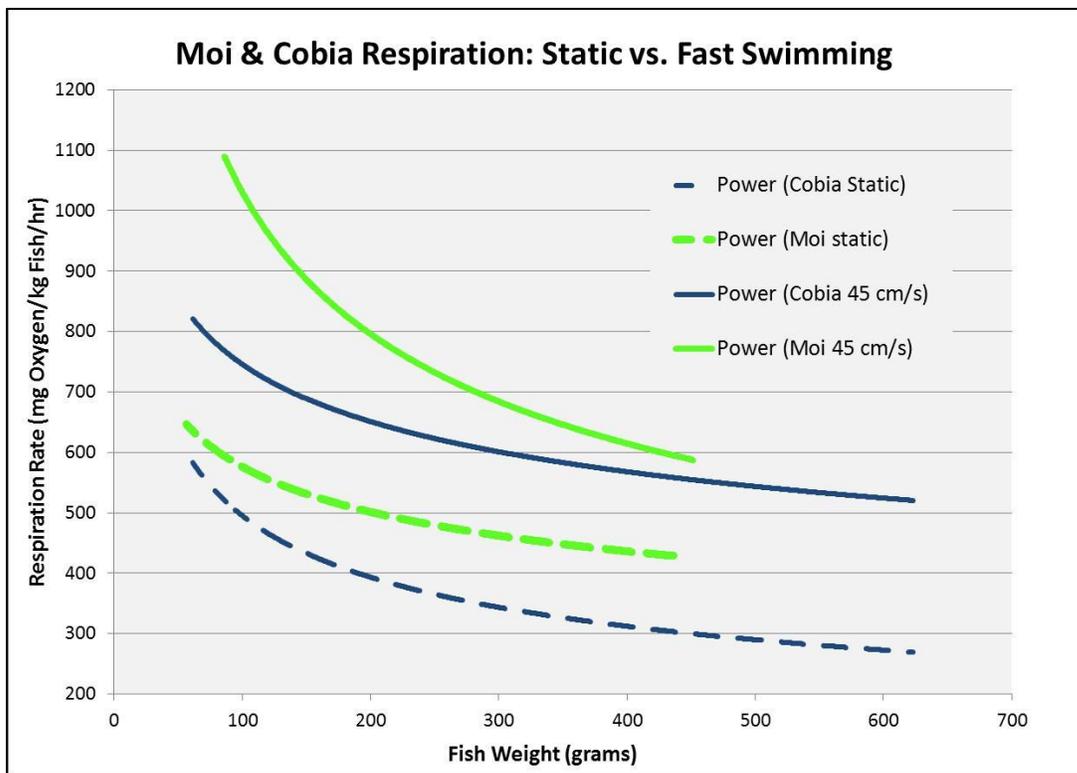


**Figure 48.  Comparison of moi and cobia respiration at static and fast swimming speeds.**

As a benchmark to compare these results, we refer to a generalized plot of standard (resting) respiration rates initially prepared by Brett and Groves (1979) and revised by Wootton (1990) (see Figure 49).
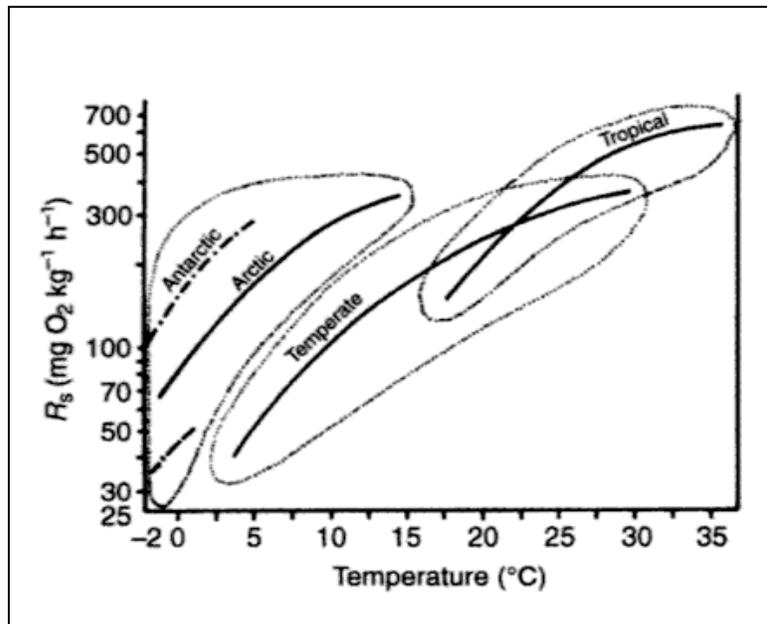


**Figure 49. Schematic diagram of the effect of temperature on standard metabolism rate ($R_s$) for polar, temperate and tropical fish (show as solid lines) with range of variability around each as dotted line. From Wooton (1998) as simplified and drawn from Brett and Groves (1979).**

As Wootton states, such generalized figures are not representative of all fish under all conditions. The plot shows that our results (at 26°C) are above the generalized and expected range, and much higher than the average expected of ~400 mg kg$^{-1}$ hr$^{-1}$ D.O. at the given temperature. In nature and the laboratory moi are a very active and schooling species and given their surf zone habitat in the ocean, higher than normal rates of respiration would be expected. If we error, it is conservatively more as it would show more effect than a lower than true rate.

Standard metabolism (SM) is defined as the energy required to keep the animal alive and is similar to basal metabolism measured in humans. Because of the difficulty of obtaining a "motionless" animal, the definition of basal metabolism is not applicable to fish. When fish are restrained to a motionless condition they struggle to free themselves and use more energy than if allowed to swim freely in still water. SM is the minimum heat production of an undisturbed fish in the "post absorptive" state in still water. For the purposes of this study, we approximated SM by not having any flow in the respirometer during measurement for the zero velocity rate category.

Figure 50 shows a different type of plot we used, this one for fish tested at the highest velocity rate of 45 cm sec$^{-1}$ (~0.9 knots). All the replicates were judged satisfactory although one fish indicated as the red squares, displayed non-linear and abruptly

changing respiration rate. Such variability is to be expected in biological testing such as this. Accordingly, slopes of other lines were similar but also somewhat different as is expected in this type of biological analysis.
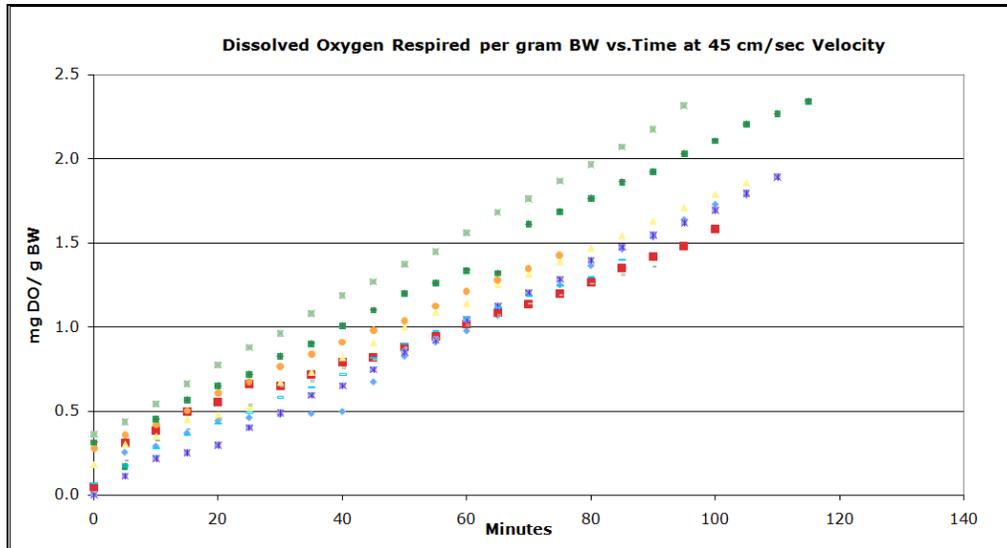


**Figure 50. Plot of relative respiration rates of individual small moi swimming at 45 cm sec^{-1}.**

# Excretion Results

Prior to this study, there were no data on the excretion rates of moi and the species of nitrogen involved. There were studies of cobia, but only of very small post larval sized fish that are not applicable to grow out situations. Many teleost fishes produce both inorganic ammonia nitrogen and (organic) urea, often the latter in lesser or much lesser quantities.

We conducted short term static bioassays in aerated containers to measure these components in two ways:

1) As ammonium + nitrite + nitrate and separate urea measurements for increase over time. Because we were aware that the sum of all the above waste products of fish excretion products does not reflect the total amount of nitrogen produced by fish (see Kajimura et al. 2004) we decided to take an extra measure to reach a more conservative estimate of N production by fish.

2) We also measured the increase of total dissolved nitrogen by filtering samples immediately upon collection and using the inexpensive but accurate CHN analyzer system available at the University of Washington Routine Chemistry Laboratory in the Oceanography Department.

In both cases, duplicate samples were drawn from about 15% of the samples as a means of quality control and assessed and analyzed for precision by the Relative Percent Difference (RPD) methodology as follows:

**RPD = 2 * [A - B] / A + B * (100)**

Where:

- RPD is the relative percent difference between duplicate determinations.
- A and B are the results for the duplicate determinations.
- [A-B] is the absolute difference between the determinations
- Result consistently showed RPD to average > 1%.


Figures 51 and 52 summarize total ammonia nitrogen production rates in trials post feeding to assess rates of change. For moi (Figure 51), the ammonia production peaked near three hours for large moi but was probably later for small moi with maximum rates of ~15 and ~ 25 mg N/kg fish/hr. Timing of maximum N production was similar for cobia (Figure 52), but only large fish assessed as these fish continue to grow to a much larger size in culture than moi. These fish had similar but slightly higher rates of ammonia production than moi and this would be expected given their highly impressive growth rate. Brett and Zala (1975, see below Figure 53) reported large increase in ammonia production about 4 hours after feeding of sockeye salmon, but constant and relatively low rates of production of urea concurrently.

Like salmon, urea production (not shown in the figure) was relatively constant for moi at ~2 mg/kg/hr and ~ 4 mg/kg/hr for cobia. Ammonia + urea only accounted for approximately 62% of the total dissolved nitrogen produced by moi. Measured ammonia + urea production of cobia only accounted for 39% of the dissolved total dissolved nitrogen production. This was a very surprising result and could be an artifact of the experiment, but we think not as the cobia in particular were very relaxed and accepting of their fate in the static bioassays. They expressed no panic or trauma, but the moi began to do so after 9 or more hours in the containers, and some became highly stressed, bright red and died by 11 hours.
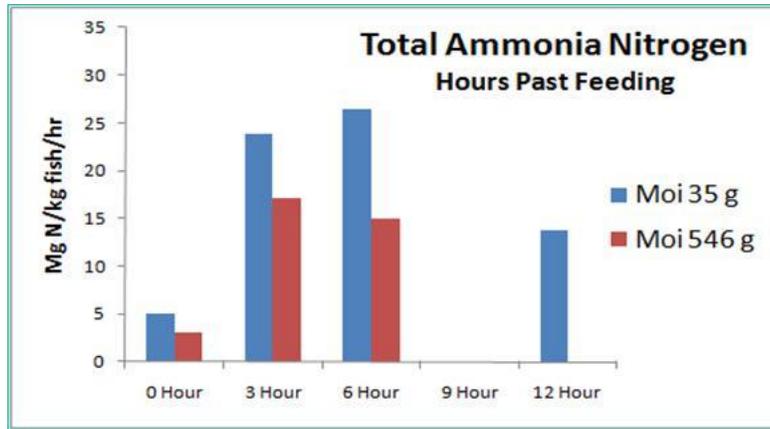
**Figure 51.  Total ammonia production of small and large moi at intervals post feeding.**
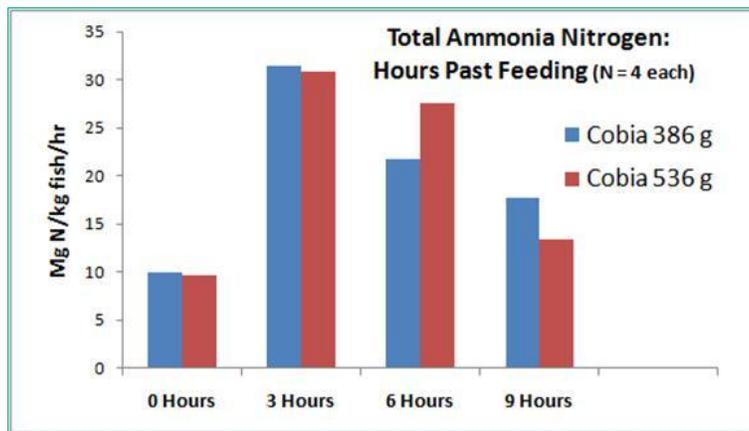


**Figure 52.  Total ammonia production of cobia at intervals post feeding.**
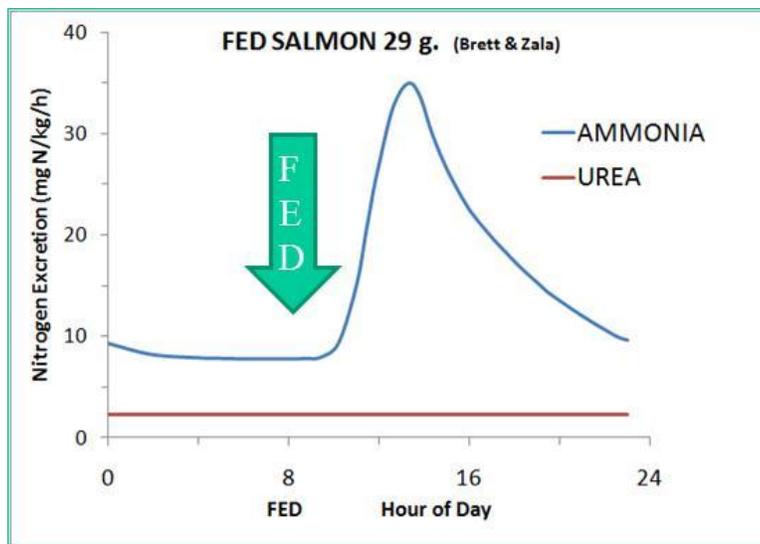


**Figure 53.  Rates of ammonia and urea production of sockeye salmon, redrawn from Brett and Zala (1975).**

Neither moi or cobia had rates of ammonia or urea production that were much different than the sockeye salmon of Brett and Zala (1975), although those fish were smaller than the average sized moi or cobia and thus not strictly comparable.

## Fecal Settling Rates Results

Using our newly devised fish fecal settling device and methodology describe above, we conducted numerous trials for both moi and cobia. These data are summarized in Figure 54.
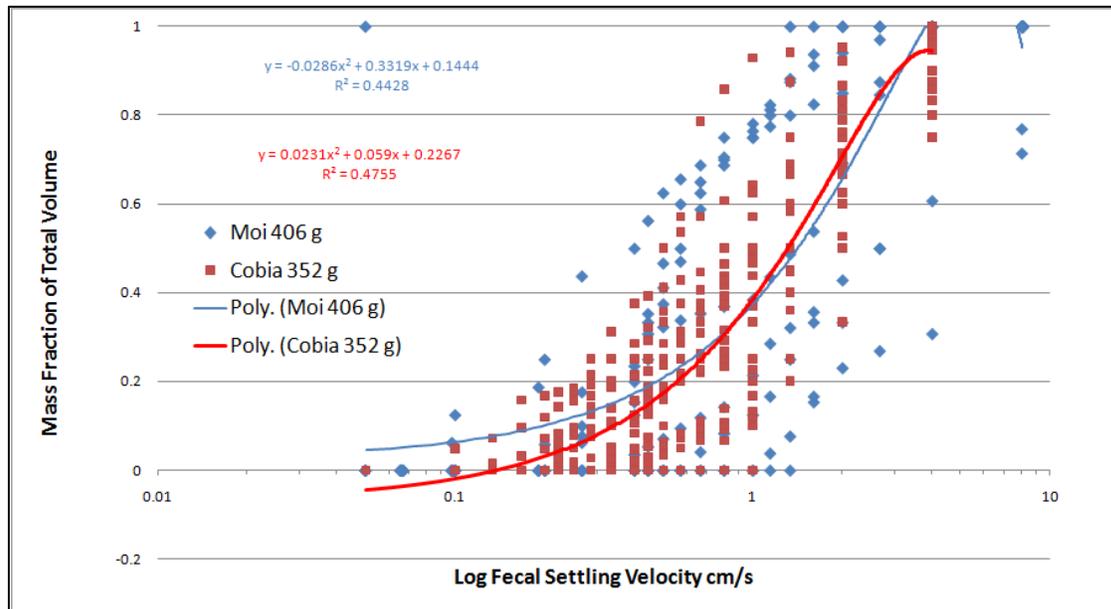


**Figure 54. Cobia and moi fecal settling rates on a semi log scale.**

A quadratic trendline fit was used in Figure 54 and produced a very similar result for both moi and cobia. The mean distributions were slightly less than 1.0 cm sec$^{-1}$, similar to other marine fish recent tested but much slower than salmon. Unlike salmon, range of rates is small regardless of fish size. Salmon fecal settling ranges from 0.5 to 9 cm sec$^{-1}$ but both moi and cobia only ranged from 0.1 to 1.2 cm sec$^{-1}$. The data was inspected and analyzed for other non normal distributions reported by others for other species of fish (.e.g., bimodal) but we believe a simple mean value adequately describes the results.

# Apparent Digestibility Results

Apparent digestibility (intake minus output) of a standard diet was determined in order to assess the mass balance flow of carbon and nitrogen in the diet. A diet containing the indigestible marker tritium oxide and formulated in the NOAA NWFSC lab has been produced to determine dry mater and protein (nitrogen) digestibility. The diet is described by Table 3 including proximate analysis.

Our methods involved anesthetizing the fish five hours after feeding and stripping the feces into a Petri dish by hand. This method worked well for cobia however moi proved difficult to strip feces from and also had a difficult time recovering from the handling stress. Because of this limited feces were available for analysis from Moi and only the dry matter ADC could be estimated (Table 4). Cobia ADC's were determined twice, because in the first run there was insufficient material to determine carbon ADC.

**Table 3. Formulation of diet used for digestibility determinations and proximate analysis.**

| Ingredient | g kg$^{-1}$ |
|---|---|
| Fish meal | 650 |
| Fish oil | 195 |
| Wheat flour | 132 |
| Vitamin Premix[1] | 10 |
| Choline Chloride (70%) | 6 |
| Vitamin C poly phosphate (Stay-C$^{tm}$) | 3 |
| Yttrium oxide | 3 |
| Trace Mineral Mix[2] | 1 |
| **Total** | **1000** |

Proximate analysis: dry weight basis 50.4% protein, 25.3% lipid, 8.1% ash

[1] Vitamin mix was ARS 704 as listed in Barrows et al. 2009.

[2] Trace mineral mix was USFWS #3 as listed by Hardy 1989.

**Table 4.  Apparent digestibility coefficients for Juvenile Moi and Cobia fed the diet in the table above.  Data are means of three trials ± Standard Deviation.**

| Species | N (protein) | Carbon | Lipid | Dry Matter |
|---|---|---|---|---|
| Cobia (A) | 75.4±4.1% | 74.1±1.2 | NA | 62.8±3.9% |
| Cobia (B) | 71.7±5.9 | NA | 84.1±6.0 | 59.6±10.8% |
| Moi | NA | NA | NA | 75.43% |

The physiological data reported here was converted into mathematical relationships using Mathmatica software and then coded into the AquaModel software program to conduct the moi fish farm theoretical siting evaluations reported later in this document.

# Task 6.  Use revised *AquaModel* to develop a mariculture information system useable in the Hawai'ian Islands

We developed a web site ([http://AquaModel.com/usda](http://AquaModel.com/usda)) to implement the Hawai'i Department of Agriculture mariculture information system.  As shown in Figure 55, this web site includes descriptions of the project objectives and study, the updated *AquaModel* features, and of the Hawai'i evaluation site.  The web site includes a dynamic demonstration simulations of the Hawai'i site that can be viewed in either GoogleMaps, GoogleEarth, or using our proprietary NetViewer internet capability.
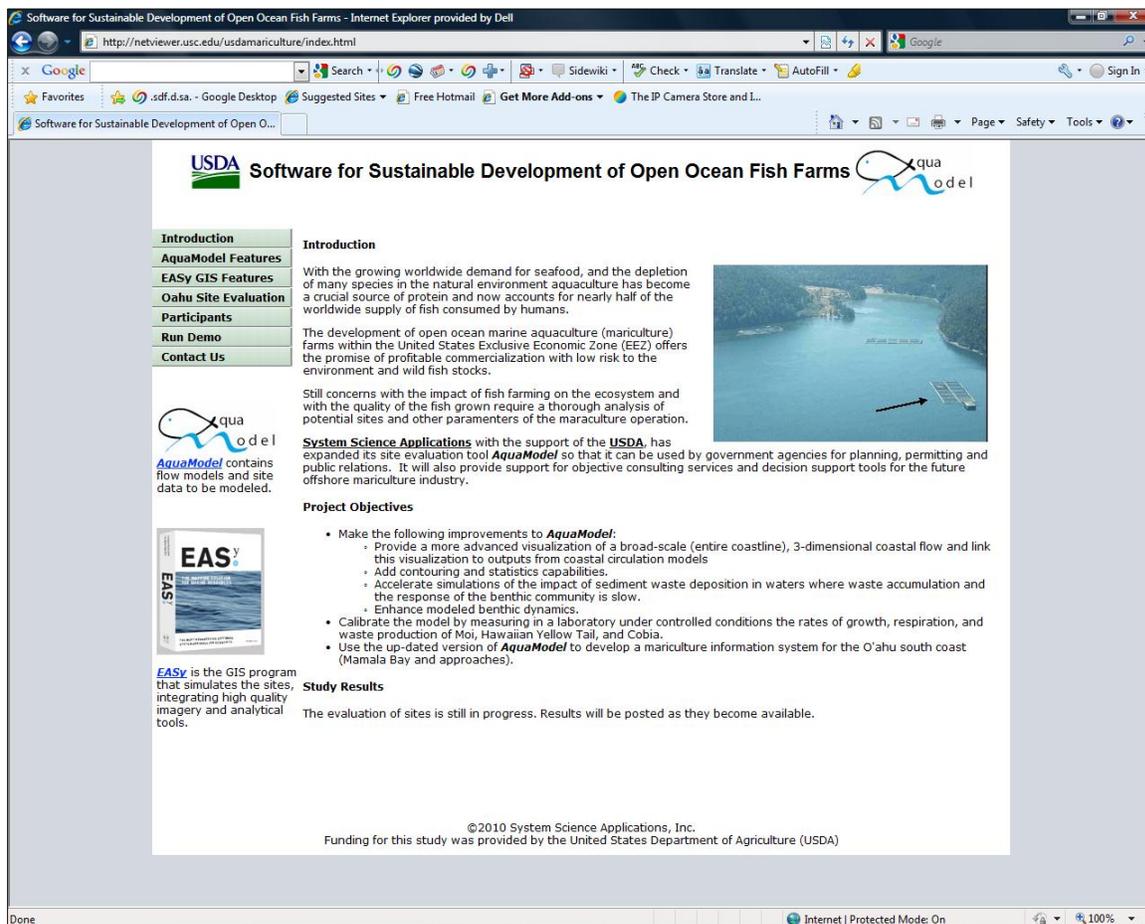


**Figure 55.   The Hawai'i Department of Agriculture mariculture information system includes study objectives, study results, description of *AquaModel*, and a dynamic simulation of the simulated Hawai'i evaluation site.**

# Single Fish Farm Model Results – Near Field

This section presents the results of a single net pen placement and operation along the northwest coast of the big island of Hawai'i. The simulation is termed "near-field" as it focuses on those conditions nearest to the pens that may be perturbed by a fish net pen including dissolved oxygen in the water column and sediments and all other sediment effects. This study location was near the site of a previous acoustic Doppler current meter recording of one month duration from 5 April 2008 to 3 May 2008 that was used to perform this two dimensional assessment. The study site was about 1.7 km offshore in 106 meters depth, relatively deep for a farm in Hawai'i or anywhere else but of similar depth to a fish farm recently planned for Southern California near San Diego. Placement of a fish farm this far offshore in deep water was done as a conservative measure to avoid nutrient plume impingement upon nearshore habitats that are sensitive to anthropogenic sources of nitrogen. Characteristics of the study site and operation are shown in Table 5 and the site vicinity and layout map is shown as Figure 56.

**Table 5. Near-field fish farm study site and facility characteristics (MT = metric ton)**

| Characteristic or Parameter | Near Field |
|---|---|
| Dimensions of a single pen footprint (L x W x D) | 50m x 50m x 12m deep |
| Volume of each net pen | 30,000 $m^3$ |
| Volume of entire fish farm (12 net pens) | 360,000 $m^3$ |
| Depth of water at study site | 106 m |
| GPS coordinates | N20.15043  W155.91445 |
| Modeling domain area | 32.08 $km^2$ * |
| Fish initial size | 10 g |
| Number of fish stocked per entire fish farm | 3.6 million |
| Duration of simulation | 7 months |
| Initial fish loading | 0.1 kg $m^{-3}$ |
| Initial loading per study site | 36 MT ** |
| Feed C composition (Fraction) | 0.44 |
| Feed N composition (Fraction) | 0.07 |
| Biomass per fish farm at harvest | 1,980 MT |
| Feed loss rate | 3% |
| Horizontal diffusion rate Kh | 0.400 $m^2 s^{-1}$ |
| Vertical diffusion rate Kv (surface / deep) | 0.010 / 0.005 $m^2 s^{-1}$ |

*141 x 91 cells, each cell 2,500 $m^2$ overlapping onto the island

**0.1 kg $m^{-3}$ x 360,000 $m^3$ each
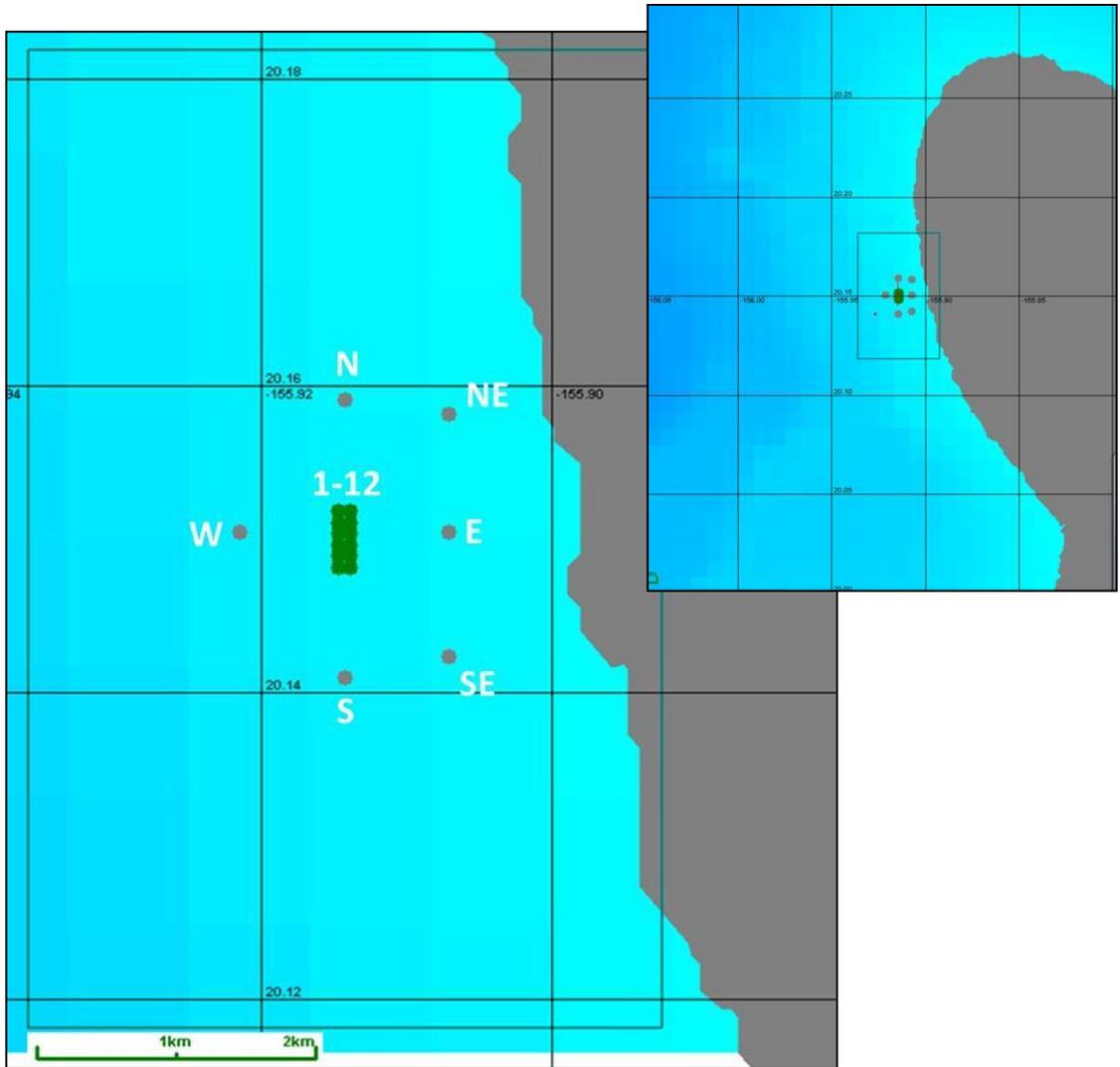
**Figure 56. Layout and location of single net pen farm of 12 cages (in green) near NW coast of Island of Hawai'i (Kohala coast). Shown with vicinity map (right) and surrounding data capture cells (grey single dots) labeled by compass direction from the fish farm.**

Most of the waste nitrogen produced by fish is in the dissolved form, and readily transported by ambient currents wherever they may flow. The waste nitrogen is, however, not a conservative component of seawater but is both diluted by horizontal and vertical mixing and cycled through the aquatic food web. The immediate concern in this case is not stimulation of phytoplankton blooms, but to avoid undue enrichment of attached benthic vegetation forms that could adversely affect nearshore reefs and waters (e.g., *Cladophora* spp). Many nearshore areas in the Hawai'ian Islands are already adversely affected by terrestrial, anthropogenic sources of nutrients that are transported by groundwater into shallow coastal areas resulting in coral reef degradation (Friedlander

et al. 2008). Numerous coral reefs occur in the studied region and it would be unacceptable to adversely impact them from net pen nutrients. Therefore this is a primary target of our studies in simulating the release and fate of such waste matter. Within any given region there may be acceptable or unacceptable sites for specified production levels of fish farming. Such analyses are impossible without a simulation model such as *AquaModel*. We begin by discussing water flow and the system used to simulate it in the modeling region.

## Hydrodynamics Single Fish Farm Site

The flow field in *AquaModel* can be either 2 or 3-dimensional or some combination of both. For the basic, single farm near field assessment, we relied on detailed acoustic Doppler current meter results collected at a suitable offshore location nearby (but not at this exact site) and depth in the middle of our modeling domain. The data was collected by a professional marine scientist from the state of Hawai'i using suitable protocols, equipment and positioning methods. The data was processed and inspected for outliers, particularly high end values and subjected to other types of analyses used to detect possible errors.

In 2-dimensional simulations advection only occurs horizontally; neither divergence nor convergence flow occurs within the array. Small scale horizontal and vertical turbulent motions are treated as described in the previous paragraph. Much of the data on circulation collected at mariculture sites come from field measurements with acoustic Doppler current profilers, drogues, or current meters. In other cases information may come from simple tidal models. Such information is well suited to 2-dimensional simulations.

Table 6 presents the mean near-surface velocity of 26.1 cm s$^{-1}$, a rate that is relatively strong for fish net pens, but in this case somewhat variable as indicated by the standard deviation of 13.3 cm s$^{-1}$. The bottom velocity is also strong, relative to the rate of flow necessary to resuspend fish fecal wastes. That velocity is unknown for moi feces but without doubt, much lower than that estimated for salmonids, which is less than 10 cm s$^{-1}$ for unconsolidated wastes. Examination of the current velocity record (not shown here for brevity) indicates no periods of sustained low current velocity, hence the degree of waste consolidation on the sea bottom at the site would be very low or non-existent. The combined circulation model generated current vectors for the entire modeling domain as shown as the differing length arrows in the screen print figures shown in this document.

**Table 6. Near surface and bottom current velocity averages and SD for near field net pen study site.**

| Measure | Near Surface (cm sec$^{-1}$) | Near Bottom (cm sec$^{-1}$) |
|---|---|---|
| Average | 26.1 | 14.4 |
| Standard Deviation | 13.3 | 7.9 |

Published estimates of the preferred range of current velocity suitable for net pen culture is typically in the range of 10 to 50 cm s$^{-1}$ but in actual practice, sustained velocity exceeding 20 cm s$^{-1}$ is a challenge to maintain net cage shape for so-called "gravity" cages. Many types of net pen cages are commercially available, but the most economical are surface cages and with the advances in HDPE cage construction, they are also suitable for open ocean conditions if properly configured and weighted in place with suitably designed circular pen weights and anchoring systems. Submersible systems such as SeaStation or AquaPod cages are arguably more suited for open ocean conditions and provide the most desirable benefit of avoidance of storm wave protection. We make no recommendation of what would be most suitable at this site as that would involve a technical analysis of wave height and frequency that is beyond the scope of this work.

Figures 57 and 58 indicate surface and near bottom current direction frequency diagrams generated from *AquaModel* data for the near field net pen study site. At the surface the strongest component was to the northeast and secondarily to the north. Near the sea bottom, the results were very different, with a dominant flow to the southeast and subdominant flow to the northwest. *AquaModel* interpolates current vectors for intermediate depths when data are not available but in this case the acoustic Doppler data was available and applied.
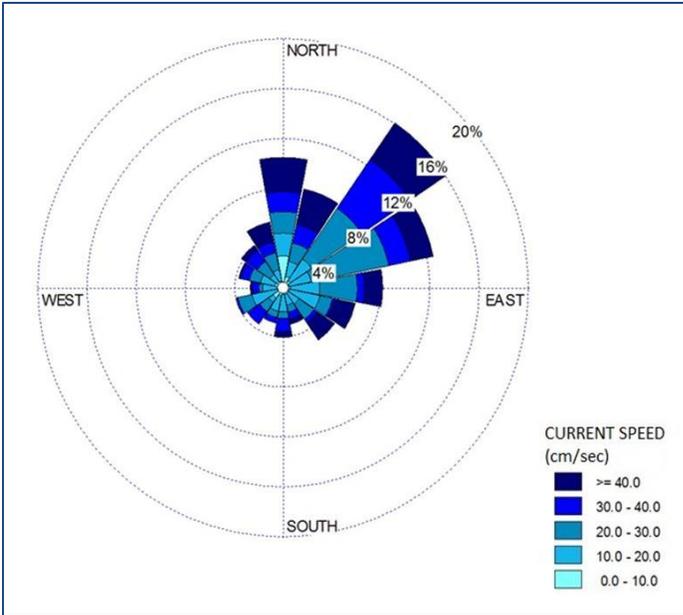
**Figure 57. Near field net pen surface current frequency distribution (cm sec⁻¹, using WRPLOT View software).**
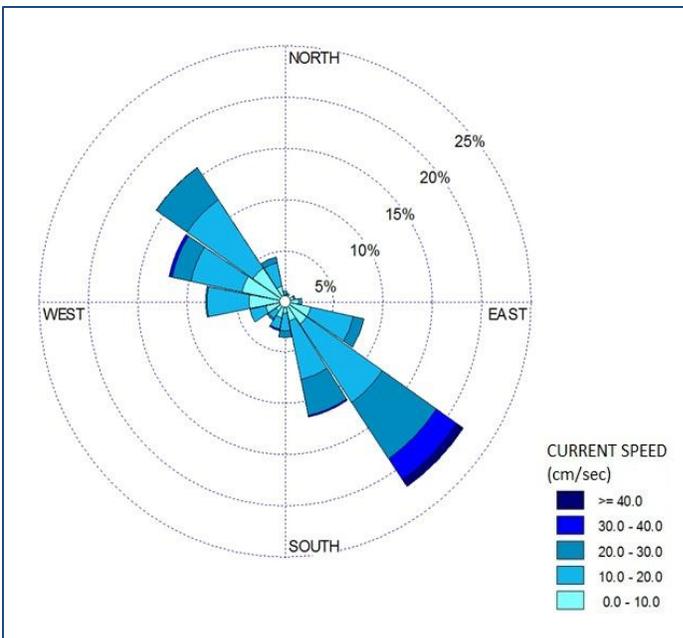


**Figure 58. Near field net pen bottom current frequency distribution (cm sec⁻¹, using WRPLOT View software).**

# Nitrogen Distribution Single Fish Farm Site

Background nitrogen concentration for the modeling simulations was set at 0.1 µM (units equivalent to µg at. $L^{-1}$ or mg at. $m^{-3}$) which is typical of this area and open subtropical and tropical Pacific Ocean conditions.

Figure 56 illustrates conditions at the start of the simulation for nitrogen distribution and assimilation. The XY plot boxes selected from a menu of about 40 options include from upper left counter clockwise include:

1) Total fish weight (biomass) in one of the replicate cages (each cage can be loaded separately with different biomass and even species);

2) nitrogen transect which illustrates a color pattern relative to the concentration along the moveable red transect line running in this case from north to south through the middle of the green circles that represent the location (but not the actual size!) of the net pens;

3) vertical profile of nitrogen at any location in the modeling domain, in this case shown as the small red dot east of the pens and near shore;

4) surface and bottom current velocity at the current time of the model run;

5) the model time, day and hour;

6) the color bar legend, in this case showing green to red, 0 to 4 µM nitrogen with current vector arrow legend below;

7) a Simulation Control Option box that includes a red slide bar on the blue time bar that allows the operator to move rapidly ahead or backwards in the simulation when in replay mode (not always shown in the screen prints herein);

8) the main image of the model showing a plan view of one or more concurrent parameters or GIS images including contours of various data. This image has geoposition shown as the user moves the mouse cursor over the image and by clicking on the image at any location. Values for that location of the presently-selected parameter are shown along the taskbar at the bottom of the window.

Figures 59 through 62 illustrate snapshots of a few of the time steps in the sequence of hundreds of images in this simulation. In most cases, the images show worst-case conditions in terms of higher concentrations of nitrogen. Captions in each figure contain an explanation of the salient features of that time step in the simulation.

Figures 63 through 65 show average overall and monthly nitrogen levels for each near field capture cell and net pen study site.
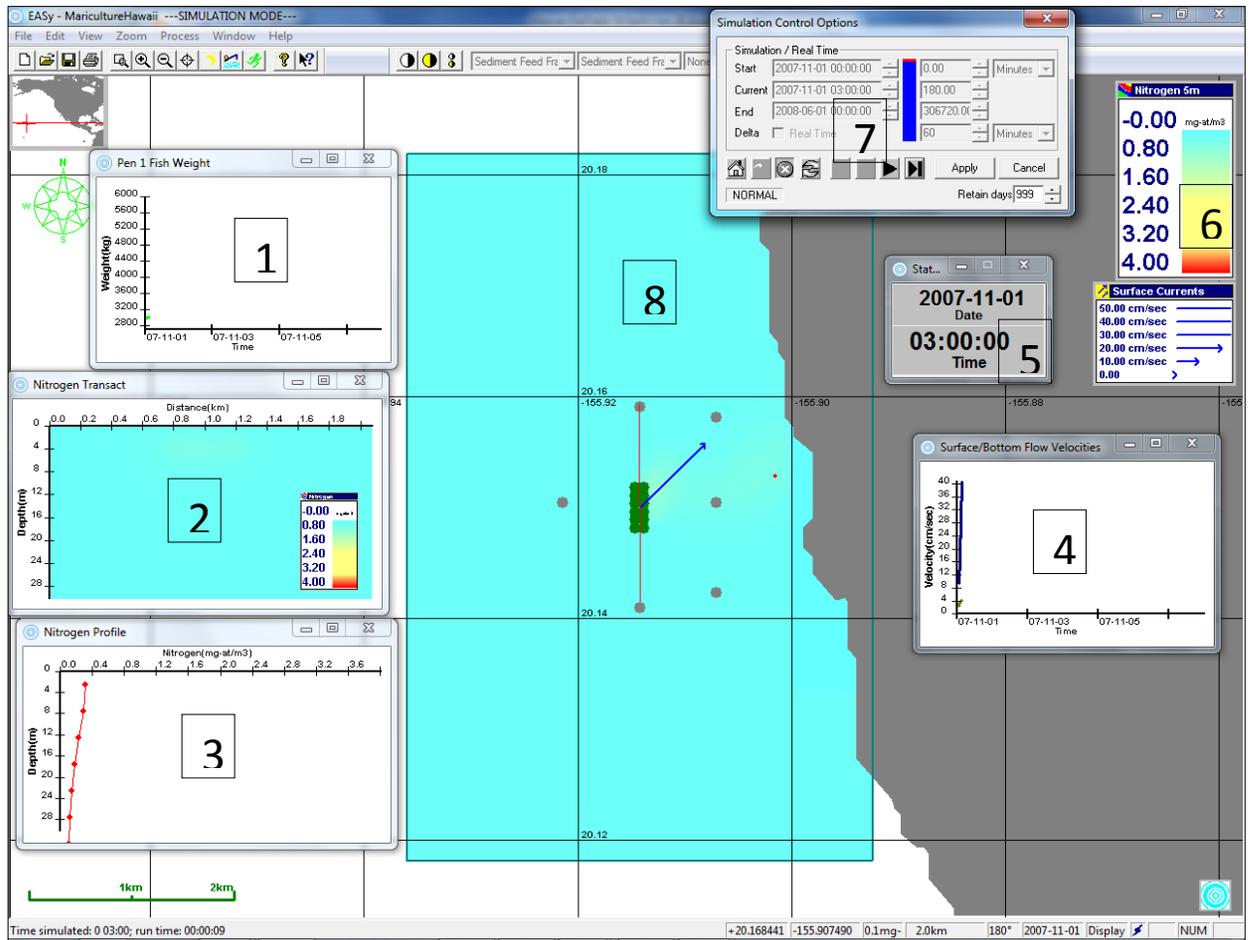
Figure 59. Dissolved nitrogen a few days into the simulation, note red profile point selected nearshore and the very small (0.2 μM, probably not measurable against background variation) increase in N about 1.5 km towards shore at that location. Current vector showing near surface conditions. Fish weight (biomass) about 3 MT per each of the 12 net pens. See prior text for explanation of the numbers superimposed on this figure.
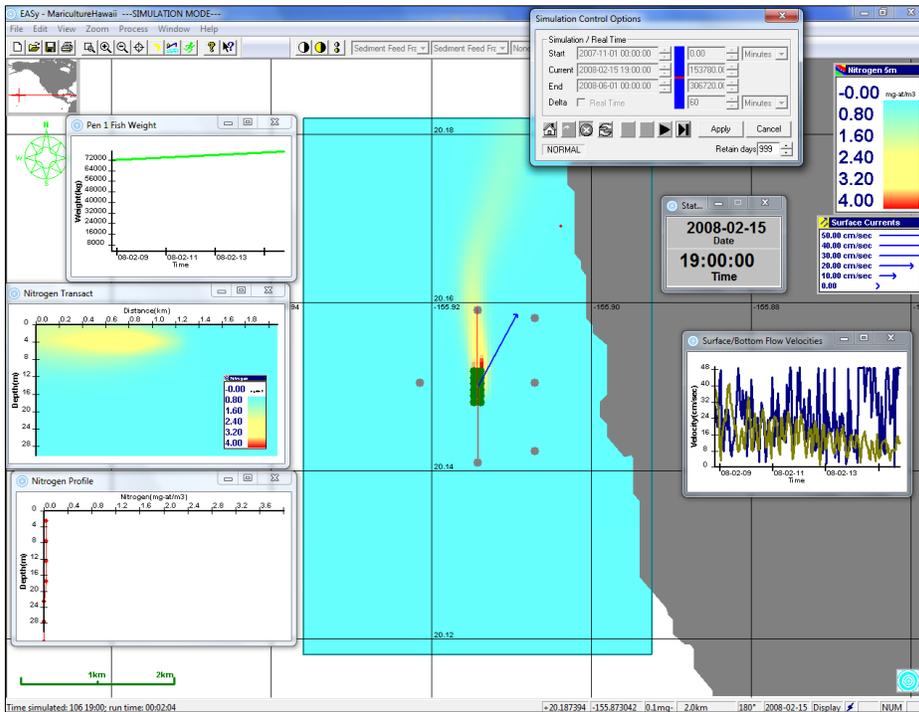
**Figure 60.** Midway through the simulation with 72 MT per net pen and a much more pronounced plume heading NW towards shore at this point in time. An increase of about 0.8 μM or less shown in the red dot profile location.
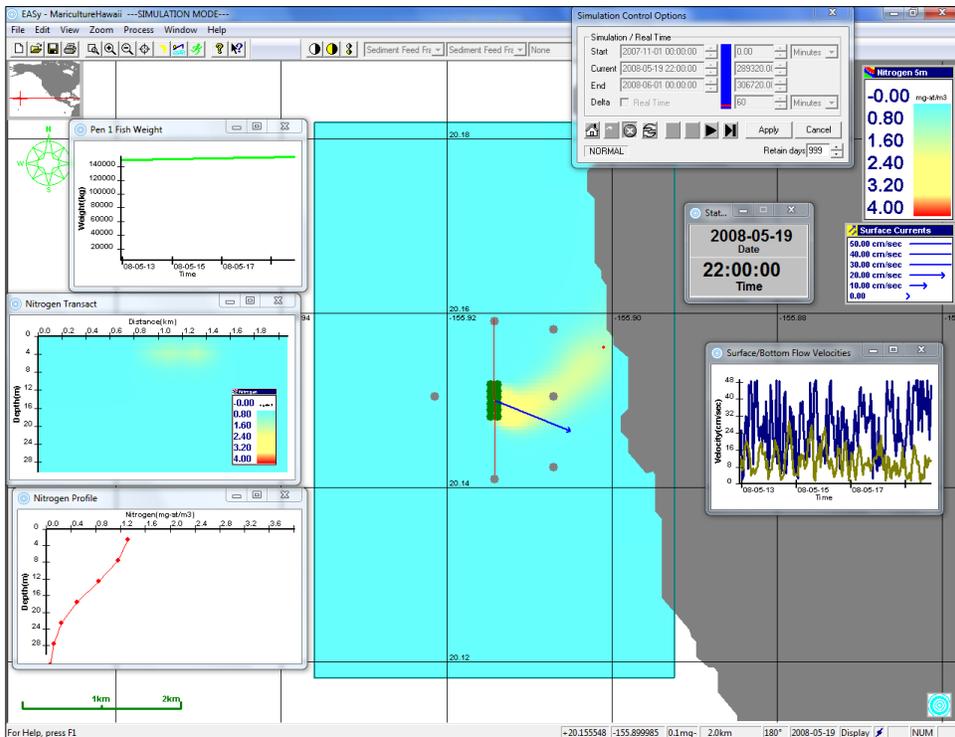


**Figure 61.** Toward the end of the grow out cycle with 140+ MT per each net pen and a much more pronounced plume heading WNW towards shore at this point in time. Note that near shore nitrogen concentration was ~ 1.2 μM.
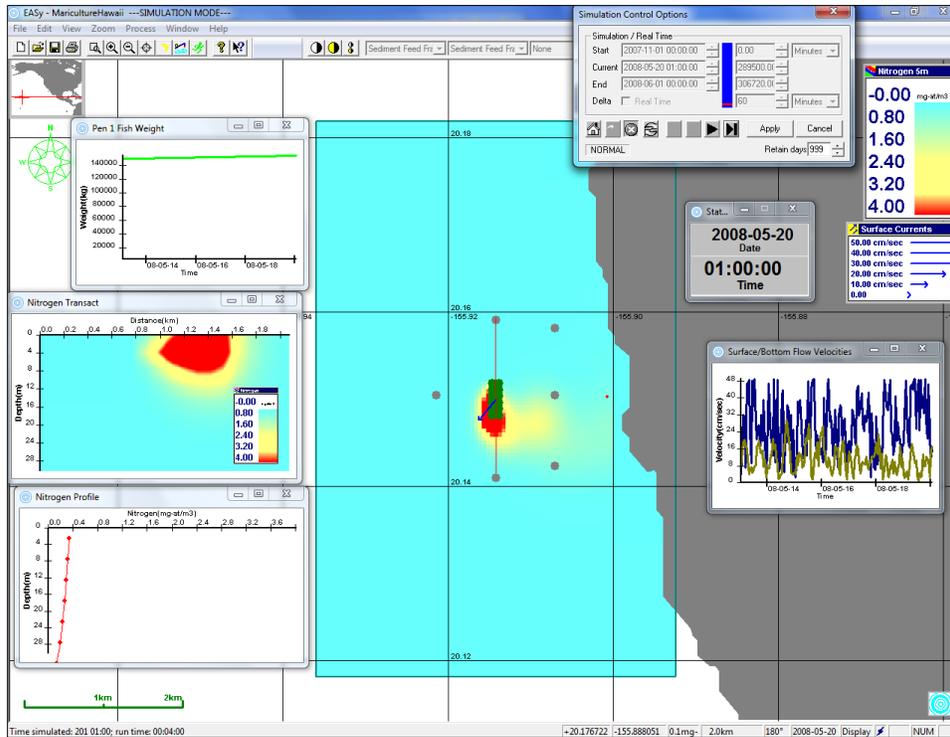
**Figure 62. Only a few hours after the prior time step, and the nitrogen plume has shifted away from the shore and centers around the pens. Nearshore dissolved nitrogen declined to < 0.4 µM, but temporary weak currents at the pens result in ~ 4.0 µM N.**
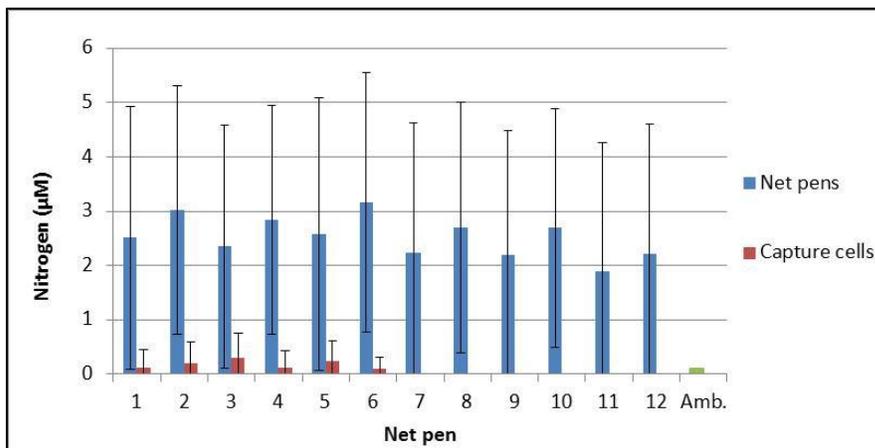


**Figure 63. Average dissolved nitrogen (µM) concentrations at nearfield net pens and associated nearshore capture cells, as well as mean ambient results in green.**
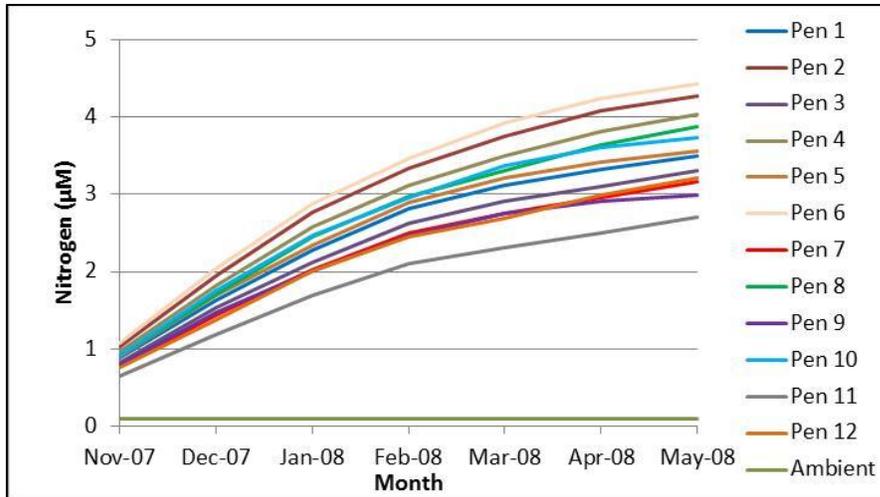
**Figure 64.** Average monthly nitrogen (μM) concentrations at nearfield net pens as well as ambient conditions.
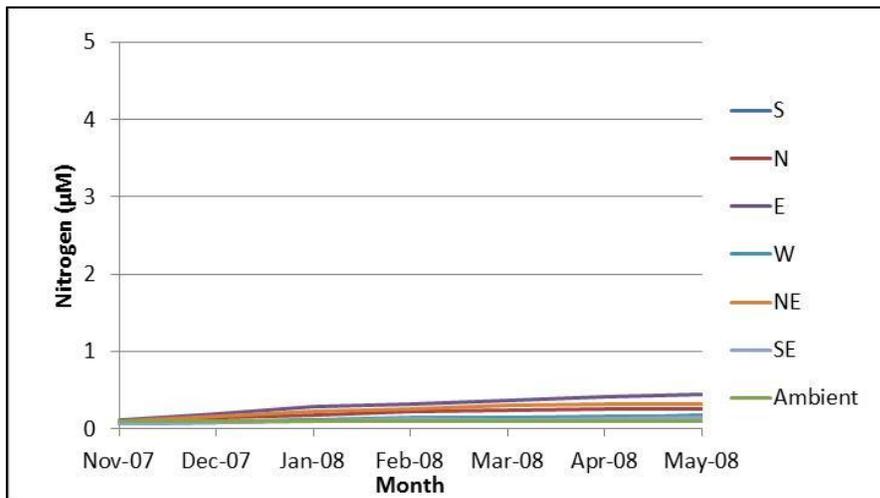


**Figure 65.** Average monthly dissolved nitrogen (μM) concentrations at nearfield capture cells as well as ambient conditions.

# Sediment Effects Single Fish Farm Site

Model results predictably showed that there would be no detectable adverse effects of moi net pens at the chosen location at any time in the production cycle due to the relatively great depth, strong currents and modest level of production selected compared to fish farms located in other locations of the world and operated by large companies.

The model results initially show a very small level of organic carbon enrichment around the net pens (Figure 66), indicated by the small yellow halo. A rule of thumb used in temperate water net pens fish farms where water temperatures in summer are approximately ½ that observed in Hawai'i is that no adverse effects occur at carbon deposition rates less than 1.0 grams carbon per m$^2$ per day (Hargrave et al. 2008). Thus for Hawai'i, a deposition rate of approximatley twice as high might be a threshold of change. Note in Figure 66 at the start of the model run that total organic carbon levels are relatively high, due to a modeling effect where a large initial load is added at the start of any model run. This results in a temporary effect on the bottom that quickly is modified by the strong currents and biological assimilation.

With higher water temperature and essentially no permanent deposition due to the frequent, strong near-bottom current velocity, the model indicates no adverse effect, no reduction of sediment interstitial dissolved oxygen, no sulfide build up, no anaerobic bacteria development, etc. (plots not shown for brevity). These results are similar to what we found in similar depths and current velocities for a site eight km offshore of Mission Beach and San Diego (Kiefer et al. 2008). Based on literature and observations worldwide discussed in that document, we would expect a very mild positive effect on the diversity and abundance of benthic infauna and no species composition change.

Figure 67 is an example of results near the end of the production cycle and fish havest. No effect is seen except a very minimal 0.02 percent total organic carbon increase from ambient immediately beneath the pens as indicated in both XY plots pertaining to total sediment fractional and waste profiles.

As a quality control check on these predictions, we observed simulated suspended sediment flux across the bottom as shown in Figures 68 and 69. In this mode, *AquaModel* shows the fish farm origin sediment flux real time in plan and sectional view. The wastes from the farm are much finer than the native coarse sand sediments and thus are easily suspended and move. A key point is that this process is NOT simply dilution, but amounts to dilution and assimilation in an aerobic fashion. Assimilation by benthic aerobes and invertebrates of the organic carbon containing solids is a key component of sustainability of properly sited fish net pens.
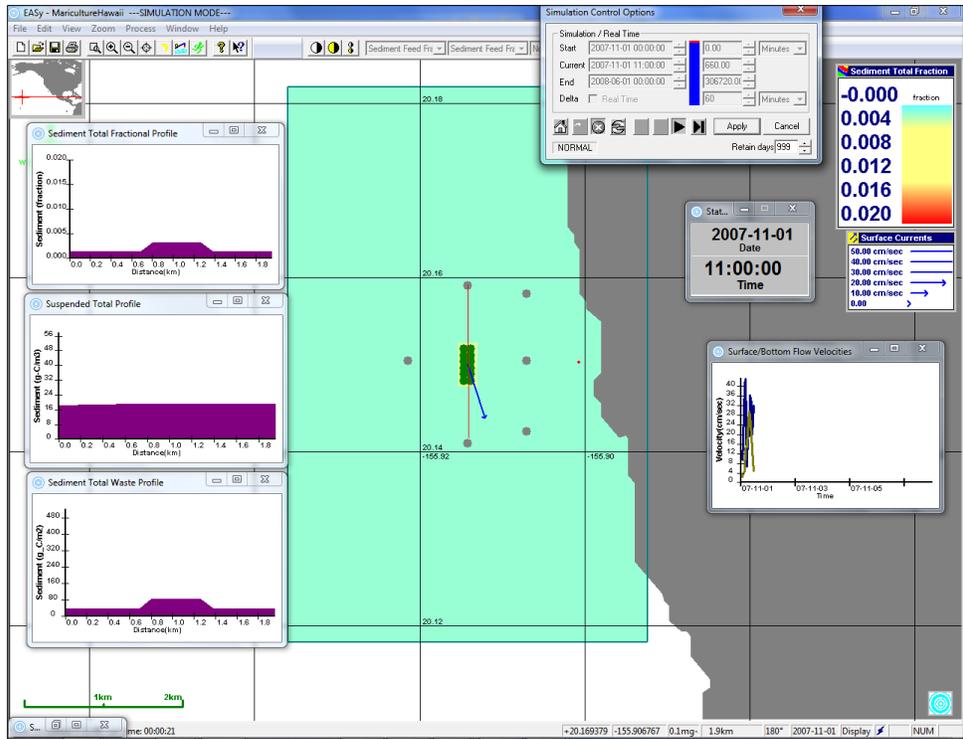
**Figure 66.  Initial effects of total organic carbon on the seabottom shown as the slight yellow halo immediately around the theoretical net pens.**
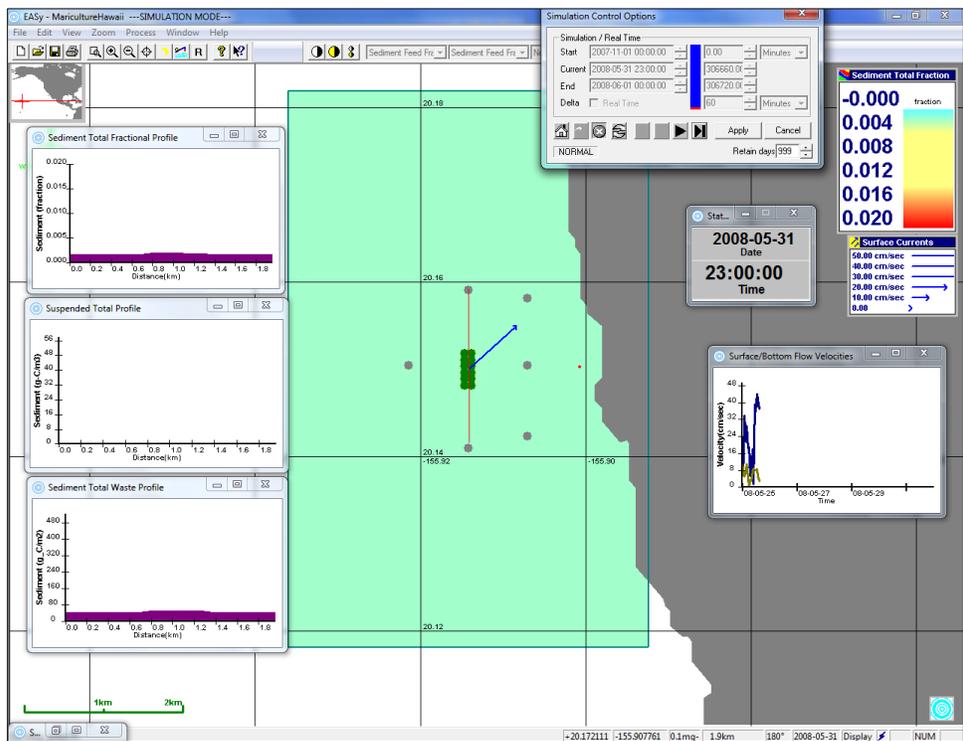


**Figure 67.  Typical result for total organic carbon at the end of a model run.**
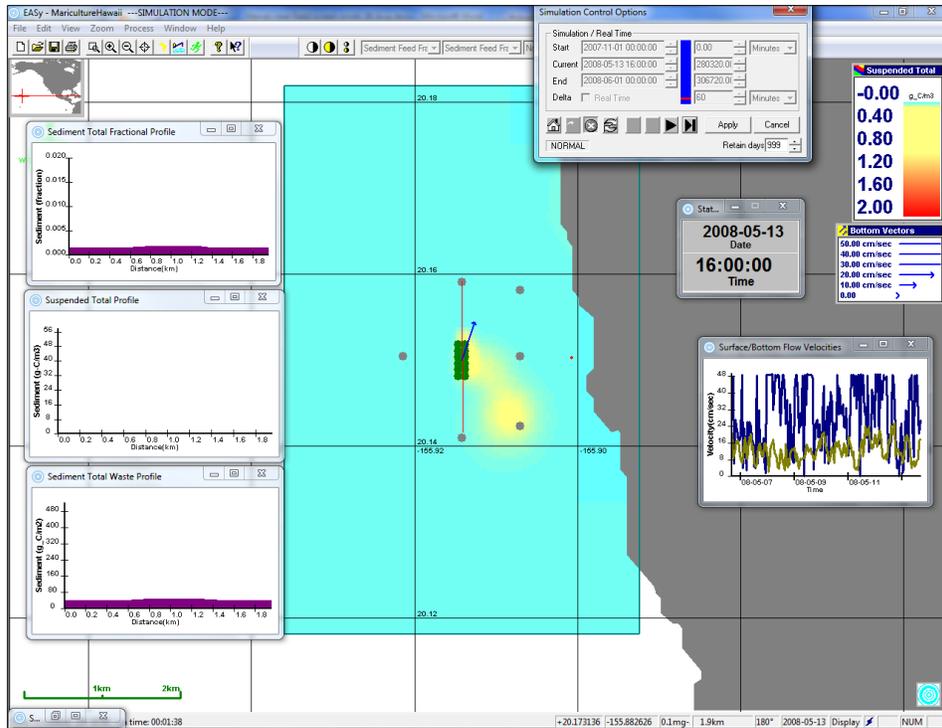
**Figure 68.** Model observation near production cycle completion indicating flow of suspended total fish farm origin sediments across the seafloor (NOT sediment TOC).
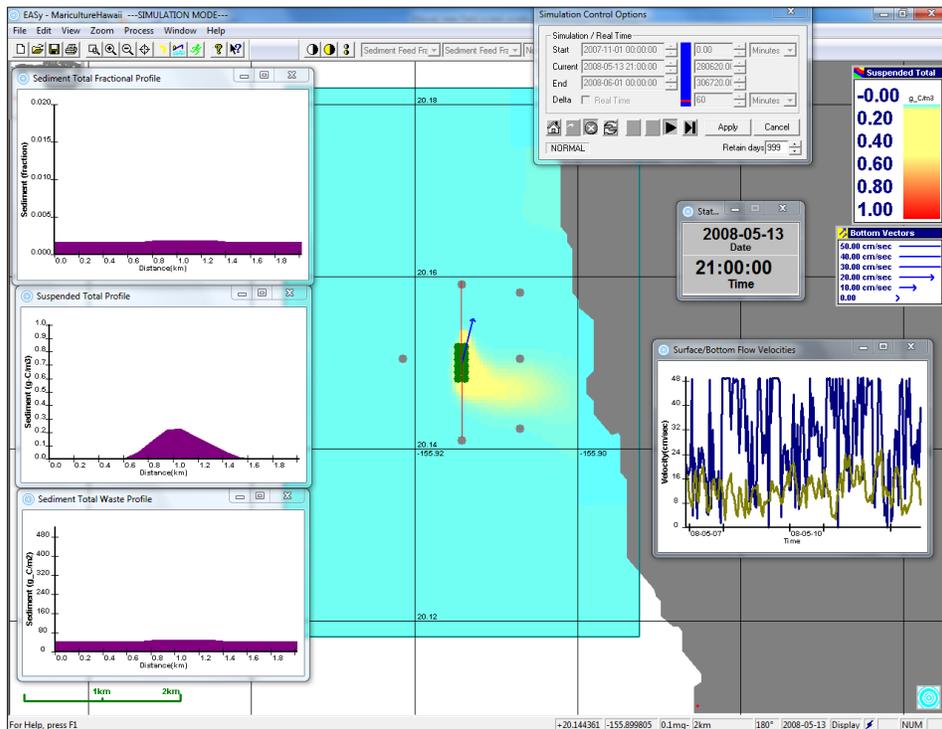


**Figure 69.** Same as the prior figure but five hours later while current velocity remained slow.

# Phytoplankton Effects Single Fish Farm Site

Directly linked to the dissolved nitrogen production, *AquaModel* calculates over time and space the resulting phytoplankton production after we input the background concentration of phytoplankton and some kinetics involving uptake and growth rate of the likely dominant species found in each ecoregion or time of year. In this case, conditions are relatively constant as well as water temperature in the mixed layer.

Figures 70 through 74 are *AquaModel* screen prints illustrating the distributions and dynamics of dissolved nitrogen (dissolved inorganic nitrogen + urea) and phytoplankton standing stock in the subject area as determined by the production of dissolved nitrogenous waste by the single, 12 cage fish farm. The simulation runs from November 1, 2007 through May 31, 2008 and periodic screen prints are presented for later in the production cycle as there was no measurable effect early on.

From the prior raster image of the 5m deep concentration of dissolved nitrogen, we can see that the farms have released sufficient nitrogen to produce large but dilute plumes of elevated nitrogen downstream of the farms. In Figures 70 through 74 we see the time delayed response (doubling times of at least a day) of the phytoplankton indicated as the yellow colored areas. In all cases the color palette was adjusted so that an effect could be shown, and in general the concentration (standing stock) of phytoplankton in the affected areas was < 0.3 µg $L^{-1}$ chlorophyll *a*. Definitions of what constitutes a bloom vary by expert and ecoregion, but very infrequent small increases of nitrogen in coastal waters doesn't necessarily indicate an ecological problem in the case of several of these theoretical net pen sites. However, nutrient effects are cumulative, so if there are other anthropogenic sources of nitrogen in affected areas, exceedence of a biological threshold could occur to create a problem. Of particular focus at this site is the dominant northeasterly current direction that tends to push water passing through the pens in that direction and towards shore. At a distance of approximately 1.6 km offshore and mean surface current velocity of 26 cm $sec^{-1}$, it would only take a few hours for a persistent current to push nitrogen bearing water on shore. Dilution and assimilation occurs, as shown by the model and basic understandings of such phenomenon, but some nitrogen would reach shore as the model demonstrates. Figures 75 and 76 show summary figures representing overall and monthly average phytoplankton levels.

It would be preferential to have the nitrogen sequestered by phytoplankton rather than flow near shore to be used by attached benthic vegetation that could adversely affect shallow coral reefs of other sensitive nearshore habitats. However, we see in these images that there is a tendency for a minor accumulation of phytoplankton in areas near the sites within Kawaihae Bay, actually more of bight than a bay along the Kohala coast.
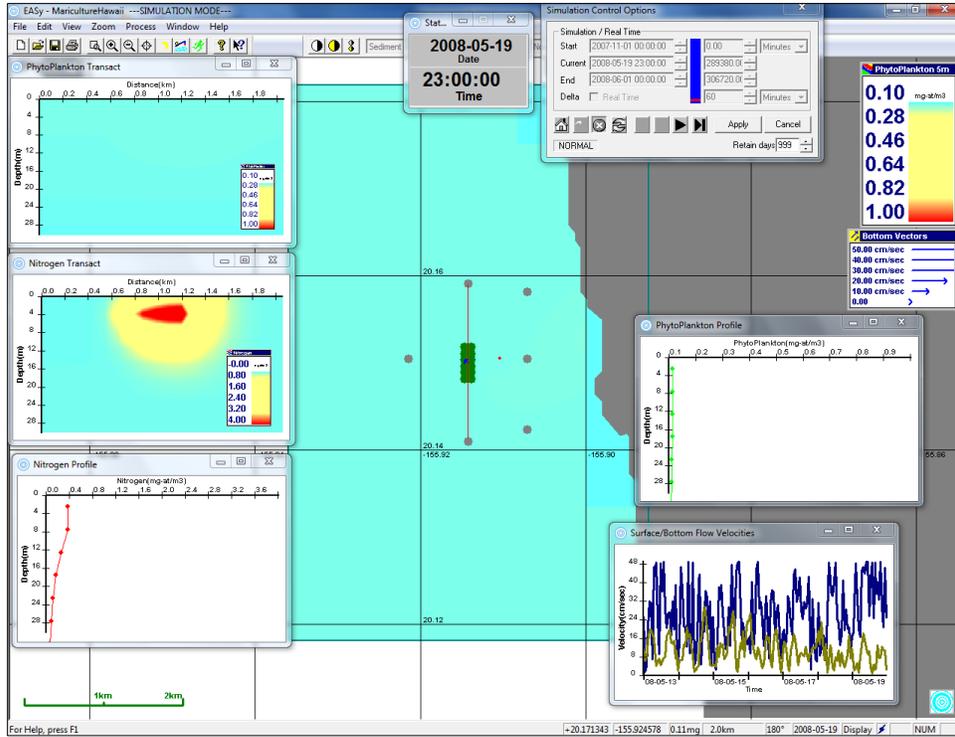
**Figure 70.** Virtually no phytoplankton accumulation with main image showing phytoplankton biomass.
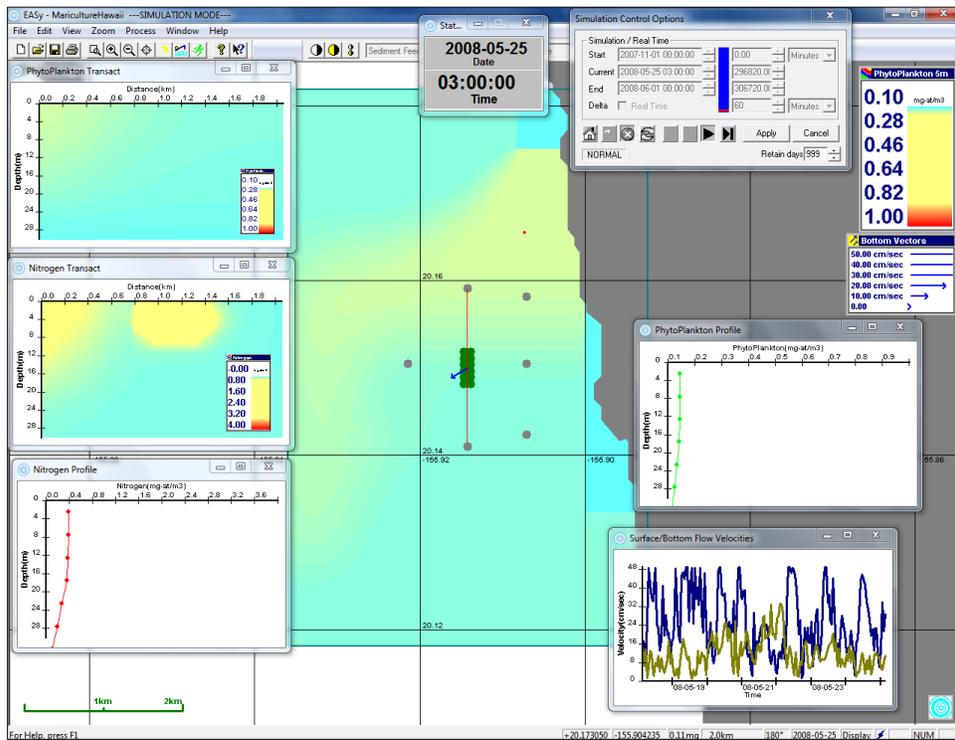


**Figure 71. Minor accumulation of phytoplankton in the region during slow current period.**
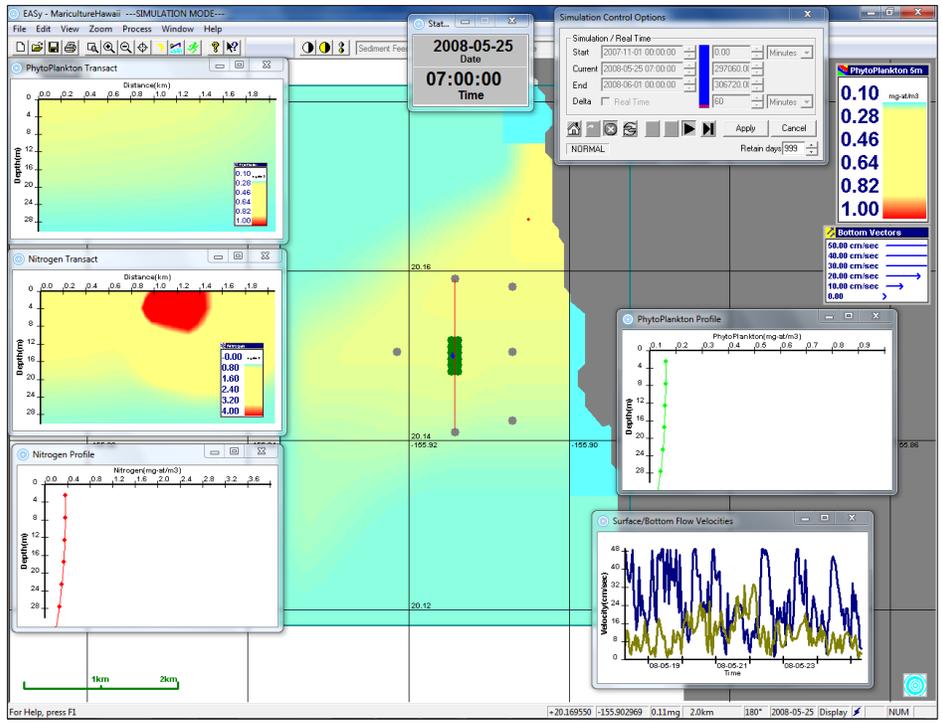
**Figure 72.** Near completion of fish production cycle showing a very small increase in phytoplankton biomass of about 0.2 µg L$^{-1}$. This image represents the worst-case seen in the entire run and was not sustained for more than part of a day.
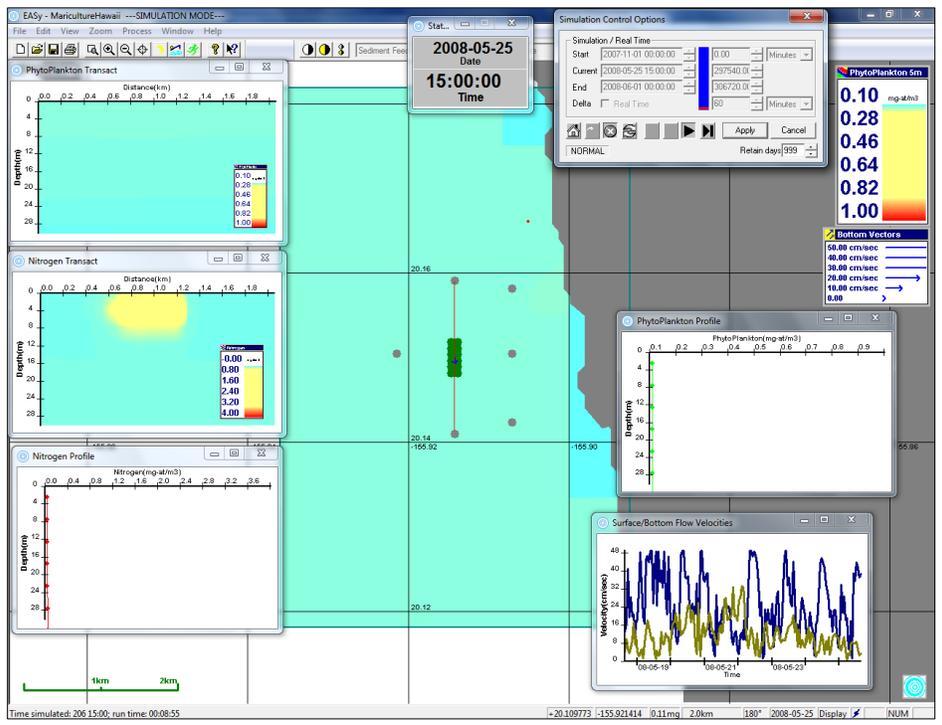


**Figure 73.** Eight hours after the prior screen print and a period of strong currents then back to weak flows but no observable phytoplankton effects.
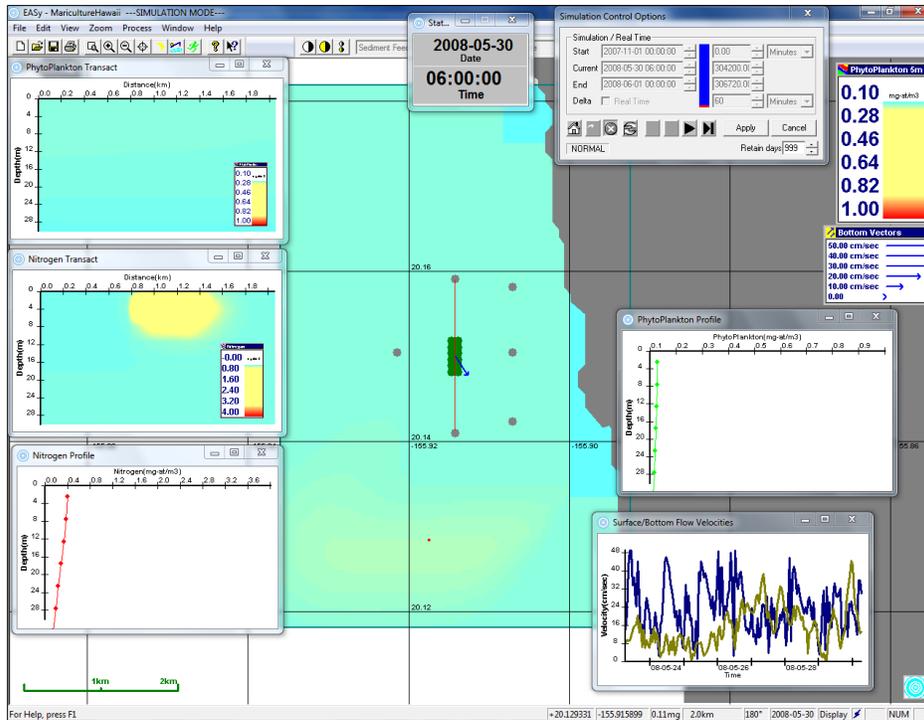
**Figure 74. Five days after the prior image and some minor accumulation of phytoplankton this time south of the fish farm in two time steps only.**
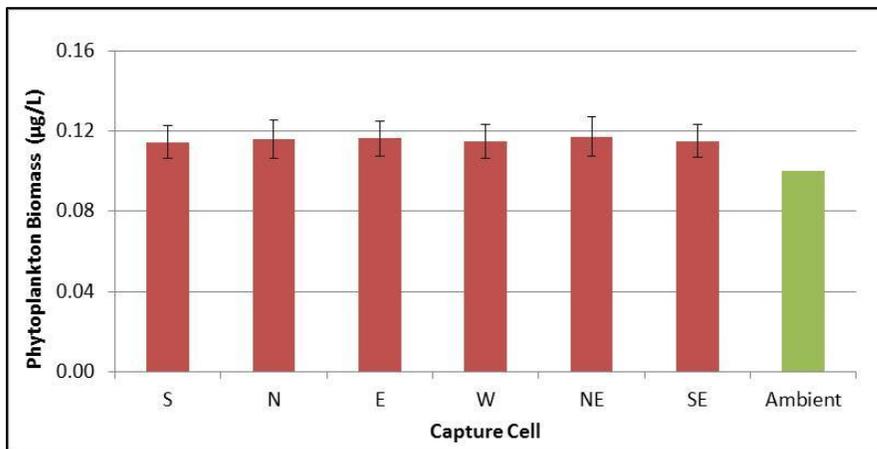


**Figure 75. Average phytoplankton biomass (μg L⁻¹) concentrations at nearfield capture cells as well as ambient conditions in green.**
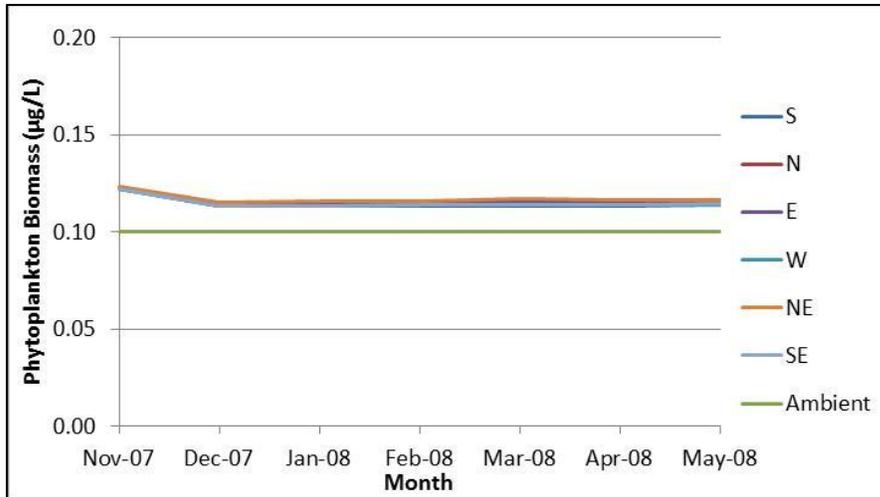
**Figure 76. Average phytoplankton biomass (µg L$^{-1}$) concentrations at nearfield capture cells as well as ambient conditions.**

The results of the phytoplankton assessment indicate that there would be small increases in phytoplankton near the fish farms and in some isolated cases near the shore, but the degree of standing stock enhancement would be on average too small to measure at the nearby capture cell locations (i.e., > 0.02 µg L$^{-1}$ chlorophyll *a*, see Figure 75).

The above plots indicate that there was little difference of phytoplankton biomass among capture cell results despite obvious differences in persistent current direction frequency. Plots of nitrogen concentration showed highest concentrations to the east and northeast, but current direction and velocity was highly variable and given the lag time for phytoplankton cells to sequester nutrient and reproduce (at least a day for a single doubling in general), it is seen that the phytoplankton effects are more diffuse. The phytoplankton effects are also highly ephemeral, mostly absent and none persistent. These data suggest that a fish farm of the size modeled here would be unlikely to have any real biological or measurable effect on phytoplankton dynamics of the subject areas, but one must consider cumulative effects if more than one farm was operated in the region. This is assessed in the next chapter using the far field model option.

# Dissolved Oxygen Single Fish Farm Site

A reduction of dissolved oxygen near large-sized fish farms is common, typically the effect is no more than 50 m distant for a really large farm but most of the prior assessments have been for salmon farms. Respiration rates are higher for most fish in tropical waters, although not linearly greater as would be expected from the Q10 temperature coefficient "rule" of standard metabolism (that averages a factor of two, but varies from 1 to 3). In any event, Figure 77 indicates that by a distance of about 0.5 to 0.8 kilometers (capture cells as red bars) there was no difference compared to the ambient value (green bar). At the farm site, this plot shows a mean reduction of slightly less than 0.2 mg L$^{-1}$, with great variability.
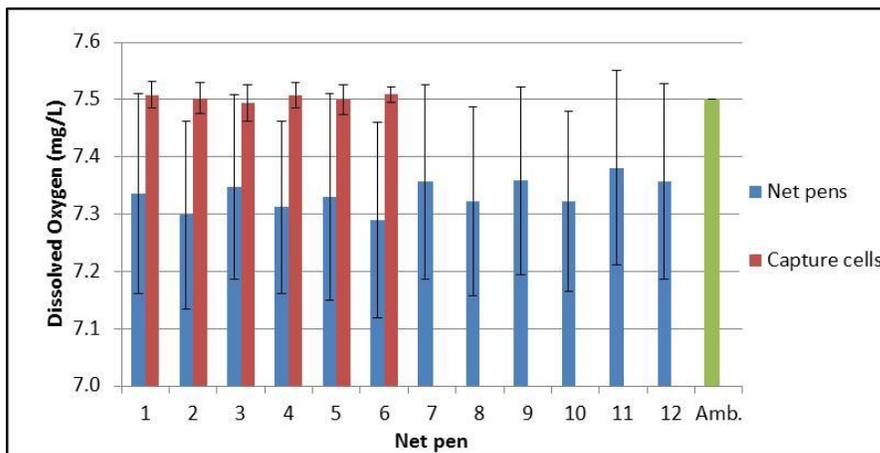


**Figure 77. Average dissolved oxygen (mg L$^{-1}$) concentrations at nearfield net pens and capture cells, as well as ambient conditions in green.**

Likewise, Figures 78 and 79 show mean monthly dissolved oxygen averages; slight decreasing dissolved oxygen levels are evident at the net pens (Figure 78) as time progresses, but at the capture cells, there is no difference compared to ambient levels (Figure 79).
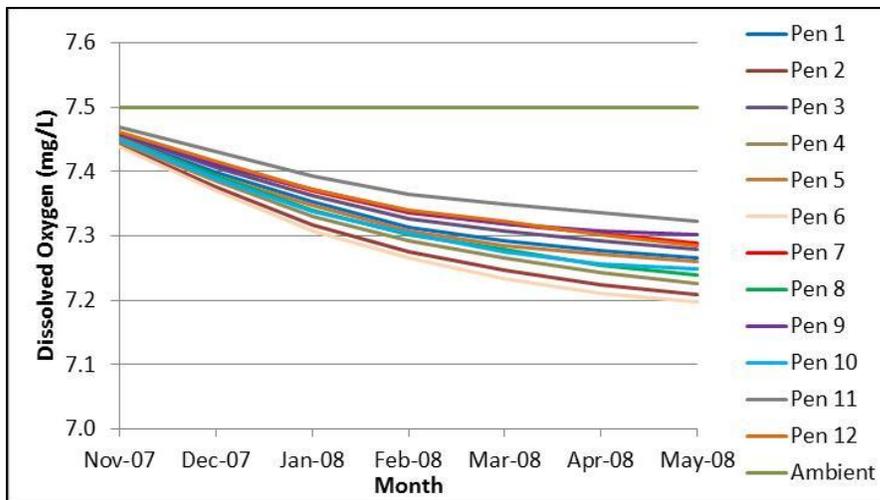
**Figure 78.** Average monthly dissolved oxygen (mg L$^{-1}$) concentrations at nearfield fish pens as well as ambient conditions.
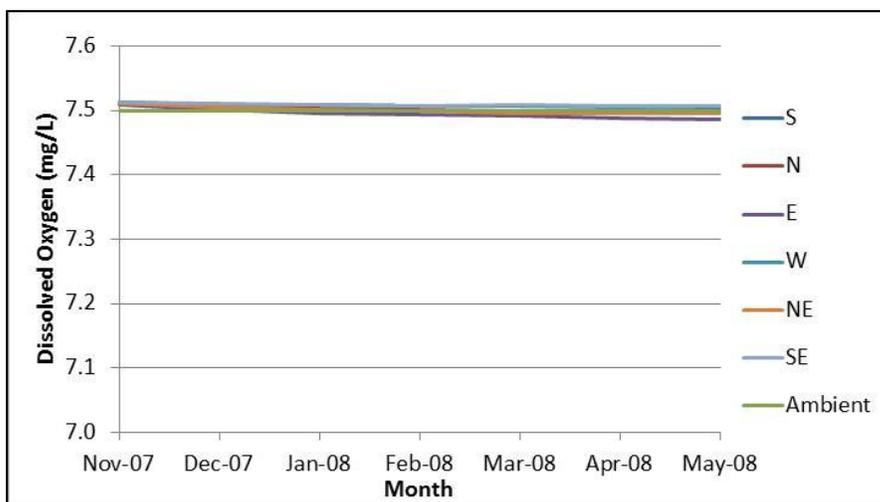


**Figure 79.** Average monthly dissolved oxygen (mg L$^{-1}$) concentrations at nearfield capture cells as well as ambient conditions.

# Multiple Fish Farm Model Results – Far Field

In order to study the effects of several farms in a region that could have cumulative effects on nearshore habitats, we developed a far field modeling system for *AquaModel* as previously described and as summarized below.  We begin by describing the hydrodynamic component of this system.

## Site Locations and Hydrodynamics

In 3-dimensional simulations there are no constraints to movement of water between adjacent cells of a simulation other than the requirement of conservation of mass. Convergent and divergent motion can be represented within the array as well as local eddies.  In addition, the water depth can vary within the array.  Since 3-dimensional flow on small spatial and temporal scales is rarely measured in the field, our 3-dimensional simulations draw upon a 3-D coastal tidal circulation model.  The spatial scale of this model is 1 km and thus small scale turbulence is not included in the output.  However, *AquaModel* provides the user the option to add specified levels of horizontal and vertical eddy diffusivity, the latter for both the surface (mixed) layer and the deep layer.  While rates of horizontal dispersion are constant throughout the computational array, the rates of vertical dispersion can be specified for two layers, the upper mixed layer and the underlying stratified waters.  The depth intervals of the mixed layer and the stratified layers vary with season as a sinusoidal oscillation.

For this far field case, we began by acquiring data from a far field tidal circulation model, with data provided by Drs. James Potemra and Brian Powell of the University of Hawai'i at Mānoa and the Hawai'i Ocean Observation System (HiOOS).  Their model computes baroclinic tides based on an annual mean stratification, which results in loss of interannual variability that might be occurring but this was judged to be a small loss.  The model outputs velocities in several layers, and since the time resolution is short (1 hour), there is too much data to store and instead tidal amplitude (sea level) and velocities at the surface, near the thermocline (around 100m) and near the bottom are recorded at 1-km resolution (pers. comm. J. Potemra to D. Harrison 28 Oct. 2010).  As tidal energy is a minor component of the water flow in this region, we needed to account for the differences by adding in actual data from the region to bring the rates of flows to a level that would actually be experienced in the field.  The tidal data were processed with *AquaModel*'s flow field assimilation subroutine and merged with detailed acoustic Doppler current meter results collected at a suitable offshore location and depth in the middle of our modeling domain as described above in the near field results section.

The combined, merged model generated current velocity estimates at the location of each of the 12 net pens within the single net pen fish farm location as summarized in Table 7. The mean near-surface velocities of each site ranged from 21.0 to 23.4 cm s$^{-1}$. The bottom velocity is also strong, relative to the rate of flow necessary to resuspend fish fecal wastes. The near bottom flow rate necessary to resuspend moi feces is, without doubt, much lower than that estimated for salmonids due to the significant differences in particle size and density. The salmonid rate is less than 10 cm s$^{-1}$ for larger fish and unconsolidated wastes. Examination of the current velocity record (not shown here for brevity) indicates no periods of sustained low current velocity, hence the degree of waste consolidation on the sea bottom at the site would be very low or non-existent. The combined circulation model generated current vectors for the entire modeling domain as shown in the screen print figures shown in this document. Figures 80 through 85 illustrate the percent current frequency results for the six different sites. They have minor variation but like the near field current direction previously described, all have a strong NE bound current direction as a result of the on-shore current regime in this region. Flows to the south to west directions are almost non-existent.

We emphasize that the locations of these study sites shown herein were more or less random and do not represent proposed aquaculture sites. Nor would the present analysis be sufficient for a permitting process, but rather be one key element of it.

**Table 7.  Summary of near surface current velocity and standard deviation at the six far field study sites.**

|  | Study Site | | | | | |
|---|---|---|---|---|---|---|
|  | 1 | 2 | 3 | 4 | 5 | 6 |
| Average | 21.9 | 23.4 | 21.0 | 21.3 | 21.1 | 21.5 |
| St. Dev. | 10.6 | 11.1 | 10.3 | 10.6 | 10.3 | 10.2 |

**Table 8.  Multiple fish farms study site characteristics.**

| Characteristic or Parameter | Far Field 1 | Far Field 2 | Far Field 3 | Far Field 4 | Far Field 5 | Far Field 6 |
|---|---|---|---|---|---|---|
| Dimensions of a single site footprint (L x W x D) | 500m x 75m x 12m | 500m x 75m x 12m | 500m x 75m x 12m | 500m x 75m x 12m | 500m x 75m x 12m | 500m x 75m x 12m |
| Volume of pens for single fish farm | 450,000 m$^3$ | 450,000 m$^3$ | 450,000 m$^3$ | 450,000 m$^3$ | 450,000 m$^3$ | 450,000 m$^3$ |
| Depth of water at study sites | 128 m | 106 m | 128 m | 106 m | 85 m | 106 m |
| GPS coordinates | N20.22880 W155.92671 | N20.11523 W155.90476 | N19.98248 W155.86701 | N19.90527 W155.93812 | N19.81223 W156.06103 | N19.58023 W155.99256 |
| Modeling domain area | 6,561 km$^2$ * | 6,561 km$^2$ * | 6,561 km$^2$ * | 6,561 km$^2$ * | 6,561 km$^2$ * | 6,561 km$^2$ * |
| Fish stocking size | 10 g | 10 g | 10 g | 10 g | 10 g | 10 g |
| Number of fish stocked per fish farm | 4.5 million | 4.5 million | 4.5 million | 4.5 million | 4.5 million | 4.5 million |
| Duration of growout to harvest | 7 months | 7 months | 7 months | 7 months | 7 months | 7 months |
| Initial fish loading density | 0.1 kg m$^{-3}$ | 0.1 kg m$^{-3}$ | 0.1 kg m$^{-3}$ | 0.1 kg m$^{-3}$ | 0.1 kg m$^{-3}$ | 0.1 kg m$^{-3}$ |
| Initial loading per study site | 45 MT** | 45 MT** | 45 MT** | 45 MT** | 45 MT** | 45 MT** |
| Feed C composition (Fraction) | 0.44 | 0.44 | 0.44 | 0.44 | 0.44 | 0.44 |
| Feed N composition (Fraction) | 0.07 | 0.07 | 0.07 | 0.07 | 0.07 | 0.07 |
| Biomass per fish farm at harvest | 297 MT | 297 MT | 297 MT | 297 MT | 297 MT | 297 MT |
| Feed loss rate | 3% | 3% | 3% | 3% | 3% | 3% |
| Horizontal diffusion rate Kh | 0.400 m$^2$ s$^{-1}$ | 0.400 m$^2$ s$^{-1}$ | 0.400 m$^2$ s$^{-1}$ | 0.400 m$^2$ s$^{-1}$ | 0.400 m$^2$ s$^{-1}$ | 0.400 m$^2$ s$^{-1}$ |
| Vertical diffusion rate Kv (surface / deep) | 0.010 / 0.005 m$^2$ s$^{-1}$ | 0.010 / 0.005 m$^2$ s$^{-1}$ | 0.010 / 0.005 m$^2$ s$^{-1}$ | 0.010 / 0.005 m$^2$ s$^{-1}$ | 0.010 / 0.005 m$^2$ s$^{-1}$ | 0.010 / 0.005 m$^2$ s$^{-1}$ |

*81 x 81 cells, each cell 1,000 m$^2$ with a significant portion overlapping onto the island

**0.1 kg m$^{-3}$ x 450000 m$^3$ each
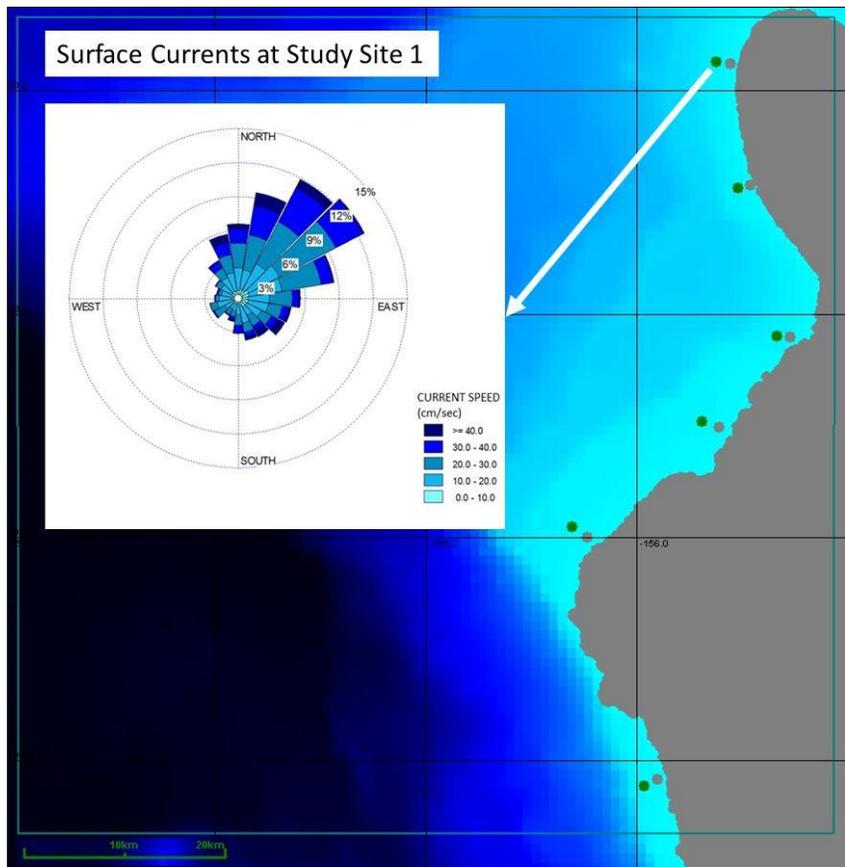
**Figure 80.  Surface Current Frequency at Study Site 1.**
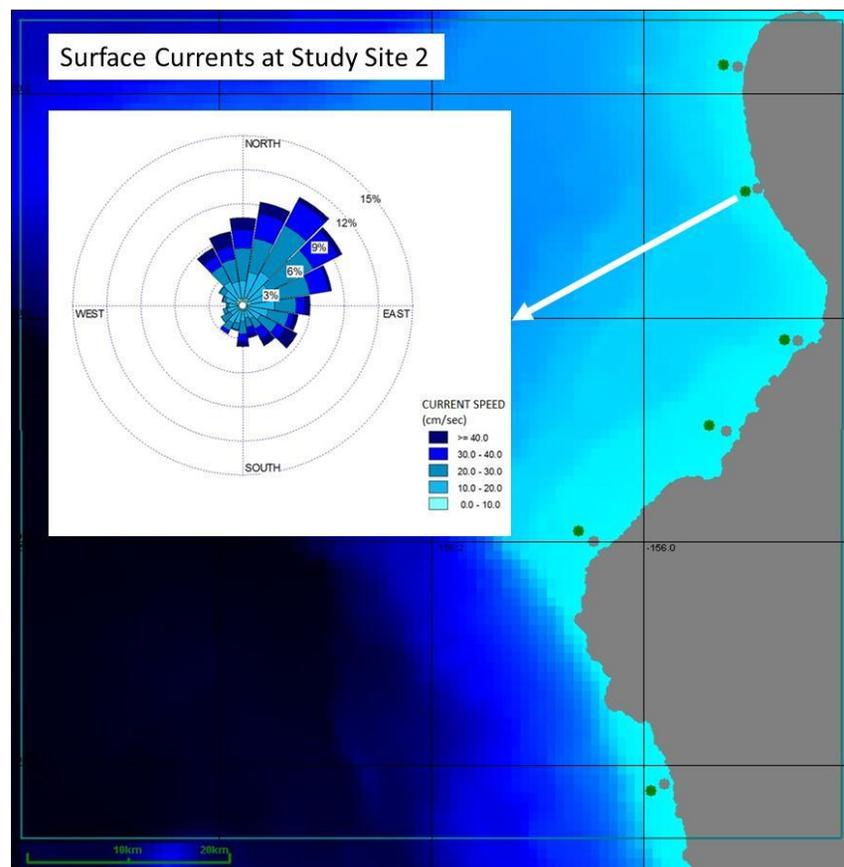


**Figure 81.  Surface Current Frequency at Study Site 2.**
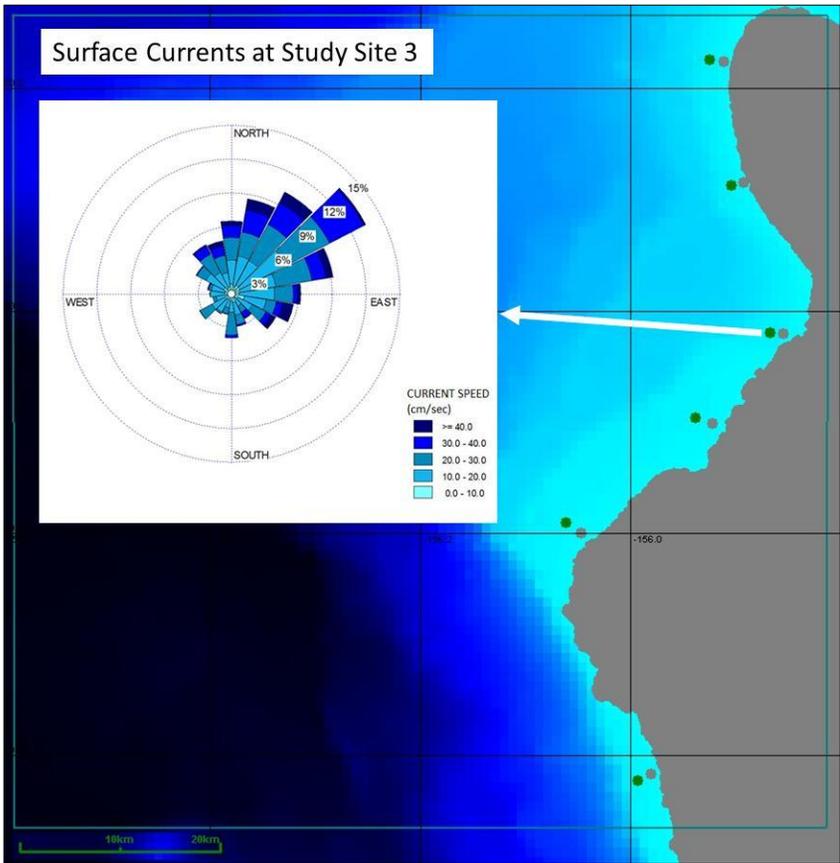
**Figure 82. Surface Current Frequency at Study Site 3.**
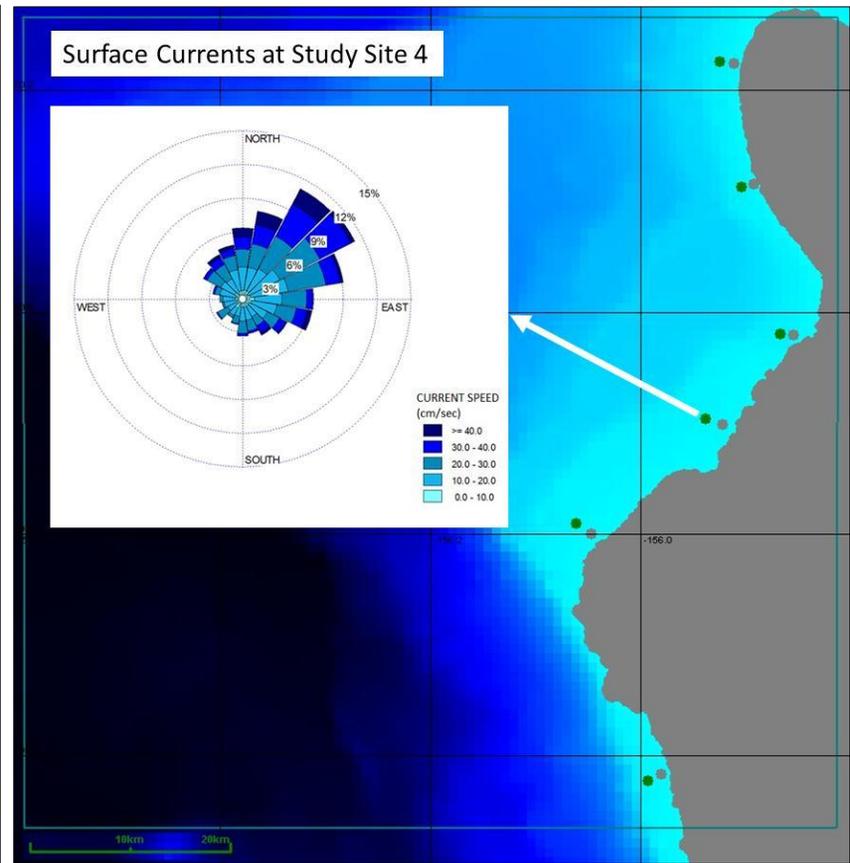


**Figure 83. Surface Current Frequency at Study Site 4.**
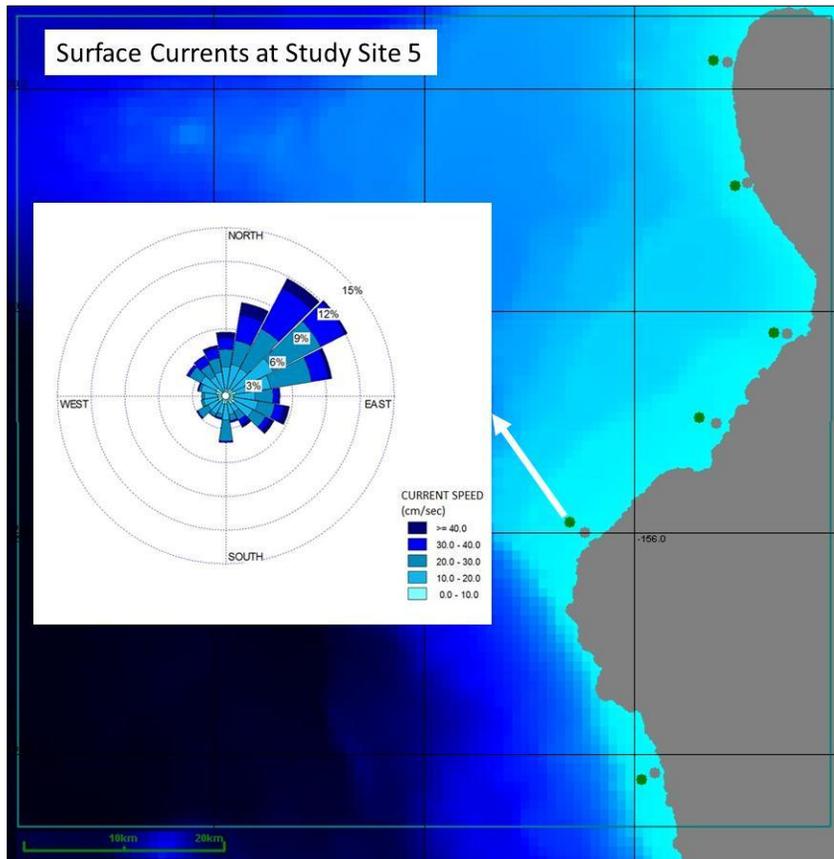
**Figure 84.  Surface Current Frequency at Study Site 5.**
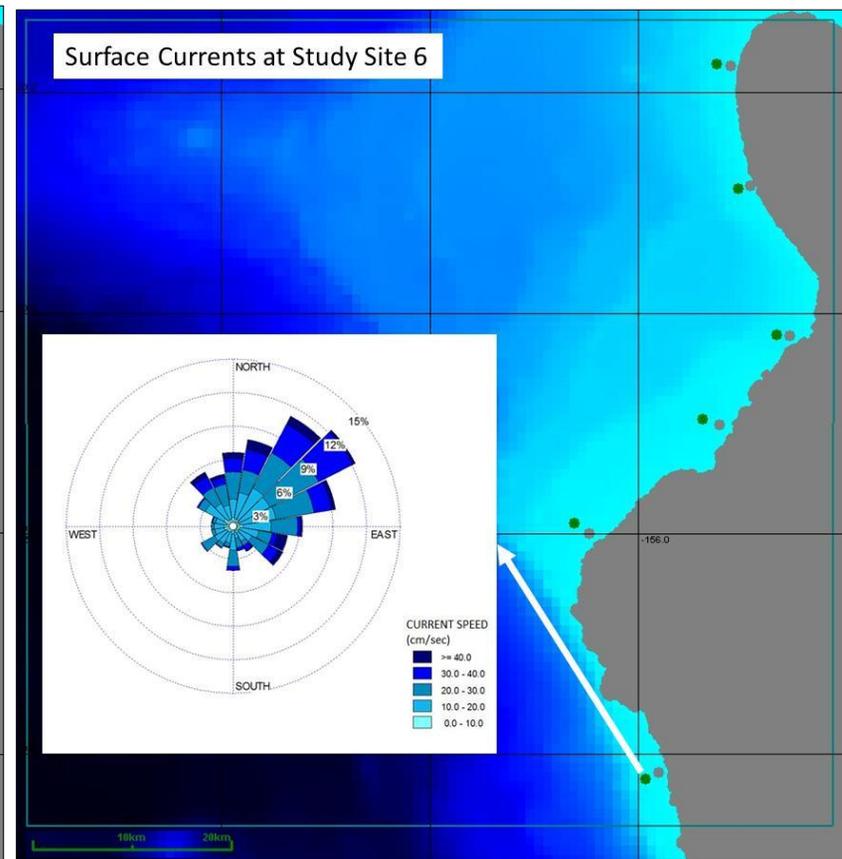


**Figure 85.  Surface Current Frequency at Study Site 6.**

## Bathymetry Multiple Fish Farms

Modeling bathymetry was accessed through the on line GEBCO (worldwide) database http://www.gebco.net/ which is relatively poor resolution for the sub-kilometer grid used here, but should *AquaModel* be needed in Hawai'i many other digital data sources are available. Three-dimensional images of the subject area are shown below in Figure 86 and 87 from the Hawai'ian Mapping Research Group at the University of Hawai'i at Mānoa. The Kohala coast is a broad, relatively shallow shelf compared to the narrowing and extremely deep Kona coast. Although the former is relatively shallow, for anchored net pens (i.e., 100m or less depth) it is a narrow band and would result in potential fish farms being placed within a few kilometers of shore.
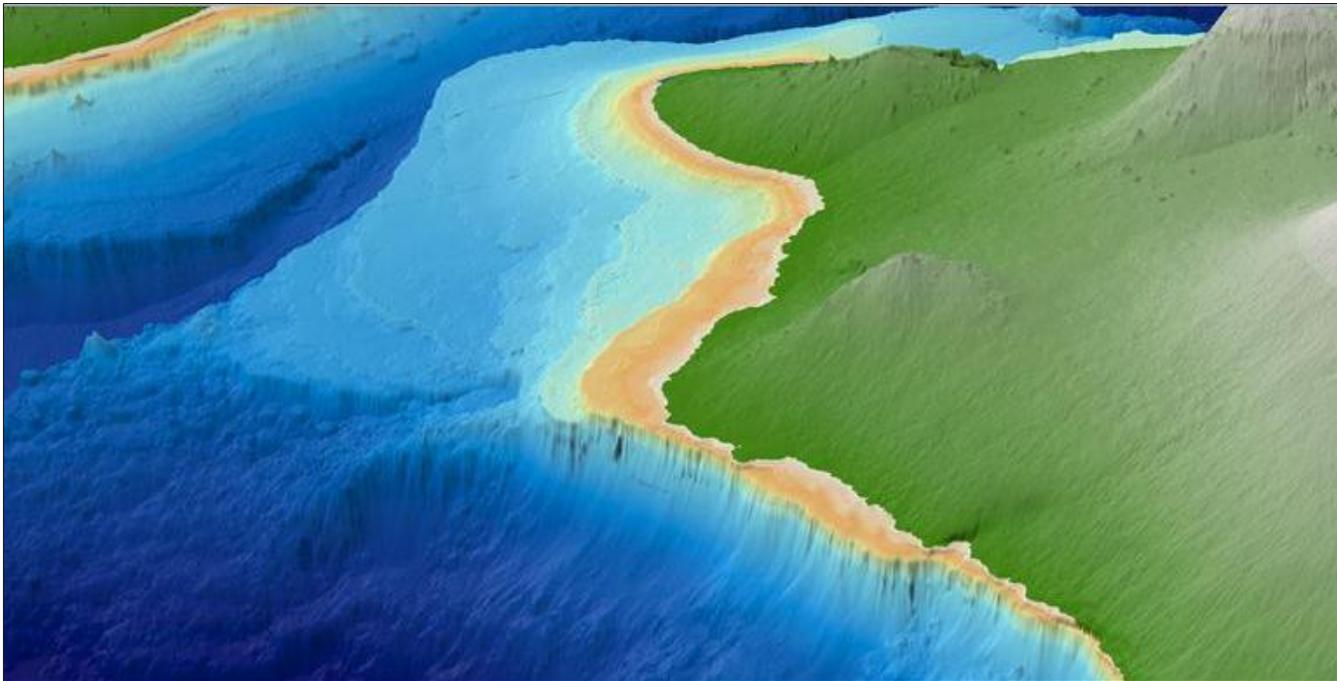


**Figure 86. Subject modeling area of the big island of Hawai'i, shown looking toward the north east. From http://www.soest.hawaii.edu/HMRG/Multibeam/index.php**
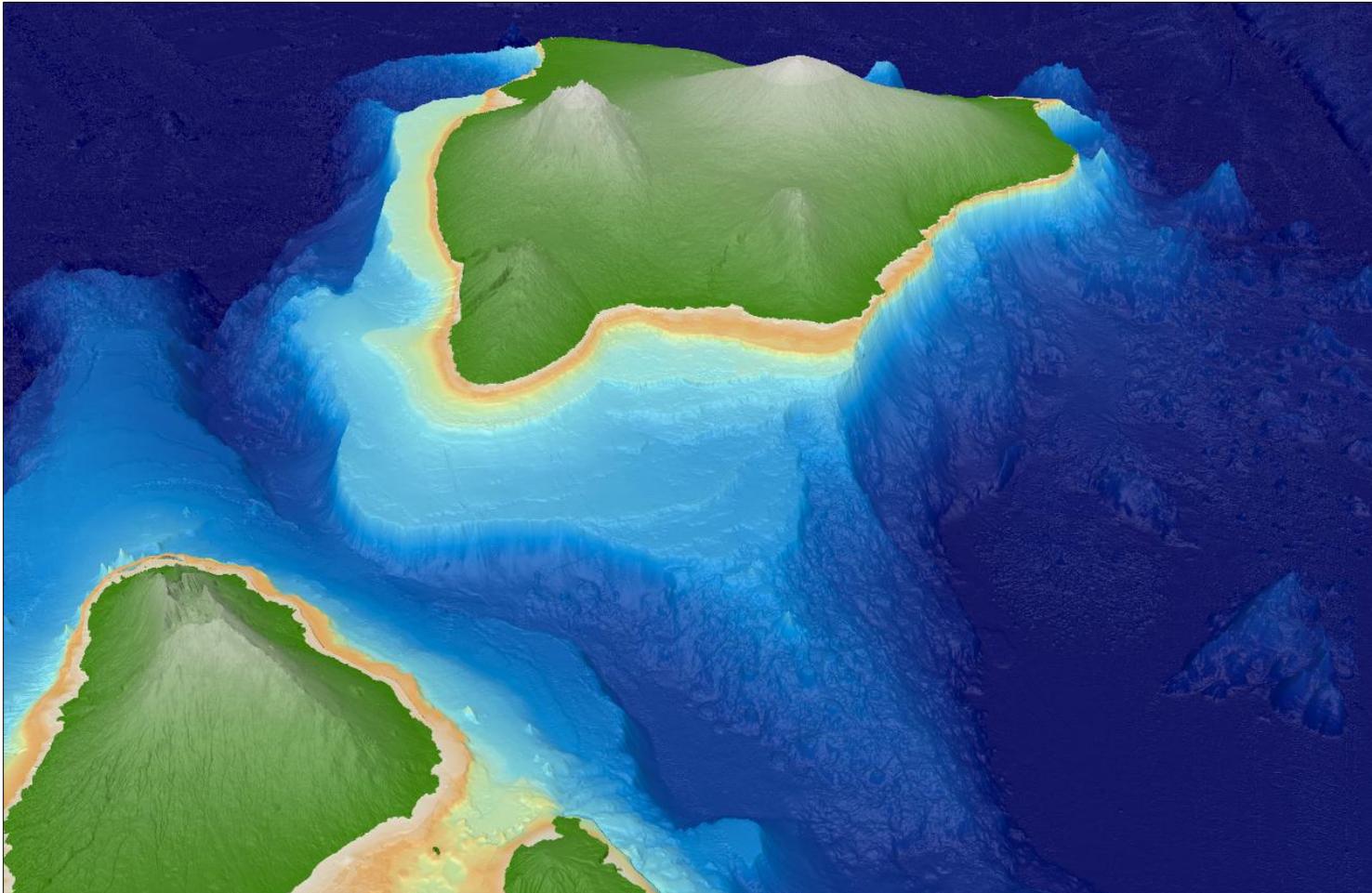
**Figure 87. Subject modeling area of the big island of Hawai'i, shown looking toward the south. From**
**http://www.soest.hawaii.edu/HMRG/Multibeam/index.php**

# Multiple Fish Farm Nitrogen Distribution and Assimilation

As in the single farm near field simulation results above, the concentrations of dissolved nitrogen from these modest sized fish farm simulations were minimal for the first 6 months of operation. As a result, we do not include screen prints showing the spatial distribution of dissolved nitrogen until the last three weeks before harvest. Figures 88-96 together show a series of screen prints which are discussed further in each figure caption. Figure 97 summarizes mean nitrogen levels at each study site compared to ambient levels.
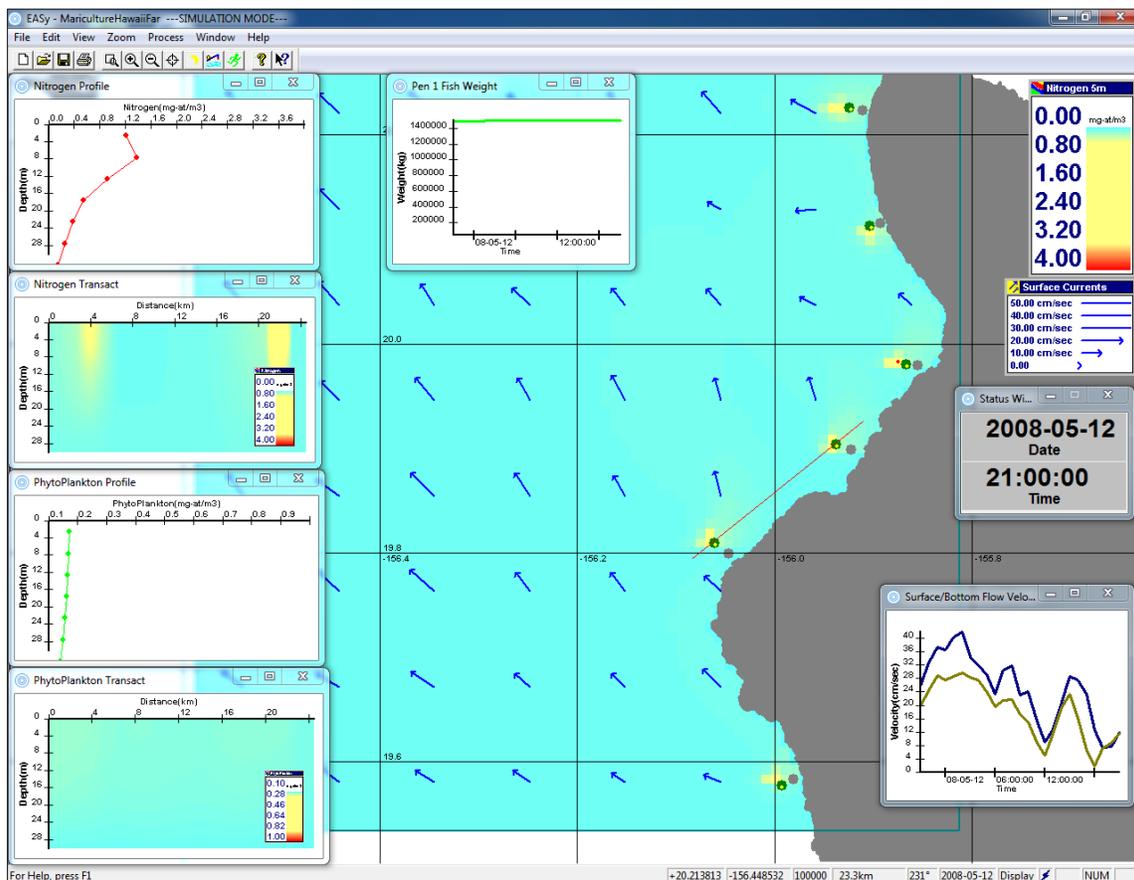


**Figure 88. Dissolved nitrogen at 5m depth distribution after 6 months of fish culture at six different sites. Nitrogen profile (upper left box) showing a maximum of ~1.4 μM N at 5 meters depth. Nitrogen transect (red) line drawn through two sites. Weak north, north-easterly water currents at this time.**
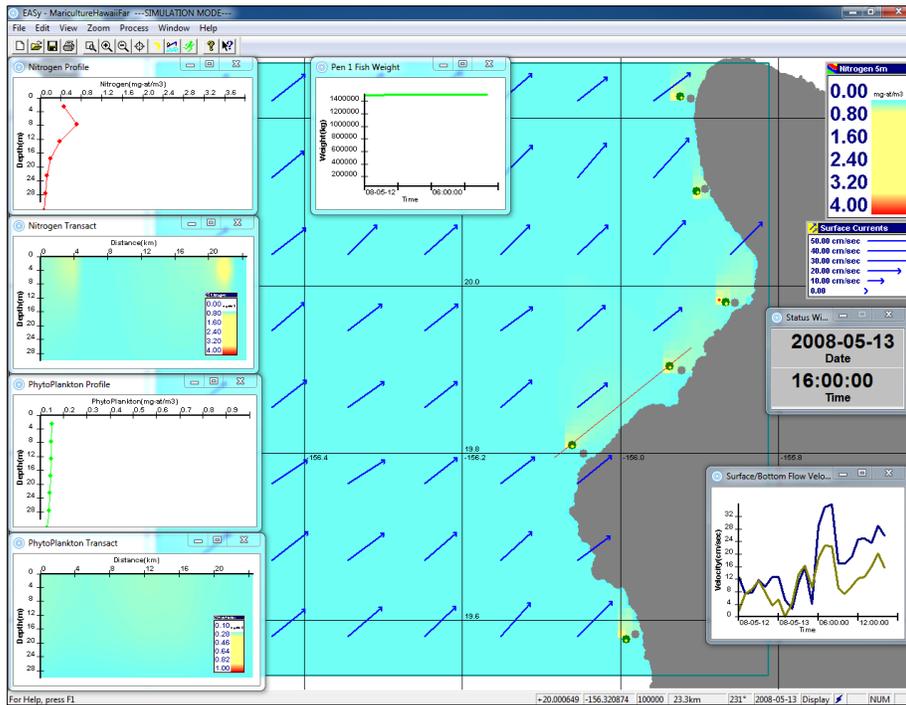
**Figure 89. 19 hours later than the above figure with increasing current velocity and dominant north easterly currents pushing water towards the North East and broader nitrogen distribution but at lower concentrations (see N profile box).**
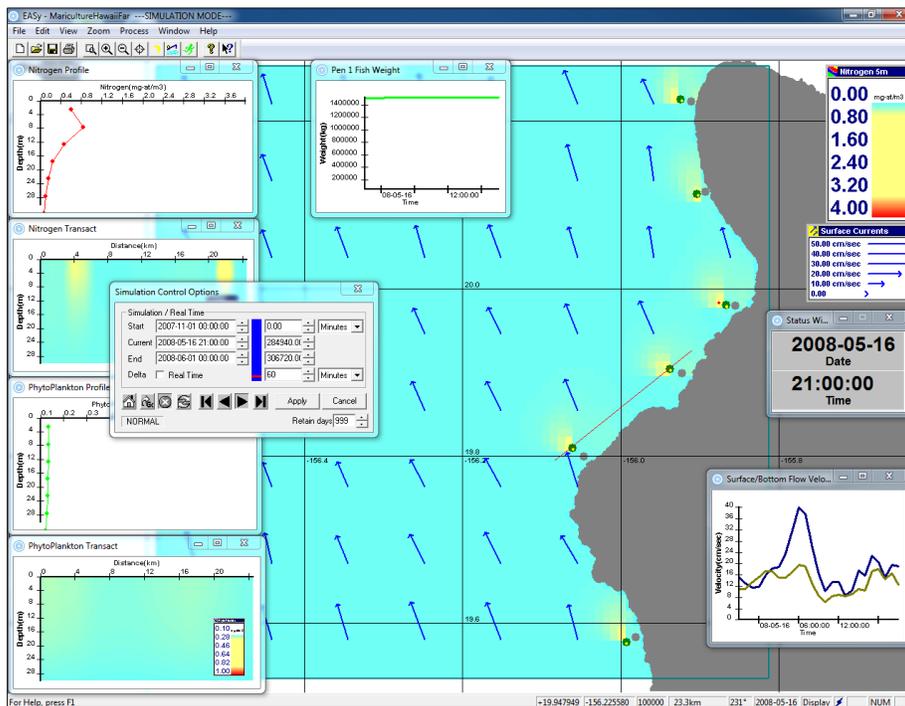


**Figure 90. Three days later during northerly current flow; similar N distribution seen.**
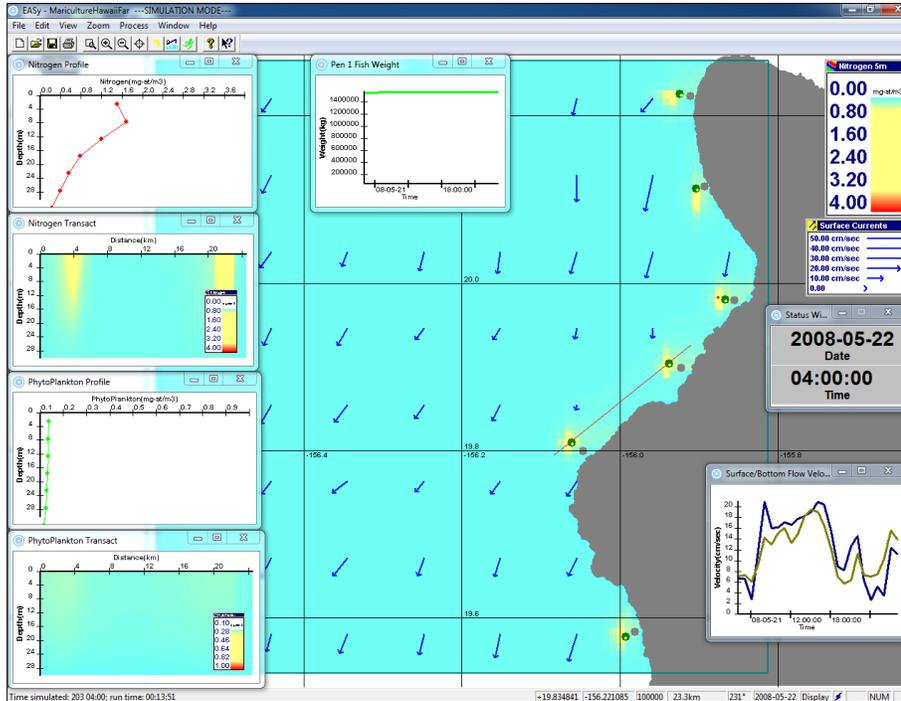
**Figure 91. Eight days left until the simulation completion, flow to the south southeast.**
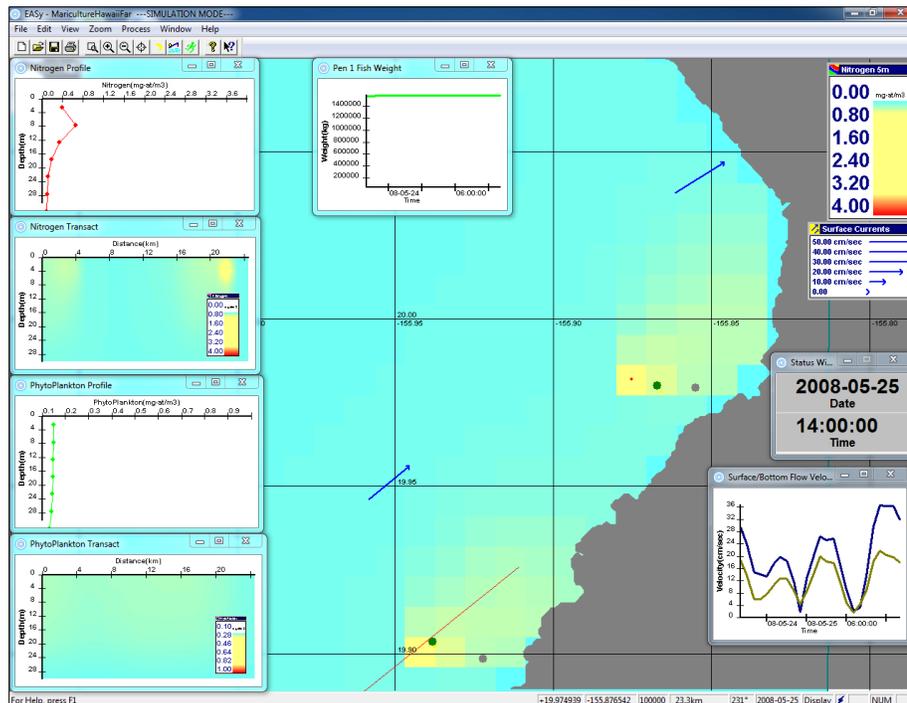


**Figure 92. Zooming in on net-pen sites numbers 3 and 4 to show N distribution. Nitrogen vertical profile (red dot near site 3) shows a concentration of 0.8 μM immediately adjacent to the farm. Nearer shore the concentrations are about 0.2 μM, compared to 0.1 μM for ambient conditions.**
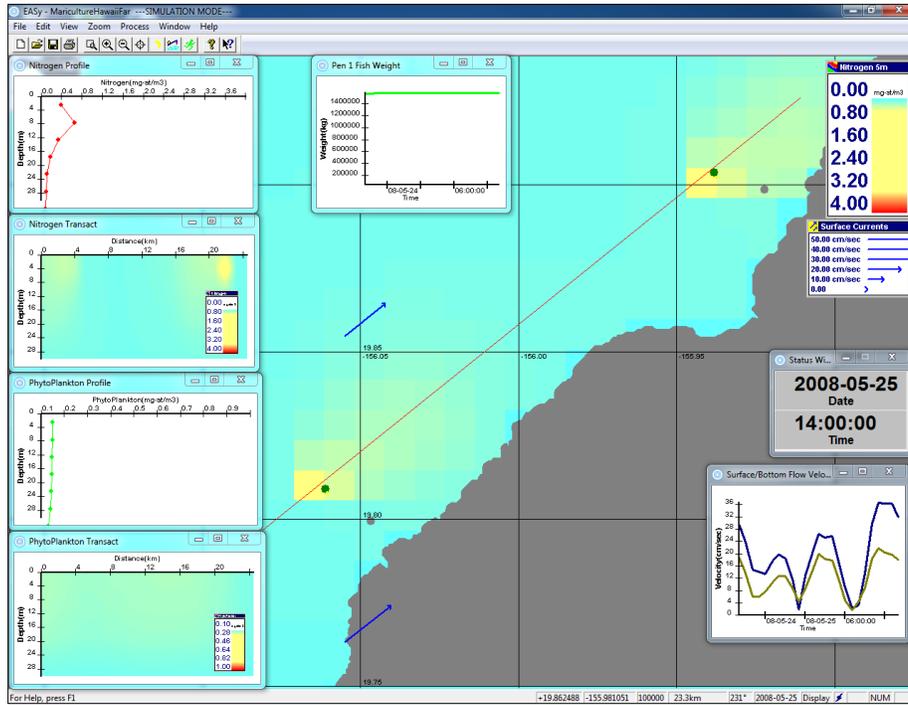
**Figure 93.** Same time frame as prior print but now showing Sites 4 (upper) and 5 (lower) and distribution of N. Note no shore contact from Site 5 but some minor contact at Site 4.
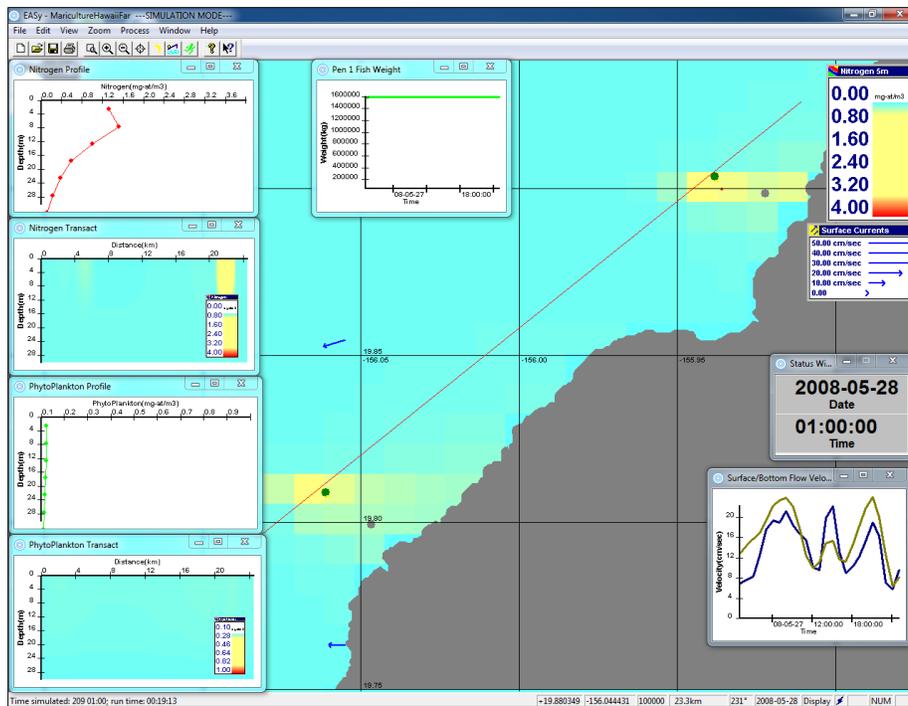


**Figure 94.** Three days later with one incident of Site 4 (upper) nitrogen incursion towards shore after strong onshore currents and a weak reversal to the west.
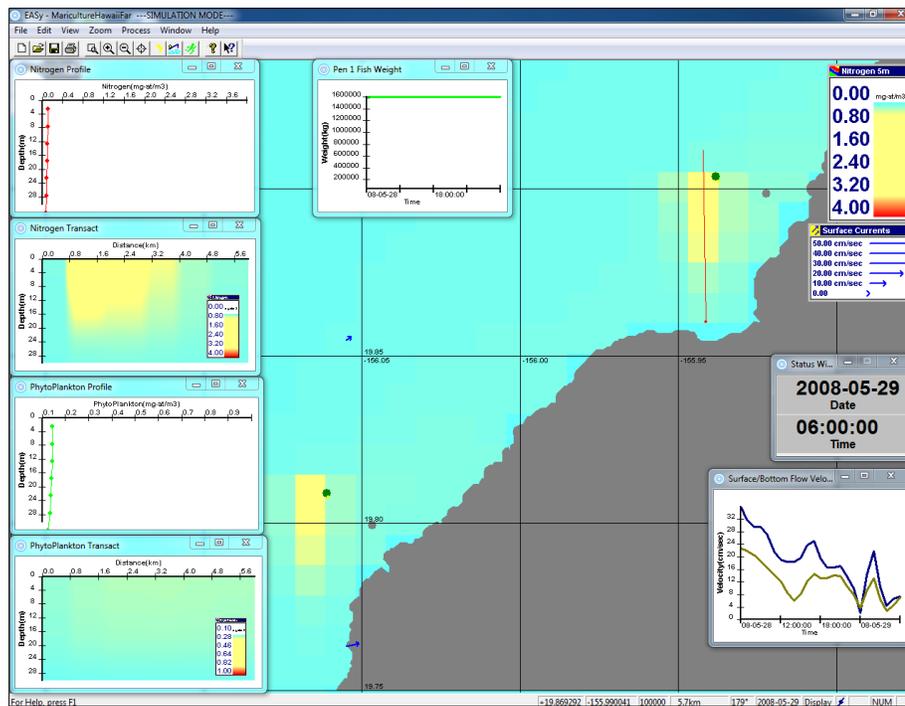
**Figure 95.  Another weak current period a day later but no on-shore N intrusion.**
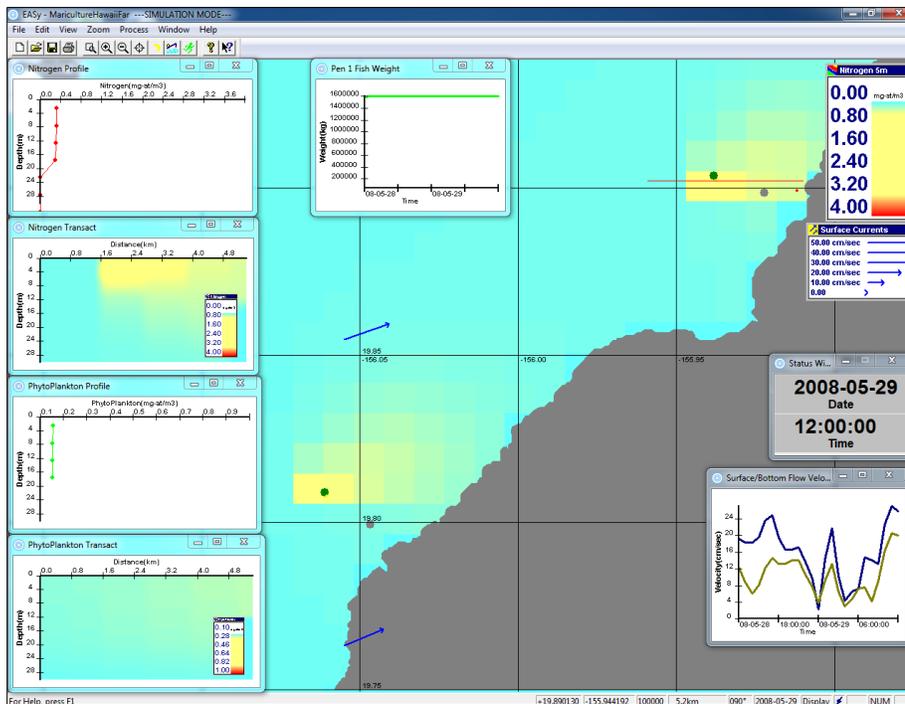


**Figure 96.  Six hours later, northeast current resumes at low rate, nearshore vertical profile shows ~ 0.2 μM N elevation at surface above ambient.  No intrusion for Site 5.**
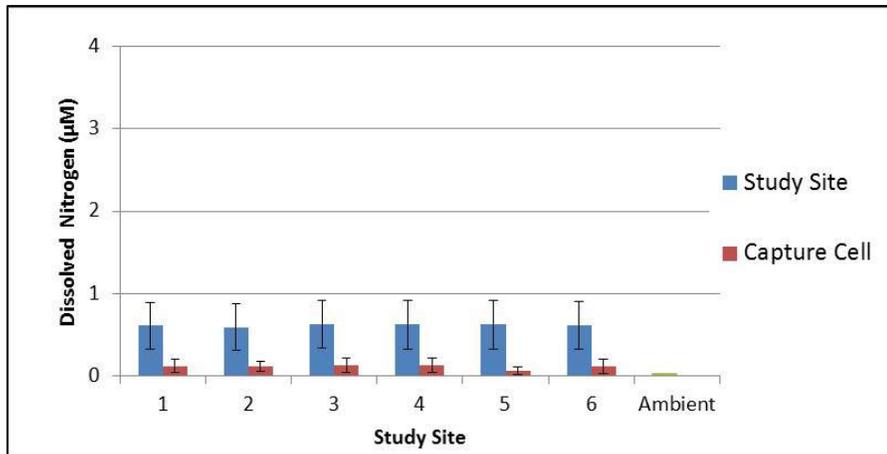
**Figure 97. Mean and standard deviation of dissolved nitrogen at each study site and associated capture cell during multiple fish farm simulation.**

To summarize this section, Figure 97 illustrates there was little difference of dissolved nitrogen concentrations recorded at each study site in the near surface waters, averaging about 0.7 μM concentration, which is ~ 0.6 μM above ambient conditions.

Nearby at the associated capture cells nearer shore, the concentrations were much less, averaging 0.12 μM at all locations except capture cell E, associated with study site 5 that averaged 0.07 μM N.

Study site 5 was located near the prominent point of land, Keahole Point and thus had better dispersion and assimilation of nitrogen near shore. However, even this would result in no significant ecological effects: these changes are about an order of magnitude less than would elicit a response from attached benthic vegetation.

Other factors are important in siting net pens, including allowing for routine navigation paths and aesthetic impacts, which are often significant around headlands such as Keahole Point. Qualitative impacts may be presented and studied through a matrix of information approach, needed to consider all the implications and effects and is not a component of this current study.

Next we examine the effects of the dissolved nitrogen production on phytoplankton stocks in the area.

# Multiple Fish Farm Phytoplankton Effects

The result of the phytoplankton simulation for the mulitple farms are illustrated in the following figures and tables found in the appendix.

There were no effects when the fish were small, so the first image we present is from 3.5 months into the simulation shown below as Figure 98.

Figures 98-108 illustrate various time points in the phytoplankton simulation. As previously, figure captions in this section present the salient points for each illustration followed by a chapter summary.
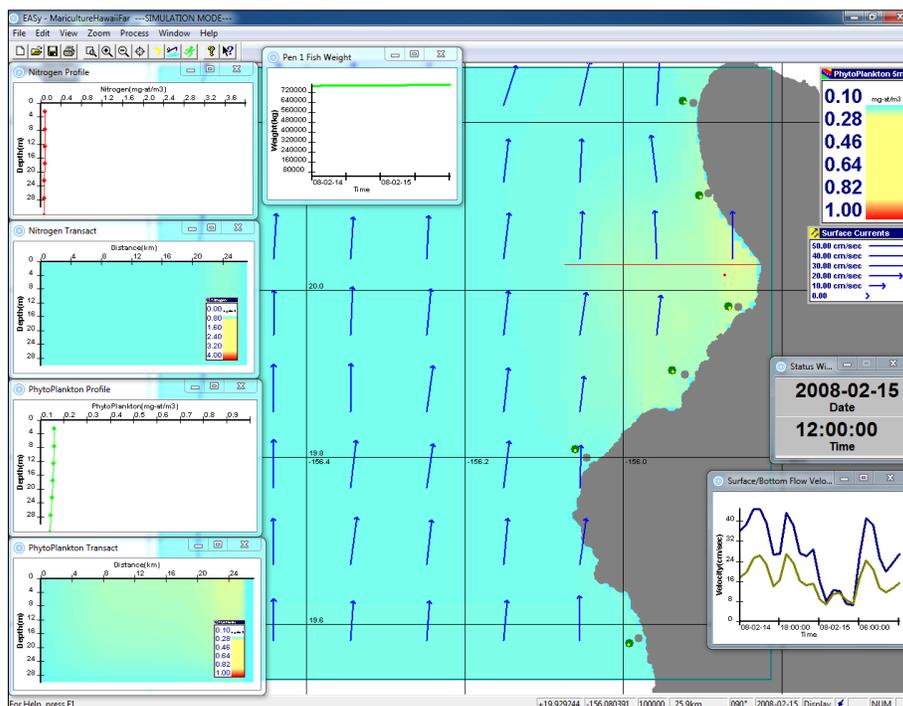


**Figure 98. After 3.5 months of simulation, a minor accumulation of phytoplankton is simulated in the bight from cumulative effects of net pen sites 3 and 4 (and possibly 5). However, the color scale is set so low that the increase over ambient is tiny, about 0.05 μg L^{-1}, which is far too little to be measurable in the field (see third plot from top left). Note concurrent, very low nitrogen values from the same location, suggesting that N uptake by the algae has occurred already.**
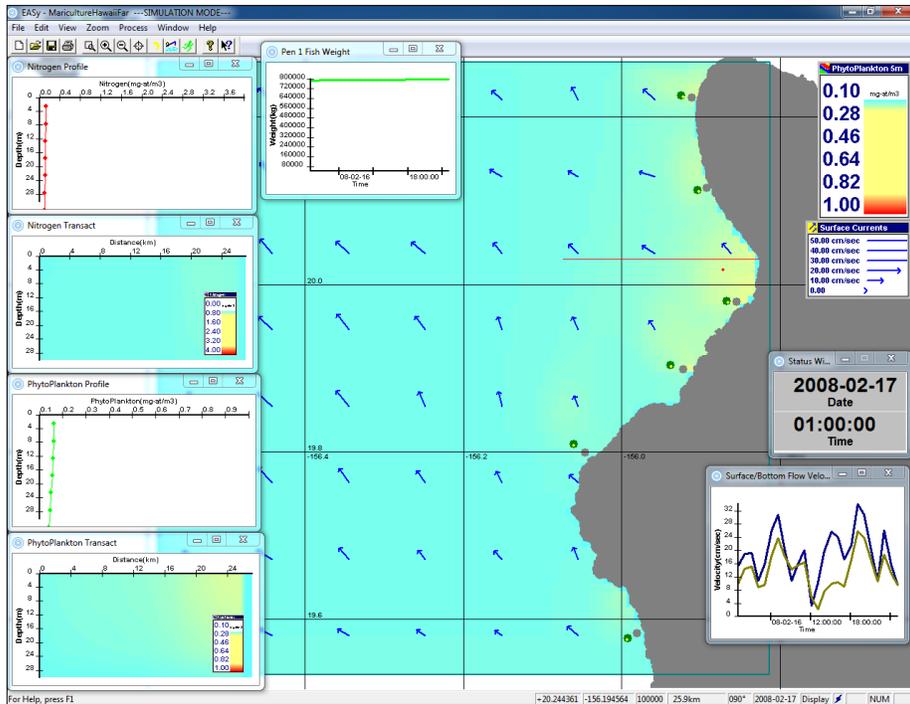
**Figure 99.** Two days later with weaker currents and a northwesterly flow, with the phytoplankton persisting in the bight and further north at very low concentrations.
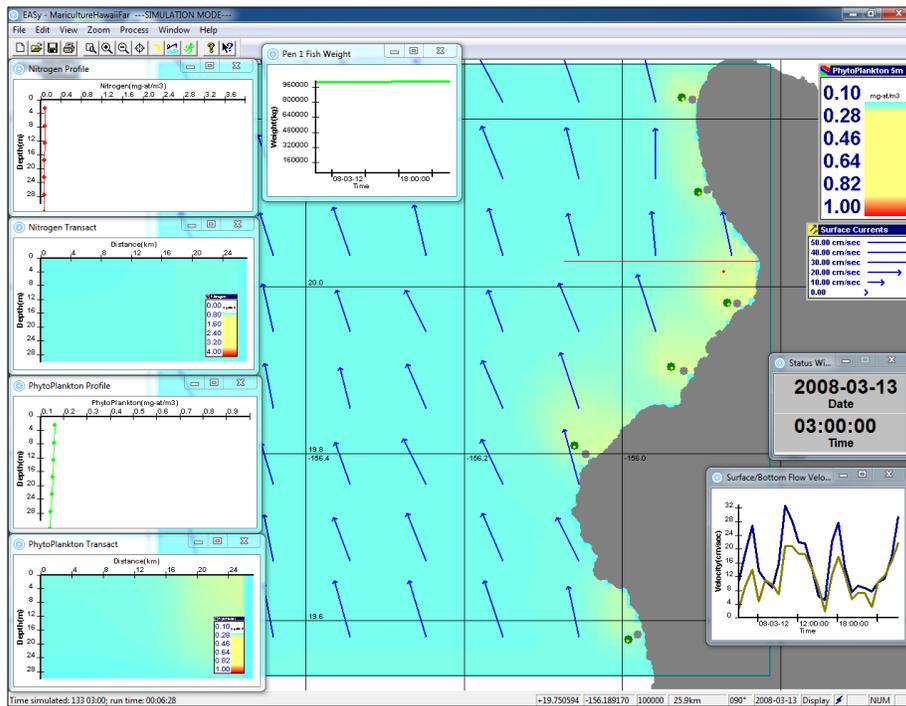


**Figure 100.** About a month later and all the sites now exhibiting some phytoplankton growth in their immediate vicinity.
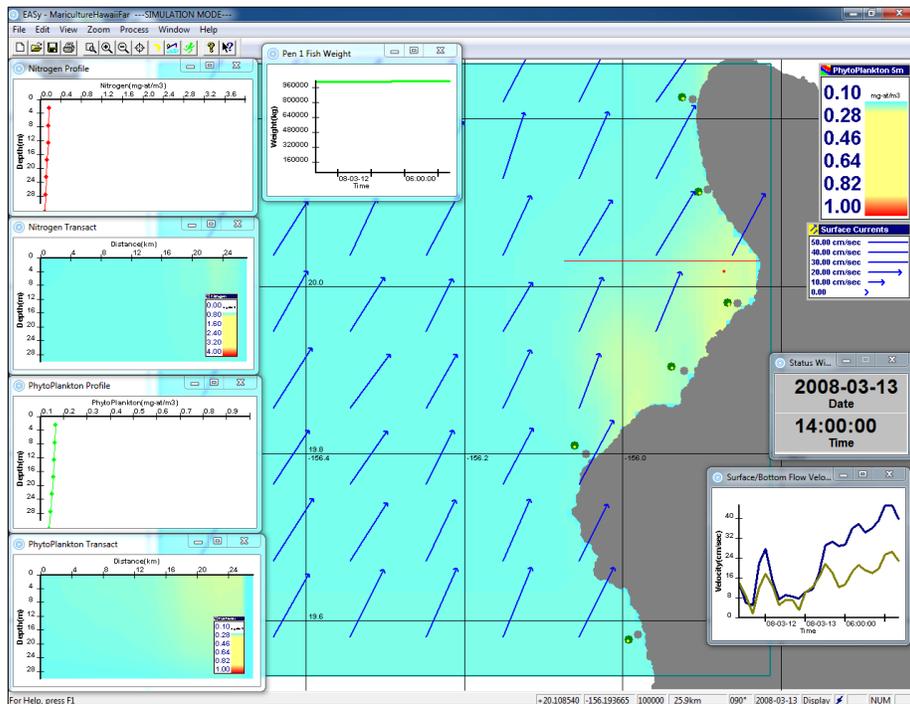
**Figure 101.** Eleven hours later and the occurrence of the usual strong northeasterly currents maintains elevated phytoplankton concentrations in the bight.
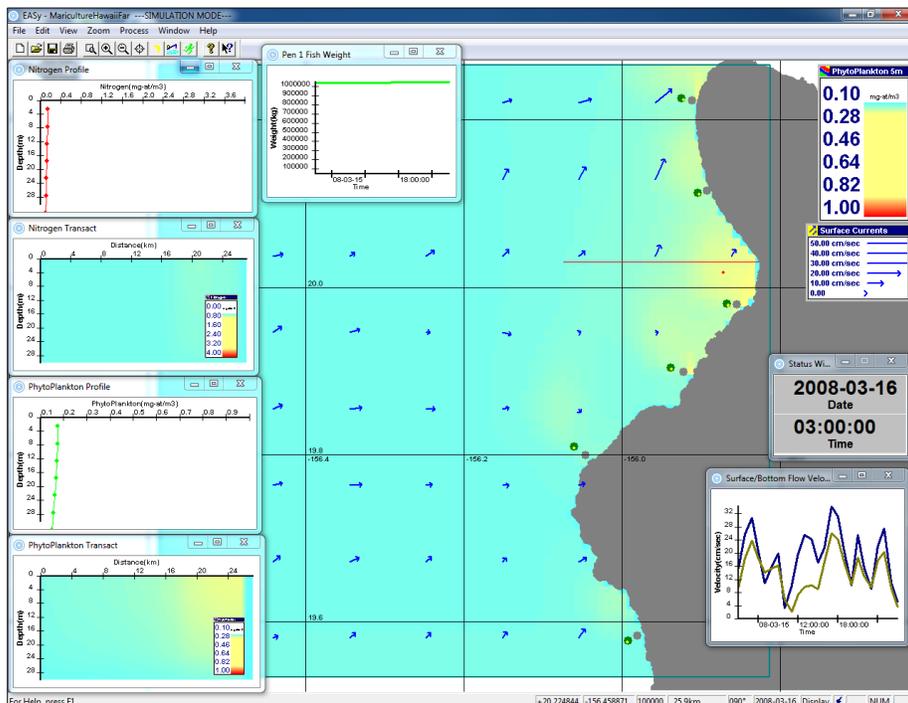


**Figure 102.** Three days later, weak currents and the same very minor level of phytoplankton occurring in the northern bight towards the north end of the island of Hawai'i.
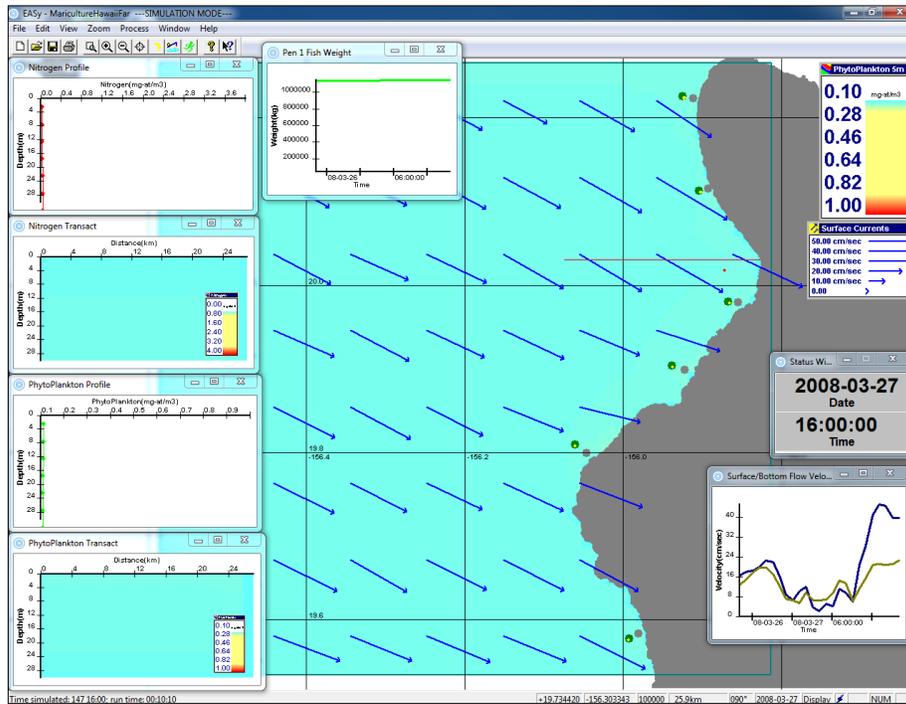
**Figure 103. Strong current period example after the above event resulting in no calculated increase in phytoplankton concentration.**
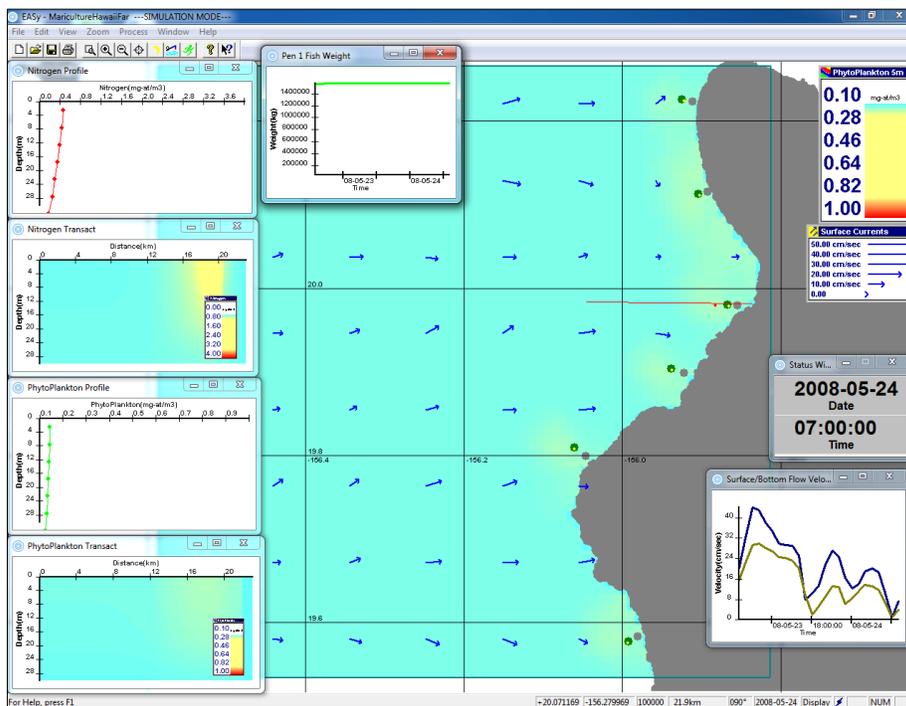


**Figure 104. Within a week of fish harvest with weak currents after a strong current period resulting in a tiny change in calculated phytoplankton biomass, as shown in the vertical profile immediately adjacent to Site 3 of about 0.01 ug L$^{-1}$ (0.01 parts per billion).**
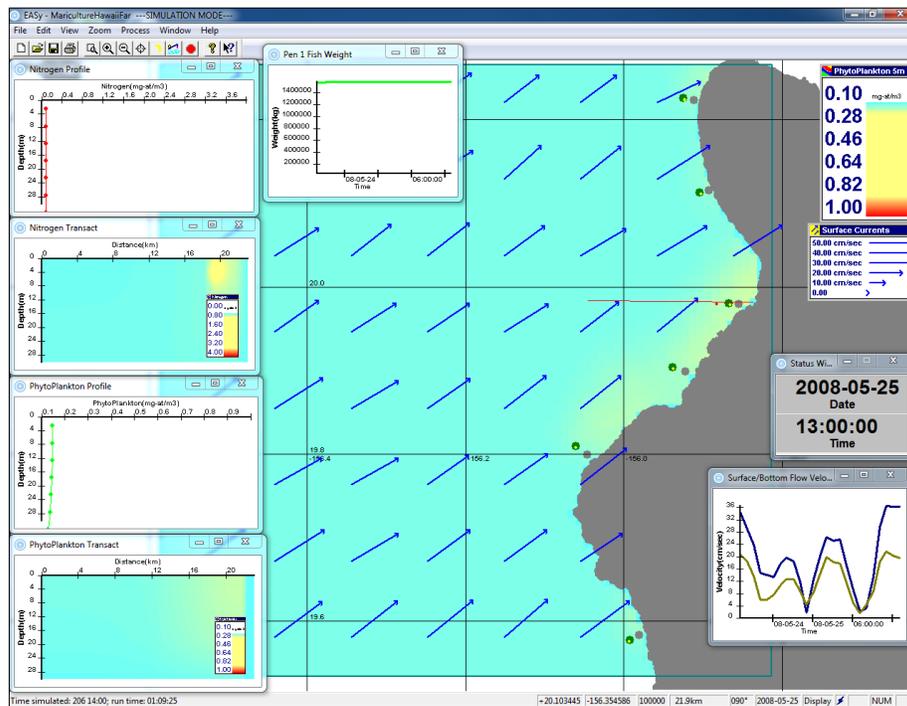
**Figure 105.** About a day later with alternating strong currents and once again tiny concentrations of phytoplankton, but this time in the south end of the bight.
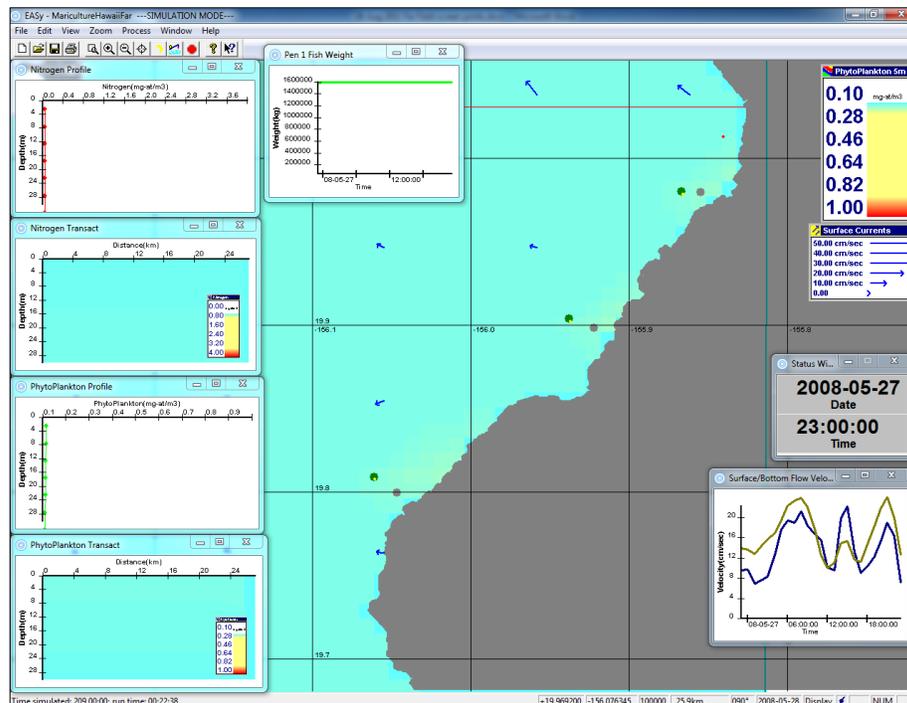


**Figure 106.** Within three days of growout completion and phytoplankton concentrations declining once again.
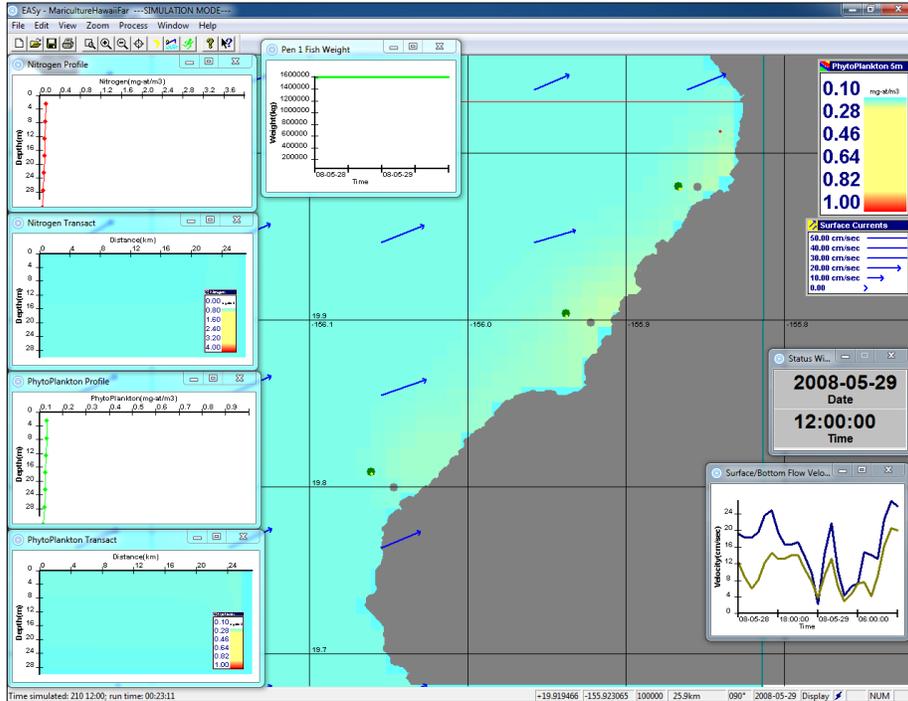
**Figure 107.** 1.5 days later, close-up of southern half of the bight showing the same extremely low levels of phytoplankton embellishment.
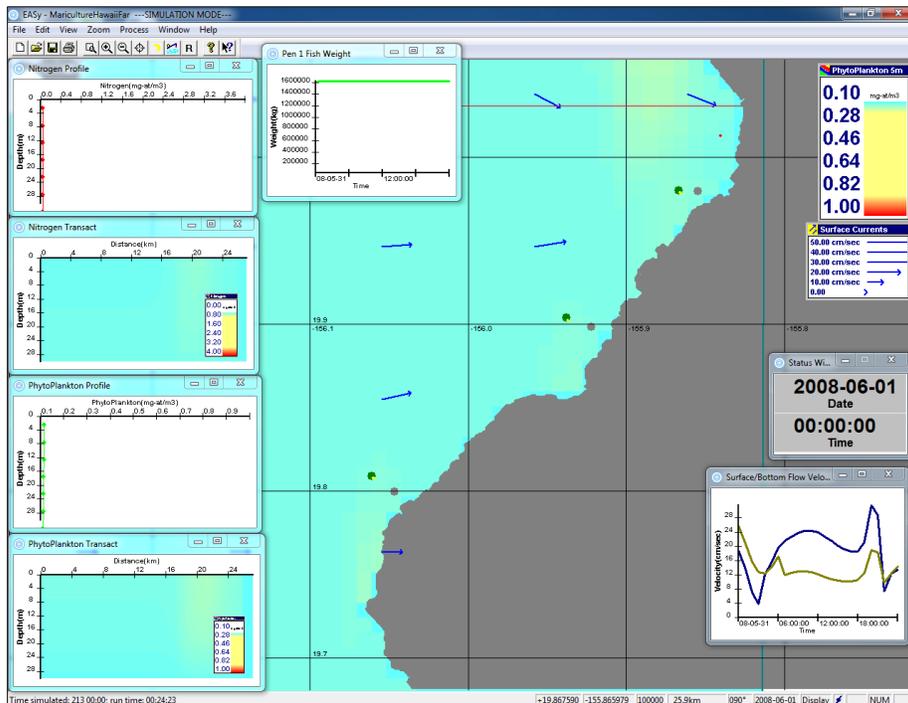


**Figure 108.** Phytoplankton concentrations at completion of grow out showing similar patterns as described above and a small focus of cells moving north but again at extremely low concentrations.

In summary, the phytoplankton analysis of the mutliple farm sites indicates that:

- Nitrogen is rapidly advected (moved) and acquired by phytoplankton in these simulations and the only location of relatively high concentrations is at the net pen sites.

- Capture cells located about one-half the distance to shore from the net pens show an order of magnitude (~ 10x) decline of dissolved nitrogen concentration due in part to dilution and uptake of nitrogen by phytoplankton.

- Effects were not forecast during much of the simulation, except toward the end when the fish biomass was attaining maximum loading. Higher levels of fish production (studied, but not shown) produced more pronounced effects nearshore.

- Some study site net pens appeared to produce less effect on nearshore zones, although at calculated concentrations and flux rates, no likely effects on attached algal productivity near shore would occur.

- Effects nearshore were most pronounced from pens located inside the Kohala Coast bight, a sort of open bay that tended to reduce water flow.

- Minimal nearfield effects were recorded for Site 5 near a major headland known as Keahole Point, due to the northeasterly currents that had no immediate nearby shore in the down current direction.

- The simulation shows evidence that dissolved nitrogen is taken up by photosnthetic phytoplankton, as downstream there are minor plumes of phytoplankton; however, the concentration of nitrogen in these plumes is similar to ambient conditions.

# Literature Cited

American Oil Chemists' Society. 1998. In: Firestone, D. (Ed.), Official Methods and Recommended Practices of the American Oil Chemists' Society, 5th edn. American Oil Chemists Society, Champaign, IL, USA.

AOAC International. 2000. In: Horwitz, W. (Ed.), Official Methods of Analysis of AOAC International, 17th edn. Arlington, VA, USA.

Austreng, E., T. Storebakken, M.S. Thomassen, S. Refstie and Y. Thomassen. 2000. Evaluation of selected trivalent metal oxides as inert markers used to estimate apparent digestibility in salmonids. Aquaculture 188: 65–78.

Bertalanffy, L. von. 1960. Principles and theory of growth. In: Wowinski, W.W. (Ed.), Fundamental aspects of normal and malignant growth, Elsevier's, Amsterdam, pp. 137-259.

Blazka P., M. Volf and M. Ceplea. 1960. A new type of respirometer for determination of the metabolism of fish in an active state. Physiologia Bohemoslovaca 9: 553-560.

Brett, J.R. 1964. The respiratory metabolism and swimming performance of young sockeye salmon. Journal of the Fisheries Research Board of Canada 21: 1183-1226.

Brett, J.R. 1976. Scope for metabolism and growth of sockeye salmon, Oncorhynchus nerka, and some related energetics. Journal of the Fisheries Research Board of Canada 33: 307-313.

Brett, J.R. and T.T.D. Groves. 1979. Physiological energetics. In: Hoar, W.S., D.J. Randall and J.R. Brett (Eds.), Fish Physiology, vol. 8, Academic Press, New York, pp. 280–352.

Brett, J.R., J.E. Shelbourne and C.T. Shoope. 1969. Growth rate and body composition of fingerling sockeye salmon, Oncorhynchus nerka, in relation to temperature and ration size. Journal of the Fisheries Research Board of Canada 26: 2363-2394.

Brett. J.R. and C.A. Zala. 1975. Daily patterns of nitrogen excretion and oxygen consumption of sockeye salmon (Oncorhynchus nerka) under controlled conditions. Journal of the Fisheries Research Board of Canada 32: 2479-2486.

Brooks, K. and C.V.W. Mahnken. 2003. Interactions of Atlantic salmon in the Pacific Northwest environment II: Organic Wastes. Fisheries Research 62: 255-293.

Chamberlain, J. and D. Stucchi. 2007. Simulating the effects of parameter uncertainty on waste model predictions of marine finfish aquaculture. Aquaculture 272: 296-311.

Cromey, C.J. and K.D. Black. 2005. Modelling the impacts of finfish aquaculture. Chapter 7 in: The Handbook of Environmental Chemistry. Environmental Effects of Marine Finfish Aquaculture. Volume 5: Water Pollution. Springer, Berlin Heidelberg New York.

Cromey, C.J., T.D. Nickell and K.D. Black. 2002a. DEPOMOD - Modelling the deposition and biological effects of waste solids from marine cage farms. Aquaculture 214: 211-239.

Cromey, C. J., T.D. Nickell, K.D. Black, P.G. Provost, and C.R. Griffiths. 2002b. Validation of a fish farm waste resuspension model by use of a particulate tracer discharged from a point source in a coastal environment. Estuaries 25: 916-929.

Cromey, C., P. Provost and K. Black. 2003. Development of monitoring guidelines and modelling tools for environmental effects from Mediterranean aquaculture. Newsletter 2. Scottish Association for Marine Science Dunstaffnage Marine Laboratory, Oban, Argyll, PA34 4AD, Scotland, UK.

Findlay, R.H., L. Watling, and L. Mayer. 1995. Environmental impact of salmon net-pen culture on marine benthic communities in Maine: A case study. Estuaries 18: 145-179.

Findlay, R.H, and L. Watling. 1997. Prediction of benthic impact for salmon net-pens based on the balance of benthic oxygen supply and demand. Marine Ecology Progress Series 155: 147-157.

Flagg, T.A. 1981. Swimming stamina and survival related to swimming fatigue in response to direct seawater entry during the Parr-Smolt transformation of Coho Salmon (Oncorhynchus kisutch). Masters Thesis, University of Washington.

Hardy, R.W. 1989. Diet preparation. In: Halver, J.E. (Ed.), Fish Nutrition. Academic Press, San Diego, CA, USA, pp. 476–548.

Hargrave, B.T., M. Holmer and C.P. Newcombe. 2008. Towards a classification of organic enrichment in marine sediments based on biogeochemical indicators. Marine Pollution Bulletin 56: 810–824.

Johnson, R.B., M.A. Cook, P.M. Nicklason and M.B. Rust. 2008. Determination of apparent protein digestibility of live Artemia and a microparticulate Diet in 8-week-old Atlantic cod Gadus morhua larvae. Aquaculture 288: 290-298.

Kajimura, M., S.J. Croke, C.N. Glover and C.M. Wood. 2004. Dogmas and controversies in the handling of nitrogenous wastes: the effect of feeding and fasting on the excretion of ammonia, urea and other nitrogenous waste products in rainbow trout. Journal of Experimental Biology 207: 1993-2002.

Kiefer, D.A., J.E. Rensel and F.J. O'Brien. 2008. *AquaModel* simulation of water column and sediment effects of fish mariculture at the proposed Hubbs-SeaWorld Research Institute Offshore Aquaculture Demonstration Project. Prepared for Hubbs SeaWorld Research Institute, San Diego, CA by Systems Science Applications, Inc. and Rensel Associates Aquatic Sciences. 68 pp. Available on request from HSWRI or SSA.

Prentice E., C. McCutcheon, T.A. Flagg and D. Park. 1986. Study to determine the biological feasibility of a new fish tagging system, Project No. 1983-31900. 97 electronic pages. (BPA Report DOE/BP-11982-2).

Revilla, M. et al. 2005. Urea analysis in coastal waters: comparison of enzymatic and direct methods. Limnology and Oceanography: Methods 3. 290-299.

Scott, T.M. and M.B. Rust. 1996. A computer-automated cold-weathered recirculating system for Aquaculture research. Aquaculture Engineering Society. Proceedings 2: Success and failures in Commercial Recirculating Aquaculture 2: 562-574.

Smith, S.L. and T.W. Newcomb. 1970. A modified version of the Blazka respirometer and exercise chamber for large fish. Journal of the Fisheries Resource Board of Canada 27: 1321-1324.

Wootton, R.J. 1998. Ecology of teleost fish. Springer Publishers. 386 p.

# Appendices

## Single Farm Near Field Data Summary

Nitrogen (DIN) (µM) nearfield net pen averages and standard deviations

| | Net Pens | | | | | |
|---|---|---|---|---|---|---|
| | **1** | **2** | **3** | **4** | **5** | **6** |
| **Average** | 2.51 | 3.03 | 2.35 | 2.84 | 2.58 | 3.15 |
| **St. Dev** | 2.43 | 2.29 | 2.24 | 2.10 | 2.52 | 2.39 |
| | **7** | **8** | **9** | **10** | **11** | **12** |
| **Average** | 2.23 | 2.70 | 2.20 | 2.69 | 1.88 | 2.22 |
| **St. Dev** | 2.39 | 2.31 | 2.29 | 2.19 | 2.37 | 2.38 |

Nitrogen (DIN) (µM) nearfield capture cell averages and standard deviations

| | Capture Cells | | | | | |
|---|---|---|---|---|---|---|
| | **S** | **N** | **E** | **W** | **NE** | **SE** |
| **Average** | 0.12 | 0.20 | 0.31 | 0.12 | 0.24 | 0.11 |
| **St. Dev** | 0.33 | 0.39 | 0.45 | 0.32 | 0.37 | 0.21 |

Nitrogen (DIN) (µM) nearfield net pen monthly averages and standard deviations

| Month | Net Pens | | | | | | | | | | | |
|---|---|---|---|---|---|---|---|---|---|---|---|---|
| | Pen 1 | | Pen 2 | | Pen 3 | | Pen 4 | | Pen 5 | | Pen 6 | |
| | Avg. | St. Dev. | Avg. | St. Dev. | Avg. | St. Dev. | Avg. | St. Dev. | Avg. | St. Dev. | Avg. | St. Dev. |
| **Nov-07** | 0.88 | 0.78 | 1.03 | 0.69 | 0.83 | 0.72 | 0.97 | 0.63 | 0.91 | 0.81 | 1.07 | 0.71 |
| **Dec-07** | 1.63 | 1.36 | 1.94 | 1.19 | 1.53 | 1.26 | 1.82 | 1.09 | 1.70 | 1.43 | 2.04 | 1.25 |
| **Jan-08** | 2.27 | 1.98 | 2.76 | 1.74 | 2.13 | 1.82 | 2.58 | 1.58 | 2.34 | 2.05 | 2.89 | 1.82 |
| **Feb-08** | 2.81 | 2.37 | 3.34 | 2.11 | 2.62 | 2.19 | 3.12 | 1.92 | 2.90 | 2.50 | 3.47 | 2.23 |
| **Mar-08** | 3.12 | 2.70 | 3.74 | 2.40 | 2.90 | 2.47 | 3.49 | 2.17 | 3.21 | 2.80 | 3.92 | 2.50 |
| **Apr-08** | 3.33 | 2.82 | 4.08 | 2.50 | 3.11 | 2.60 | 3.82 | 2.28 | 3.42 | 2.92 | 4.25 | 2.59 |
| **May-08** | 3.49 | 2.90 | 4.28 | 2.61 | 3.30 | 2.70 | 4.03 | 2.39 | 3.56 | 3.00 | 4.43 | 2.73 |
| | Pen 7 | | Pen 8 | | Pen 9 | | Pen 10 | | Pen 11 | | Pen 12 | |
| | Avg. | St. Dev. | Avg. | St. Dev. | Avg. | St. Dev. | Avg. | St. Dev. | Avg. | St. Dev. | Avg. | St. Dev. |
| **Nov-07** | 0.78 | 0.75 | 0.92 | 0.70 | 0.78 | 0.75 | 0.92 | 0.67 | 0.66 | 0.76 | 0.76 | 0.75 |
| **Dec-07** | 1.44 | 1.34 | 1.71 | 1.24 | 1.47 | 1.32 | 1.76 | 1.19 | 1.19 | 1.35 | 1.38 | 1.32 |
| **Jan-08** | 2.02 | 1.94 | 2.46 | 1.79 | 2.00 | 1.88 | 2.47 | 1.71 | 1.70 | 1.96 | 2.01 | 1.91 |
| **Feb-08** | 2.49 | 2.35 | 2.97 | 2.19 | 2.47 | 2.30 | 2.96 | 2.09 | 2.10 | 2.36 | 2.45 | 2.33 |
| **Mar-08** | 2.76 | 2.64 | 3.31 | 2.46 | 2.75 | 2.56 | 3.37 | 2.34 | 2.31 | 2.70 | 2.68 | 2.63 |
| **Apr-08** | 2.97 | 2.77 | 3.64 | 2.60 | 2.91 | 2.68 | 3.61 | 2.42 | 2.50 | 2.85 | 3.00 | 2.83 |
| **May-08** | 3.17 | 2.89 | 3.87 | 2.73 | 2.99 | 2.77 | 3.73 | 2.58 | 2.71 | 2.99 | 3.22 | 2.96 |

Nitrogen (DIN) (µM) nearfield capture cell monthly averages and standard deviations

| Month | \| Capture Cells | | | | | | | | | | |
|---|---|---|---|---|---|---|---|---|---|---|---|
| | \| S | | \| N | | \| E | | \| W | | \| NE | | \| SE | |
| | Avg. | St. Dev. | Avg. | St. Dev. | Avg. | St. Dev. | Avg. | St. Dev. | Avg. | St. Dev. | Avg. | St. Dev. |
| Nov-07 | 0.06 | 0.11 | 0.09 | 0.13 | 0.12 | 0.14 | 0.06 | 0.11 | 0.09 | 0.10 | 0.06 | 0.07 |
| Dec-07 | 0.09 | 0.20 | 0.15 | 0.24 | 0.20 | 0.26 | 0.10 | 0.20 | 0.16 | 0.21 | 0.08 | 0.12 |
| Jan-08 | 0.11 | 0.28 | 0.18 | 0.32 | 0.29 | 0.38 | 0.11 | 0.27 | 0.23 | 0.32 | 0.10 | 0.17 |
| Feb-08 | 0.12 | 0.34 | 0.22 | 0.41 | 0.32 | 0.45 | 0.14 | 0.33 | 0.25 | 0.37 | 0.13 | 0.23 |
| Mar-08 | 0.13 | 0.36 | 0.25 | 0.46 | 0.36 | 0.50 | 0.14 | 0.36 | 0.30 | 0.43 | 0.12 | 0.23 |
| Apr-08 | 0.14 | 0.42 | 0.25 | 0.48 | 0.41 | 0.56 | 0.15 | 0.41 | 0.31 | 0.45 | 0.13 | 0.26 |
| May-08 | 0.17 | 0.48 | 0.25 | 0.49 | 0.44 | 0.60 | 0.15 | 0.41 | 0.32 | 0.48 | 0.14 | 0.27 |

Dissolved oxygen (mg/L) nearfield net pen averages and standard deviations

| | Net Pens | | | | | |
|---|---|---|---|---|---|---|
| | 1 | 2 | 3 | 4 | 5 | 6 |
| Average | 7.34 | 7.30 | 7.35 | 7.31 | 7.33 | 7.29 |
| St. Dev | 0.17 | 0.16 | 0.16 | 0.15 | 0.18 | 0.17 |
| | 7 | 8 | 9 | 10 | 11 | 12 |
| Average | 7.36 | 7.32 | 7.36 | 7.32 | 7.38 | 7.36 |
| St. Dev | 0.17 | 0.17 | 0.16 | 0.16 | 0.17 | 0.17 |

Dissolved oxygen (mg/L) nearfield capture cell averages and standard deviations

| | Capture Cells | | | | | |
|---|---|---|---|---|---|---|
| | S | N | E | W | NE | SE |
| Average | 7.51 | 7.50 | 7.49 | 7.51 | 7.50 | 7.51 |
| St. Dev | 0.02 | 0.03 | 0.03 | 0.02 | 0.03 | 0.01 |

Dissolved oxygen (mg/L) nearfield net pen monthly averages and standard deviations

| Month | \| Net Pens | | | | | | | | | | |
|---|---|---|---|---|---|---|---|---|---|---|---|---|
| | \| Pen 1 | | \| Pen 2 | | \| Pen 3 | | \| Pen 4 | | \| Pen 5 | | \| Pen 6 | |
| | Avg. | St. Dev. | Avg. | St. Dev. | Avg. | St. Dev. | Avg. | St. Dev. | Avg. | St. Dev. | Avg. | St. Dev. |
| Nov-07 | 7.5 | 0.1 | 7.4 | 0.0 | 7.5 | 0.1 | 7.4 | 0.0 | 7.5 | 0.1 | 7.4 | 0.1 |
| Dec-07 | 7.4 | 0.1 | 7.4 | 0.1 | 7.4 | 0.1 | 7.4 | 0.1 | 7.4 | 0.1 | 7.4 | 0.1 |
| Jan-08 | 7.4 | 0.1 | 7.3 | 0.1 | 7.4 | 0.1 | 7.3 | 0.1 | 7.3 | 0.1 | 7.3 | 0.1 |
| Feb-08 | 7.3 | 0.2 | 7.3 | 0.2 | 7.3 | 0.2 | 7.3 | 0.1 | 7.3 | 0.2 | 7.3 | 0.2 |
| Mar-08 | 7.3 | 0.2 | 7.2 | 0.2 | 7.3 | 0.2 | 7.3 | 0.2 | 7.3 | 0.2 | 7.2 | 0.2 |
| Apr-08 | 7.3 | 0.2 | 7.2 | 0.2 | 7.3 | 0.2 | 7.2 | 0.2 | 7.3 | 0.2 | 7.2 | 0.2 |
| May-08 | 7.3 | 0.2 | 7.2 | 0.2 | 7.3 | 0.2 | 7.2 | 0.2 | 7.3 | 0.2 | 7.2 | 0.2 |
| | \| Pen 7 | | \| Pen 8 | | \| Pen 9 | | \| Pen 10 | | \| Pen 11 | | \| Pen 12 | |
| | Avg. | St. Dev. | Avg. | St. Dev. | Avg. | St. Dev. | Avg. | St. Dev. | Avg. | St. Dev. | Avg. | St. Dev. |
| Nov-07 | 7.5 | 0.1 | 7.5 | 0.1 | 7.5 | 0.1 | 7.5 | 0.0 | 7.5 | 0.1 | 7.5 | 0.1 |
| Dec-07 | 7.4 | 0.1 | 7.4 | 0.1 | 7.4 | 0.1 | 7.4 | 0.1 | 7.4 | 0.1 | 7.4 | 0.1 |
| Jan-08 | 7.4 | 0.1 | 7.3 | 0.1 | 7.4 | 0.1 | 7.3 | 0.1 | 7.4 | 0.1 | 7.4 | 0.1 |
| Feb-08 | 7.3 | 0.2 | 7.3 | 0.2 | 7.3 | 0.2 | 7.3 | 0.1 | 7.4 | 0.2 | 7.3 | 0.2 |
| Mar-08 | 7.3 | 0.2 | 7.3 | 0.2 | 7.3 | 0.2 | 7.3 | 0.2 | 7.4 | 0.2 | 7.3 | 0.2 |
| Apr-08 | 7.3 | 0.2 | 7.3 | 0.2 | 7.3 | 0.2 | 7.3 | 0.2 | 7.3 | 0.2 | 7.3 | 0.2 |
| May-08 | 7.3 | 0.2 | 7.2 | 0.2 | 7.3 | 0.2 | 7.2 | 0.2 | 7.3 | 0.2 | 7.3 | 0.2 |

Dissolved oxygen (mg/L) nearfield capture cell monthly averages and standard deviations

| Month | Capture Cells | | | | | | | | | | | |
|---|---|---|---|---|---|---|---|---|---|---|---|---|
| | S | | N | | E | | W | | NE | | SE | |
| | Avg. | St. Dev. | Avg. | St. Dev. | Avg. | St. Dev. | Avg. | St. Dev. | Avg. | St. Dev. | Avg. | St. Dev. |
| Nov-07 | 7.5 | 0.0 | 7.5 | 0.0 | 7.5 | 0.0 | 7.5 | 0.0 | 7.5 | 0.0 | 7.5 | 0.0 |
| Dec-07 | 7.5 | 0.0 | 7.5 | 0.0 | 7.5 | 0.0 | 7.5 | 0.0 | 7.5 | 0.0 | 7.5 | 0.0 |
| Jan-08 | 7.5 | 0.0 | 7.5 | 0.0 | 7.5 | 0.0 | 7.5 | 0.0 | 7.5 | 0.0 | 7.5 | 0.0 |
| Feb-08 | 7.5 | 0.0 | 7.5 | 0.0 | 7.5 | 0.0 | 7.5 | 0.0 | 7.5 | 0.0 | 7.5 | 0.0 |
| Mar-08 | 7.5 | 0.0 | 7.5 | 0.0 | 7.5 | 0.0 | 7.5 | 0.0 | 7.5 | 0.0 | 7.5 | 0.0 |
| Apr-08 | 7.5 | 0.0 | 7.5 | 0.0 | 7.5 | 0.0 | 7.5 | 0.0 | 7.5 | 0.0 | 7.5 | 0.0 |
| May-08 | 7.5 | 0.0 | 7.5 | 0.0 | 7.5 | 0.0 | 7.5 | 0.0 | 7.5 | 0.0 | 7.5 | 0.0 |

Phytoplankton (µg/L) nearfield capture cell averages and standard deviations

| | Capture Cells | | | | | |
|---|---|---|---|---|---|---|
| | S | N | E | W | NE | SE |
| Average | 0.11 | 0.12 | 0.12 | 0.11 | 0.12 | 0.12 |
| St. Dev | 0.01 | 0.01 | 0.01 | 0.01 | 0.01 | 0.01 |

Phytoplankton (µg/L) nearfield capture cell monthly averages and standard deviations

| Month | Capture Cells | | | | | | | | | | | |
|---|---|---|---|---|---|---|---|---|---|---|---|---|
| | S | | N | | E | | W | | NE | | SE | |
| | Avg. | St. Dev. | Avg. | St. Dev. | Avg. | St. Dev. | Avg. | St. Dev. | Avg. | St. Dev. | Avg. | St. Dev. |
| Nov-07 | 0.12 | 0.02 | 0.12 | 0.02 | 0.12 | 0.02 | 0.12 | 0.02 | 0.12 | 0.02 | 0.12 | 0.02 |
| Dec-07 | 0.11 | 0.00 | 0.11 | 0.01 | 0.11 | 0.00 | 0.11 | 0.00 | 0.12 | 0.01 | 0.11 | 0.00 |
| Jan-08 | 0.11 | 0.00 | 0.11 | 0.01 | 0.11 | 0.01 | 0.11 | 0.00 | 0.12 | 0.01 | 0.11 | 0.00 |
| Feb-08 | 0.11 | 0.01 | 0.11 | 0.01 | 0.12 | 0.01 | 0.11 | 0.01 | 0.12 | 0.01 | 0.11 | 0.01 |
| Mar-08 | 0.11 | 0.01 | 0.12 | 0.01 | 0.12 | 0.01 | 0.11 | 0.01 | 0.12 | 0.01 | 0.11 | 0.01 |
| Apr-08 | 0.11 | 0.01 | 0.12 | 0.01 | 0.12 | 0.01 | 0.11 | 0.01 | 0.12 | 0.01 | 0.11 | 0.01 |
| May-08 | 0.11 | 0.01 | 0.12 | 0.01 | 0.12 | 0.01 | 0.11 | 0.01 | 0.12 | 0.01 | 0.11 | 0.01 |

Nearfield model ambient conditions at 5m depth

| Ambient conditions @ 5m | |
|---|---|
| Nitrogen (DIN) (µM) | 0.10 |
| Dissolved oxygen (mg/L) | 7.50 |
| Phytoplankton (µg/L) | 0.10 |
| Zooplankton N (µM) | 0.10 |

## Multiple Farm Far Field Data Summary

Average current velocities (cm/sec) at surface of farfield study sites

| | Study Site | | | | | |
|---|---|---|---|---|---|---|
| | **1** | **2** | **3** | **4** | **5** | **6** |
| **Average** | 21.9 | 23.4 | 21.0 | 21.3 | 21.1 | 21.5 |
| **St. Dev.** | 10.6 | 11.1 | 10.3 | 10.6 | 10.3 | 10.2 |

Nitrogen (DIN) (µM) farfield study site averages and standard deviations

| | Study Site | | | | | |
|---|---|---|---|---|---|---|
| | **1** | **2** | **3** | **4** | **5** | **6** |
| **Average** | 0.61 | 0.60 | 0.63 | 0.63 | 0.62 | 0.62 |
| **St. Dev.** | 0.28 | 0.28 | 0.30 | 0.30 | 0.30 | 0.29 |

Nitrogen (DIN) (µM) farfield capture cell averages and standard deviations

| | Capture Cell | | | | | |
|---|---|---|---|---|---|---|
| | **A** | **B** | **C** | **D** | **E** | **F** |
| **Average** | 0.12 | 0.12 | 0.13 | 0.13 | 0.07 | 0.12 |
| **St. Dev.** | 0.08 | 0.07 | 0.09 | 0.09 | 0.05 | 0.09 |

Nitrogen (DIN) (µM) farfield study site monthly averages and standard deviations

| Month | Study Site | | | | | | | | | | | |
|---|---|---|---|---|---|---|---|---|---|---|---|---|
| | Site 1 | | Site 2 | | Site 3 | | Site 4 | | Site 5 | | Site 6 | |
| | Avg. | St. Dev. | Avg. | St. Dev. | Avg. | St. Dev. | Avg. | St. Dev. | Avg. | St. Dev. | Avg. | St. Dev. |
| **Nov-07** | 0.23 | 0.08 | 0.22 | 0.08 | 0.23 | 0.08 | 0.23 | 0.08 | 0.23 | 0.08 | 0.23 | 0.08 |
| **Dec-07** | 0.41 | 0.13 | 0.40 | 0.13 | 0.42 | 0.13 | 0.42 | 0.13 | 0.41 | 0.13 | 0.41 | 0.14 |
| **Jan-08** | 0.56 | 0.18 | 0.56 | 0.18 | 0.58 | 0.18 | 0.58 | 0.18 | 0.57 | 0.18 | 0.57 | 0.19 |
| **Feb-08** | 0.67 | 0.20 | 0.66 | 0.21 | 0.69 | 0.21 | 0.68 | 0.21 | 0.69 | 0.21 | 0.68 | 0.22 |
| **Mar-08** | 0.74 | 0.22 | 0.72 | 0.22 | 0.77 | 0.23 | 0.76 | 0.23 | 0.77 | 0.24 | 0.75 | 0.24 |
| **Apr-08** | 0.80 | 0.23 | 0.78 | 0.23 | 0.83 | 0.24 | 0.83 | 0.25 | 0.83 | 0.26 | 0.81 | 0.25 |
| **May-08** | 0.85 | 0.25 | 0.82 | 0.25 | 0.88 | 0.26 | 0.88 | 0.27 | 0.87 | 0.27 | 0.85 | 0.25 |

Nitrogen (DIN) (µM) farfield capture cell monthly averages and standard deviations

| Month | Capture Cell | | | | | | | | | | | |
|---|---|---|---|---|---|---|---|---|---|---|---|---|
| | A | | B | | C | | D | | E | | F | |
| | Avg. | St. Dev. | Avg. | St. Dev. | Avg. | St. Dev. | Avg. | St. Dev. | Avg. | St. Dev. | Avg. | St. Dev. |
| Nov-07 | 0.06 | 0.02 | 0.06 | 0.02 | 0.06 | 0.02 | 0.06 | 0.02 | 0.04 | 0.01 | 0.06 | 0.02 |
| Dec-07 | 0.09 | 0.04 | 0.09 | 0.04 | 0.09 | 0.04 | 0.09 | 0.05 | 0.05 | 0.03 | 0.08 | 0.05 |
| Jan-08 | 0.12 | 0.06 | 0.12 | 0.05 | 0.12 | 0.07 | 0.12 | 0.07 | 0.06 | 0.04 | 0.11 | 0.07 |
| Feb-08 | 0.13 | 0.07 | 0.13 | 0.06 | 0.14 | 0.08 | 0.13 | 0.08 | 0.07 | 0.04 | 0.13 | 0.08 |
| Mar-08 | 0.14 | 0.08 | 0.14 | 0.07 | 0.15 | 0.09 | 0.15 | 0.09 | 0.07 | 0.05 | 0.14 | 0.09 |
| Apr-08 | 0.15 | 0.09 | 0.14 | 0.07 | 0.17 | 0.10 | 0.17 | 0.10 | 0.08 | 0.06 | 0.16 | 0.10 |
| May-08 | 0.16 | 0.10 | 0.15 | 0.08 | 0.18 | 0.10 | 0.17 | 0.11 | 0.08 | 0.06 | 0.16 | 0.11 |

Dissolved oxygen (mg/L) farfield study site averages and standard deviations

| | Study Site | | | | | |
|---|---|---|---|---|---|---|
| | 1 | 2 | 3 | 4 | 5 | 6 |
| Average | 7.46 | 7.47 | 7.46 | 7.46 | 7.46 | 7.46 |
| St. Dev. | 0.02 | 0.02 | 0.02 | 0.02 | 0.02 | 0.02 |

Dissolved oxygen (mg/L) farfield capture cell averages and standard deviations

| | Capture Cell | | | | | |
|---|---|---|---|---|---|---|
| | A | B | C | D | E | F |
| Average | 7.50 | 7.50 | 7.50 | 7.50 | 7.50 | 7.50 |
| St. Dev. | 0.01 | 0.00 | 0.01 | 0.01 | 0.00 | 0.01 |

Dissolved oxygen (mg/L) farfield study site monthly averages and standard deviations

| Month | Study Site | | | | | | | | | | | |
|---|---|---|---|---|---|---|---|---|---|---|---|---|
| | Site 1 | | Site 2 | | Site 3 | | Site 4 | | Site 5 | | Site 6 | |
| | Avg. | St. Dev. | Avg. | St. Dev. | Avg. | St. Dev. | Avg. | St. Dev. | Avg. | St. Dev. | Avg. | St. Dev. |
| Nov-07 | 7.5 | 0.0 | 7.5 | 0.0 | 7.5 | 0.0 | 7.5 | 0.0 | 7.5 | 0.0 | 7.5 | 0.0 |
| Dec-07 | 7.5 | 0.0 | 7.5 | 0.0 | 7.5 | 0.0 | 7.5 | 0.0 | 7.5 | 0.0 | 7.5 | 0.0 |
| Jan-08 | 7.5 | 0.0 | 7.5 | 0.0 | 7.5 | 0.0 | 7.5 | 0.0 | 7.5 | 0.0 | 7.5 | 0.0 |
| Feb-08 | 7.5 | 0.0 | 7.5 | 0.0 | 7.5 | 0.0 | 7.5 | 0.0 | 7.5 | 0.0 | 7.5 | 0.0 |
| Mar-08 | 7.5 | 0.0 | 7.5 | 0.0 | 7.5 | 0.0 | 7.5 | 0.0 | 7.5 | 0.0 | 7.5 | 0.0 |
| Apr-08 | 7.5 | 0.0 | 7.5 | 0.0 | 7.5 | 0.0 | 7.4 | 0.0 | 7.4 | 0.0 | 7.4 | 0.0 |
| May-08 | 7.4 | 0.0 | 7.4 | 0.0 | 7.4 | 0.0 | 7.4 | 0.0 | 7.4 | 0.0 | 7.4 | 0.0 |

Dissolved oxygen (mg/L) farfield capture cell monthly averages and standard deviations

| Month | Capture Cell | | | | | | | | | | | |
|---|---|---|---|---|---|---|---|---|---|---|---|---|
| | A | | B | | C | | D | | E | | F | |
| | Avg. | St. Dev. | Avg. | St. Dev. | Avg. | St. Dev. | Avg. | St. Dev. | Avg. | St. Dev. | Avg. | St. Dev. |
| Nov-07 | 7.5 | 0.0 | 7.5 | 0.0 | 7.5 | 0.0 | 7.5 | 0.0 | 7.5 | 0.0 | 7.5 | 0.0 |
| Dec-07 | 7.5 | 0.0 | 7.5 | 0.0 | 7.5 | 0.0 | 7.5 | 0.0 | 7.5 | 0.0 | 7.5 | 0.0 |
| Jan-08 | 7.5 | 0.0 | 7.5 | 0.0 | 7.5 | 0.0 | 7.5 | 0.0 | 7.5 | 0.0 | 7.5 | 0.0 |
| Feb-08 | 7.5 | 0.0 | 7.5 | 0.0 | 7.5 | 0.0 | 7.5 | 0.0 | 7.5 | 0.0 | 7.5 | 0.0 |
| Mar-08 | 7.5 | 0.0 | 7.5 | 0.0 | 7.5 | 0.0 | 7.5 | 0.0 | 7.5 | 0.0 | 7.5 | 0.0 |
| Apr-08 | 7.5 | 0.0 | 7.5 | 0.0 | 7.5 | 0.0 | 7.5 | 0.0 | 7.5 | 0.0 | 7.5 | 0.0 |
| May-08 | 7.5 | 0.0 | 7.5 | 0.0 | 7.5 | 0.0 | 7.5 | 0.0 | 7.5 | 0.0 | 7.5 | 0.0 |

Phytoplankton (µg/L) farfield capture cell averages and standard deviations

|  | Capture Cell |  |  |  |  |
|---|---|---|---|---|---|---|
|  | **A** | **B** | **C** | **D** | **E** | **F** |
| **Average** | 0.13 | 0.13 | 0.14 | 0.13 | 0.12 | 0.12 |
| **St. Dev.** | 0.01 | 0.01 | 0.02 | 0.01 | 0.01 | 0.01 |

Phytoplankton (µg/L) farfield capture cell monthly averages and standard deviations

| Month | Capture Cell | | | | | | | | | | | |
|---|---|---|---|---|---|---|---|---|---|---|---|---|
|  | A | | B | | C | | D | | E | | F | |
|  | Avg. | St. Dev. | Avg. | St. Dev. | Avg. | St. Dev. | Avg. | St. Dev. | Avg. | St. Dev. | Avg. | St. Dev. |
| **Nov-07** | 0.12 | 0.01 | 0.12 | 0.01 | 0.12 | 0.01 | 0.12 | 0.00 | 0.11 | 0.00 | 0.11 | 0.00 |
| **Dec-07** | 0.12 | 0.01 | 0.12 | 0.01 | 0.13 | 0.01 | 0.12 | 0.01 | 0.12 | 0.01 | 0.12 | 0.01 |
| **Jan-08** | 0.12 | 0.01 | 0.12 | 0.01 | 0.13 | 0.01 | 0.13 | 0.01 | 0.12 | 0.01 | 0.12 | 0.01 |
| **Feb-08** | 0.13 | 0.01 | 0.13 | 0.01 | 0.14 | 0.01 | 0.13 | 0.01 | 0.12 | 0.01 | 0.12 | 0.01 |
| **Mar-08** | 0.13 | 0.01 | 0.13 | 0.01 | 0.14 | 0.01 | 0.13 | 0.01 | 0.12 | 0.01 | 0.12 | 0.01 |
| **Apr-08** | 0.13 | 0.02 | 0.13 | 0.02 | 0.14 | 0.02 | 0.13 | 0.01 | 0.12 | 0.01 | 0.12 | 0.01 |
| **May-08** | 0.13 | 0.02 | 0.13 | 0.02 | 0.14 | 0.02 | 0.14 | 0.01 | 0.12 | 0.01 | 0.12 | 0.01 |

Farfield model ambient conditions at 5m depth

| Ambient conditions @ 5m | |
|---|---|
| Nitrogen (DIN) (µM) | 0.03 |
| Dissolved oxygen (mg/L) | 7.50 |
| Phytoplankton (µg/L) | 0.11 |
| Zooplankton N (µM) | 0.16 |

# GIS data accessible through AquaModel for Study Sites

## Aquamodel Single Fish Farm Siting



**Legend**

| Symbol | Description |
|---|---|
| × | Bottom Type |
| + | Unexploded Ordnance |
| ▪ | Navigational Aid |
| ▪ | FAD |
| ◆ | Obstruction |
| ◆ | obstructions_2 |
| ● | Offshore Installation |
| ▪ | Submerged Buoy |
| ✱ | Wreck |
| ─── | Perennial_streams |
| | Ag_Lands |
| | wetlnds_py_n83_Buffer |
| | mma |
| | Coral Reefs_nc |
| | corals |
| | Danger - Restricted Zone |
| | Dumping Area |
| | Explosive Dumping Area |
| | Kauai Safety Zone |
| | Prohibited Area |
| | Small Arms Firing Area |
| | Submerged Submarine Area |
| | A Waters |
| | AA Waters |
| | Anchorage |
| | FAD Area |
| | coast_names83 |
| | 3-mile Boundary |
| | 12-mile Boundary |

# Aquamodel Multiple Fish Farm Siting



Legend

| | |
|---|---|
| + | Unexploded Ordnance |
| ▪ | Navigational Aid |
| ▪ | FAD |
| ♦ | Obstruction |
| ♦ | obstructions_2 |
| ▪ | Offshore Installation |
| ▪ | Submerged Buoy |
| ✷ | Wreck |
| —— | Perennial_streams |
| - - - | Cable |
| —— | Sewerline |
| | Ag_Lands |
| | Coral Reefs_nc |
| | corals |
| | Danger - Restricted Zone |
| | Dumping Area |
| | Explosive Dumping Area |
| | Kauai Safety Zone |
| | Prohibited Area |
| | Small Arms Firing Area |
| | Submerged Submarine Area |
| | Anchorage |
| | FAD Area |
| | coast_names83 |
| | 12-mile Boundary |
| OO | Fish Farm Site |